UNIVERSITY OF OKLAHOMA

GRADUATE COLLEGE

THEORETICAL STUDIES OF MULTI-MODE NOON STATES FOR APPLICATIONS IN QUANTUM METROLOGY AND PROPOSALS OF EXPERIMENTAL SETUPS FOR THEIR GENERATION

A DISSERTATION

SUBMITTED TO THE GRADUATE FACULTY

in partial fulfillment of the requirements for the

Degree of

DOCTOR OF PHILOSOPHY

By

LU ZHANG
Norman, Oklahoma
2018

THEORETICAL STUDIES OF MULTI-MODE NOON STATES FOR APPLICATIONS IN QUANTUM METROLOGY AND PROPOSALS OF EXPERIMENTAL SETUPS FOR THEIR GENERATION

A DISSERTATION APPROVED FOR THE
SCHOOL OF ELECTRICAL AND COMPUTER ENGINEERING

BY

Dr. Kam Wai Clifford Chan, Chair

Dr. Pramode Verma

Dr. Alberto Marino

Dr. Samuel Cheng

Dr. Gregory MacDonald

Dr. Robert Huck

Acknowledgements

I would like to express my deepest appreciation to my committee chair Dr. Kam Wai Cliff Chan, who has been a supportive and accommodating advisor to me. For the past five years, we have been working together on multiple projects in the field of quantum metrology, in which he has valuable insight, and always provides helpful comments and suggestions. With his help, I learned time management skills to work more efficiently, how to think like a scientist, and how to become a researcher. I truly appreciate his trust in me and the financial support from him and Dr. Verma, which made it possible for me to complete my doctorate degree.

I am also extremely grateful of all the other committee members, Dr. Pramode Verma, Dr. Alberto Marino, Dr. Samuel Cheng, Dr. Gregory MacDonald, and Dr. Robert Huck, for their help over the past few years and precious comments on the dissertation. Moreover, I would like to thank all my colleagues, Kyrus M. Kuplicki, Guangyu Fang, Bhagyashri Darunkar-Punekar, Mayssaa El Rifai, Rasha El Hajj, etc., who gave me useful suggestions from different aspects.

I would also like to thank all my friends and family, who supported me both emotionally and financially throughout the entire time of my degree. Special thanks to my parents Dawei Zhang and Xiaozhi Gu, and my grandparents Ming Zhang,

Sumin Zhang, and Guilan Dong, for your love, encouragement, and always supporting every decision I have made. Specifically, I want to thank my grandfather Ming Zhang, who introduced me to the quantum field with Heisenberg's uncertainty principle. I also want to extend a huge thank you to my husband Tyler Osterhaus, for your love, support, and patience in working on a long distance relationship for the past three years until I eventually graduate.

Table of Contents

List of Tables

List of Figures

List of Abbreviations

BCH Baker-Campbell-Hausdorff formula

BS beam splitter

ECS entangled coherent state

EM electromagnetic field

ESCS entangled squeezed coherent state

ESVS entangled squeezed vacuum state

FSF Fock state filter

GHZ Greenberger-Horne-Zeilinger state

HL Heisenberg limit

HOM Hong-Ou-Mandel effect

HV horizontal-vertical polarization

MZI Mach-Zehnder interferometer

NLC nonlinear crystal

OCM optical centroid measurement

PBS polarizing beam splitter

PNR photon-number-resolving detector

POVM positive operator-valued measure

PS phase shifter

QCRB quantum Cramér-Rao bound

QIP quantum information processing

QL quantum lithography

SLD symmetric logarithmic derivative

SMSV single-mode squeezed vacuum state

SPCD single photon coincidence detection

SPDC spontaneous parameter down-conversion process

SQL standard quantum limit

TMSV two-mode squeezed vacuum state

Abstract

Quantum entanglement is a fascinating physical resource that is central to the field of quantum information processing with important applications in such areas as quantum computing, quantum communication, quantum metrology, and quantum imaging. It describes the physical phenomenon in which the quantum state of a multipartite system cannot be written as consisting of constituents that are independent of each other. In this case, the state of the system is called an entangled state. In this dissertation, the entanglement of photons–the elementary excitations of the quantized electromagnetic field–is studied. A focus is made on a particular type of entangled states of light called the d-mode N-photon NOON state, which consists of N photons with the N photons as an ensemble appearing at d orthogonal modes simultaneously and are inseparable.

In quantum metrology, a field that investigates the ultimate precision of measurements of unknown physical parameters, the two-mode NOON state has been studied extensively with respect to its ability to achieve super-resolution and super-sensitivity in the estimation of a single parameter. A lot of theoretical research has been conducted on the generation of two-mode NOON states, and two-mode NOON states with up to 4 photons have been experimentally and efficiently produced. On the

other hand, recently there has been increasing interest in the study of the simultaneous estimation of multiple parameters. Accordingly, the multi-mode NOON state has been attracting more and more attention in view of its potential for enhanced efficiency as compared to using multiple two-mode NOON states separately to estimate the parameters. Nevertheless, no known generation method of multi-mode NOON states with more than 2 photons or 2 modes exists so far.

In this dissertation, several scalable generation methods of multi-mode NOON states are proposed. These methods take advantage of multi-photon quantum interference and they can theoretically be applied to produce NOON states with an arbitrary number of modes and an arbitrary number of photons. The intrinsic generation probability for each method is calculated, and the methods are compared in regards to their feasibility and efficiency. The advantages of using multi-mode NOON states in quantum metrology are also analyzed and discussed in detail.

Chapter 1: Introduction

1.1. Motivation

Quantum entanglement, which was first introduced by Schrödinger [1], is a physical phenomenon describing the strong, nonclassical correlations between two spatially separated quantum systems. In some sense, the elementary light particles (photons) are prepared in such a way that the quantum states of different ensembles of photons cannot be separated. In fact, it has been found that the quantum law behind entanglement is inherently nonlocal; that is, the measurement results obtained at one position can affect the outcome at the other positions. Einstein famously called this "spooky action at a distance". As one of the most important quantum properties of light, entanglement has been studied as an essence of quantum physics, and entanglement has applications in the following areas: quantum computing, quantum communication, quantum metrology, and quantum imaging.

Another important quantum property of light is squeezing, which describes the phenomenon in which the measurement noise of two orthogonal quadratures of light particles can be reduced in one component at the expense of increased fluctuations in the other. According to Heisenberg's uncertainty principle [2], there is a fundamental limit to the measurement precision of two complementary variables of a particle,

such as its position x and its momentum p. Here, the two complementary variables refer to variables whose operators do not commute. Mathematically, this principle is presented using their standard deviations Δ_x and Δ_p as

$$\Delta_x \Delta_p \geq \frac{\hbar}{2}, \tag{1.1}$$

where $\hbar$ is the reduced Planck constant. This indicates that two complementary variables cannot be known exactly, simultaneously. The more precisely the position variable is measured, the less precisely the momentum can be determined, and vice versa. Squeezed states are a type of minimum-uncertainty state with the equality in Eq. (1.1) being saturated, and the quantum noise for measuring one variable can be reduced at the cost of increased measurement noise for the other variable. In common preparations of squeezed states through nonlinear processes, the photons in the states tend to appear in pairs, which is a favorable property for enhanced-precision measurement in quantum metrology. In a sense, squeezing can be regarded as a manifestation of quantum entanglement.

Another even more interesting entangled state of light is called the NOON state [3, 4], which is a quantum state with exactly N photons and all the N photons as an ensemble are entangled and appear at different orthogonal modes simultaneously. A related but different entangled state, called the Greenberger-Horne-Zeilinger (GHZ) state [5], is a multi-mode state with entanglement among multiple single photons (at least 3) in different modes, such as polarization modes or orbital angular momentum modes. The NOON state provides a simple and intuitive way to see how beneficial

entanglement is in quantum metrology. It has the ability to achieve super-resolution and super-sensitivity with respect to the ultimate precision of measurements of unknown physical parameters. The GHZ state, on the other hand, is the fundamental unit for quantum computing, and it is of enormous benefit to quantum communication protocols. In this dissertation, I focus on the NOON state and its applications in quantum metrology.

A wealth of theoretical research has been conducted on the generation of two-mode NOON states [3, 4, 6–20], and their experimental realizations with up to 4 photons have been demonstrated [21–23]. Two-mode NOON states can achieve enhanced resolution [21, 22, 24–26] and enhanced sensitivity [4, 27–30] in the single parameter estimation problem with a relatively low number of photons (low intensity). Thus, they have been of great importance in biological microscopy that deals with target samples that are sensitive to light. In this regard, the NOON state has been successfully deployed as an imaging light source in such applications as tissue imaging using quantum optical coherence tomography [31], refractive index sensing [32], super-resolution fluorescent microscopy [33,34], enhanced phase contrast microscopy [35,36], etc. Aside from the NOON state, other quantum probes have also been considered for quantum metrology, such as the cat state [37], the Holland-Bernett state [38–40], and the entangled coherent state [41, 42], among others [43, 44].

Recently, there has been increasing interest in the simultaneous estimation of multiple parameters with respect to the potential for enhanced measurement efficiency [45–56]. In this respect, the multi-mode NOON state could prove to be advantageous. Nevertheless, the problem of how to generate multi-mode NOON states

with more than 2 photons and two modes is still unsolved. This leads to the pressing research topic of how to generate multi-mode NOON states.

The contributions of this dissertation are as follows:

1. The advantages of using NOON states in quantum metrology are discussed. In particular, a class of generalized multi-mode NOON-like states is introduced and studied in the effort to achieve super-sensitivity in the simultaneous estimation of multiple parameters more efficiently as compared with individual estimations. The multi-mode NOON state is a special case in that class. The analytical form of the lower bound of the uncertainty (the quantum Cramér-Rao bound) using this class of state is calculated. On the other hand, an example of maximum-likelihood measurement for the polarization of light with an arbitrary photon number is presented, which is an optimal measurement in the sense that it maximizes the likelihood function, instead of saturating the quantum Cramér-Rao bound.

2. Several special cases of NOON-like states are compared with respect to their achievable measurement precision, including multi-mode NOON states, entangled coherent states, entangled squeezed vacuum states, and entangled squeezed coherent states. It has been proved that the entangled squeezed vacuum state, with both entanglement and squeezing properties, could result in the best precision among these four cases with the same mean photon number.

3. Several approaches for creating the multi-mode NOON state with at least three modes are proposed. The first method deploys cross-Kerr nonlinearity in order to achieve the entanglement from a single Fock state, while the second method utilizes multiple Fock states and keeps reducing photons from one of the multiple modes

without the knowledge of the mode number in order to introduce entanglement among different modes. Other methods take advantage of the Fock state filters, to reduce non-NOON state components from an input state containing both NOON components and non-NOON components, using either fixed-photon-number input states or nondeterministic-photon-number input states with post-selection.

4. The intrinsic generation probability for each method is calculated and comparisons are made among them with respect to their feasibility and efficiency. It has been shown that the method using multiple squeezed vacuum states as the input sources is the most efficient method, and relatively more feasible to implement since it requires the least number of optical devices, such as photon detectors, under the same expected numbers of modes and photons.

This dissertation is organized as follows. In the rest of Chapter 1, the quantization of the electromagnetic field is described as a preparation for future analyses in the quantum picture. Then, several important states of light, including NOON states, and basic optical devices are introduced with their mathematical representations. Two types of measurement methods are introduced at the end of the chapter. In Chapter 2, the advantages of the two-mode NOON state in quantum metrology are shown, where the state's ability to enhance resolution and sensitivity is demonstrated. Moreover, the performance of a class of multi-mode NOON-like states in the simultaneous multi-phase estimation is analyzed. In Chapter 3, the previous methods of generating two-mode NOON states are summarized. In Chapter 4, the proposed methods for multi-mode NOON states with at least 3 modes and a high photon number are discussed in detail. These methods are then compared with respect to their feasibility and

generation efficiency. In Chapter 5, conclusions from this research are made, followed by the potential future work.

1.2. Quantization of the electromagnetic field

Light is an electromagnetic (EM) radiation that exhibits the properties of both waves and particles, referred to as the wave-particle duality. In this dissertation, I focus on the quantum mechanical features of light. These features require the quantization of the EM field, such that light can be described as being emitted and absorbed in quantized energy packages called photons.

The quantization of the EM field can be derived from the classical Maxwell equations. For convenience, at the beginning, the source-free Maxwell equations [57] are adopted:

$$\begin{aligned} \nabla \cdot \mathbf{B} &= 0, \\ \nabla \times \mathbf{E} &= -\frac{\partial \mathbf{B}}{\partial t}, \\ \nabla \cdot \mathbf{E} &= 0, \\ \nabla \times \mathbf{B} &= \frac{1}{c^2}\frac{\partial \mathbf{E}}{\partial t}, \end{aligned} \tag{1.2}$$

where $c = 1/\sqrt{\mu_0 \epsilon_0}$, μ_0 and ϵ_0 are the magnetic permeability and the electric permittivity of free space, and $\mathbf{E}$ and $\mathbf{B}$ are the electric field and the magnetic field. Since the Maxwell equations are gauge invariant under the source-free scenario, the Coulomb gauge is chosen for analysis as a convention. Under the Coulomb gauge, $\mathbf{E}$

and $\mathbf{B}$ are determined from the vector potential $\mathbf{A}(\mathbf{r}, t)$ as:

$$\begin{aligned} \mathbf{B} &= \nabla \times \mathbf{A}, \\ \mathbf{E} &= -\frac{\partial \mathbf{A}}{\partial t}, \end{aligned} \tag{1.3}$$

with the Coulomb gauge condition

$$\nabla \cdot \mathbf{A} = 0. \tag{1.4}$$

Combining equations (1.2), (1.3), adn (1.4), one can solve and obtain $\mathbf{A}(\mathbf{r}, t) = \mathbf{A}^{(+)}(\mathbf{r}, t) + \mathbf{A}^{(-)}(\mathbf{r}, t)$, with

$$\mathbf{A}^{(+)}(\mathbf{r}, t) = (\mathbf{A}^{(-)}(\mathbf{r}, t))^* = \sum_k c_k \mathbf{u}_k(\mathbf{r}) e^{-i\omega_k t}, \tag{1.5}$$

which is expanded using a discrete set of orthogonal mode functions $\mathbf{u}_k(\mathbf{r})$ with the Fourier coefficient c_k and frequency ω_k for the kth mode. ω_k satisfies

$$(\nabla^2 + \frac{\omega_k^2}{c^2})\mathbf{u}_k(\mathbf{r}) = 0, \tag{1.6}$$

and the mode functions form a complete orthonormal set

$$\int_V \mathbf{u}_k^*(\mathbf{r}) \mathbf{u}_{k'}(\mathbf{r}) d\mathbf{r} = \delta_{kk'}. \tag{1.7}$$

Using the periodic boundary conditions, one can rewrite the vector potential as

$$\mathbf{A}(\mathbf{r},t)=\sum_k\left(\frac{\hbar}{2\omega_k\epsilon_0}\right)^{1/2}\left[a_k\mathbf{u}_k(\mathbf{r})e^{-i\omega_k t}+a_k^\dagger\mathbf{u}_k^*(\mathbf{r})e^{i\omega_k t}\right], \tag{1.8}$$

with † denoting the complex conjugate transposition operation. Then the electric field is obtained using Eq. (1.3):

$$\mathbf{E}(\mathbf{r},t)=i\sum_k\left(\frac{\hbar\omega_k}{2\epsilon_0}\right)^{1/2}\left[a_k\mathbf{u}_k(\mathbf{r})e^{-i\omega_k t}-a_k^\dagger\mathbf{u}_k^*(\mathbf{r})e^{i\omega_k t}\right]. \tag{1.9}$$

The normalization factors are chosen properly, such that the amplitudes a_k and $a_k^\dagger$ are dimensionless.

In classical EM theory, a_k and $a_k^\dagger$ are complex numbers. In order to quantize the EM field, a_k and $a_k^\dagger$ are chosen to be mutually adjoint operators, which satisfy the boson commutation relations

$$[a_k,a_{k'}]=[a_k^\dagger,a_{k'}^\dagger]=0,\ [a_k,a_{k'}^\dagger]=\delta_{kk'}, \tag{1.10}$$

where $[a,b]=ab-ba$ is the commutator of two elements a and b. a_k and $a_k^\dagger$ are recognized as the field operators, which can be adopted to describe the properties of the EM field quantitatively in the quantum picture.

1.3. Basic states of light

In this section, after the quantum field operators a_k and $a_k^\dagger$ are introduced, several interesting states of light and their properties are discussed. Particularly, the photon

statistics for each state are denoted using field operators. In the quantum picture, a state of light in mode k is usually represented using bracket notation $|\phi\rangle_k$ with a certain parameter ϕ, where the mode can be a spatial mode, a polarization mode, etc. In the following subsections, three types of basic states are introduced: Fock states $|N\rangle$, coherent states $|\alpha\rangle$, and squeezed vacuum states $|r\rangle$, where N, α and r are the photon number, the coherent amplitude, and the squeezing factor, respectively. An introduction to the NOON state is given afterwards.

1.3.1 The Fock state

The Fock state is also called the photon number state, and it is a single mode quantum state of light with exactly N photons, where the N photons are operated/measured as an ensemble and are indistinguishable. Mathematically, the Fock state $|n\rangle_k$ in mode k is an eigenstate of the photon number operator defined as $a_k^\dagger a_k$:

$$a_k^\dagger a_k |n\rangle_k = n|n\rangle_k, \tag{1.11}$$

and the eigenvalue n is the number of photons for $|n\rangle_k$. When there are no photons in the system, the state $|0\rangle$ is called the vacuum state. The vacuum state in the quantum picture is different from the vacuum state in classical optics since the former has non-zero fluctuation. Using Eqs. (1.10) and (1.11), one can derive the following useful

equations for calculations:

$$\begin{aligned} a_k|n\rangle_k &= \sqrt{n}|n-1\rangle_k, \\ a_k^\dagger|n\rangle_k &= \sqrt{n+1}|n+1\rangle_k, \end{aligned} \tag{1.12}$$

which can be explained as that $a_k^\dagger$ (a_k) working on a Fock state $|n\rangle_k$ creates (destroys) one photon from the mode k. Since destroying one photon from a vacuum state is impossible, a_k working on a vacuum state gives zero probability; i.e., $a_k|0\rangle = 0$. Because of this property, $a_k^\dagger$ and a_k are called the creation operator and the annihilation operator, respectively.

A Fock state can also be represented by successively applying $a_k^\dagger$ to the vacuum state:

$$|n\rangle_k = \frac{a_k^{\dagger n}}{\sqrt{n!}}|0\rangle_k, \ n = 0, 1, 2, \cdots . \tag{1.13}$$

It is noticeable that the Fock state $|n\rangle_k$ is a fixed-photon-number state, whose photon number variance is 0. Currently, there is no uniform strategy of generating the Fock state with an arbitrary photon number perfectly. However, research has been done in effectively creating Fock states with six photons using a superconducting quantum circuit [58]. Higher photon-number Fock states were theoretically shown to be achievable with schemes that make use of certain recycling strategies [59].

Specifically, when $n = 1$, $|1\rangle_k$ is a single photon state, which is the quantum bit unit with main applications in quantum key distribution and quantum computing. Single photons can be created deterministically using quantum dots [60], or conditionally using a spontaneous parametric down-conversion process (SPDC) [61].

In order to present a multi-mode quantum state, a tensor product is used as an operator to connect different modes, denoted by $\otimes$. As an example, the quantum state for two Fock states with n_1 photons in mode 1 and n_2 photons in mode 2 can be written as $|n_1\rangle_1 \otimes |n_2\rangle_2$. In this case, the tensor product $\otimes$ can be omitted, i.e., $|n_1\rangle_1 \otimes |n_2\rangle_2 = |n_1\rangle_1|n_2\rangle_2 = |n_1, n_2\rangle_{12} = a_1^{\dagger n_1} a_2^{\dagger n_2}|0,0\rangle_{12}/\sqrt{n_1! n_2!}$. In the discussion of single-mode quantum states, the mode number k is omitted in the following text for convenience.

1.3.2 The coherent state

The coherent state $|\alpha\rangle$ is a mathematical characterization of the output of an ideal single-mode laser [62], which is the most common classical light source used in experiments. It is the eigenstate of the annihilation operator a satisfying $a|\alpha\rangle = \alpha|\alpha\rangle$ with the complex number α being the coherent amplitude. The coherent state can also be represented using the displacement operator $D(\alpha)$ as $|\alpha\rangle = D(\alpha)|0\rangle$ [57], where

$$D(\alpha) = \exp\left(\alpha a^\dagger - \alpha^* a\right). \tag{1.14}$$

The displacement operator has the following properties:

$$\begin{aligned} &D^\dagger(\alpha)D(\alpha) = D(\alpha)D^\dagger(\alpha) = I, \\ &D^\dagger(\alpha)a^\dagger D(\alpha) = a^\dagger + \alpha^* \\ &D^\dagger(\alpha)aD(\alpha) = \left(D^\dagger(\alpha)a^\dagger D(\alpha)\right)^\dagger = a + \alpha. \end{aligned} \tag{1.15}$$

The equations in Eq. (1.15) can be proved using a lemma of the Baker-Campbell-Hausdorff formula (BCH) [63]:

$$e^X Y e^{-Y} = Y + [X,Y] + \frac{1}{2!}[X,[X,Y]] + \frac{1}{3!}[X,[X,[X,Y]]] + \cdots . \tag{1.16}$$

As an example,

$$\begin{aligned}
&D^\dagger(\alpha) a^\dagger D(\alpha) = \exp\left(\alpha^* a - \alpha a^\dagger\right) a^\dagger \exp\left(\alpha^* a - \alpha a^\dagger\right) \\
&= a^\dagger + [(\alpha^* a - \alpha a^\dagger), a^\dagger] + \frac{1}{2!}[(\alpha^* a - \alpha a^\dagger), [(\alpha^* a - \alpha a^\dagger), a^\dagger]] + \cdots \\
&= a^\dagger + \alpha^*(a a^\dagger - a^\dagger a) - \alpha(a^\dagger a^\dagger - a^\dagger a^\dagger) + \frac{1}{2!}[(\alpha^* a - \alpha a^\dagger), [(\alpha^* a - \alpha a^\dagger), a^\dagger]] + \cdots \\
&= a^\dagger + \alpha^* + \frac{1}{2!}[(\alpha^* a - \alpha a^\dagger), \alpha^*] + \cdots = a^\dagger + \alpha^*.
\end{aligned} \tag{1.17}$$

Using the Zassenhaus formula [63]:

$$e^{t(X+Y)} = e^{tX} e^{tY} e^{-t^2/2![X,Y]} e^{t^3/3!(2[Y,[X,Y]]+2[X,[X,Y]])} \cdots , \tag{1.18}$$

the displacement operator can be separated by choosing $t = 1$, $X = \alpha a^\dagger$ and $Y = -\alpha^* a$:

$$\begin{aligned}
&D(\alpha) = \exp\left(\alpha a^\dagger - \alpha^* a\right) = e^{\alpha a^\dagger} e^{-\alpha^* a} e^{-1/2[\alpha a^\dagger, -\alpha^* a]} e^{1/3!(2[Y,[X,Y]]+2[X,[X,Y]])} \cdots \\
&= e^{\alpha a^\dagger} e^{-\alpha^* a} e^{-|\alpha|^2/2} e^{1/3!\left(2[-\alpha^* a, |\alpha|^2]+2[\alpha a^\dagger, |\alpha|^2]\right)} \cdots \\
&= e^{-|\alpha|^2/2} e^{\alpha a^\dagger} e^{-\alpha^* a}.
\end{aligned} \tag{1.19}$$

One can then expand the coherent state using Fock state basis with Eq. (1.19):

$$|\alpha\rangle = e^{-\frac{|\alpha|^2}{2}} \sum_{n=0}^{\infty} \frac{\alpha^n}{\sqrt{n!}} |n\rangle. \tag{1.20}$$

As one can see from Eq. (1.20), the coherent state is a coherent superposition of different Fock state components $|n\rangle$, following the Poisson photon distribution:

$$p_{\mathrm{Coh}}(n) = \left| e^{-\frac{|\alpha|^2}{2}} \frac{\alpha^n}{\sqrt{n!}} \right|^2 = e^{-|\alpha|^2} \frac{|\alpha|^{2n}}{n!}, \tag{1.21}$$

with the mean photon number $\bar{n}_{\mathrm{Coh}} = |\alpha|^2$ and the photon number variance $\Delta^2 n_{\mathrm{Coh}} = |\alpha|^2$. The mean photon number and photon number variance for state $|\phi\rangle$ are defined as $\bar{n} = \langle\phi|a^\dagger a|\phi\rangle$ and $\Delta^2 n = \langle\phi|a^\dagger a a^\dagger a|\phi\rangle - \langle\phi|a^\dagger a|\phi\rangle^2$, respectively.

1.3.3 The squeezed state

The single-mode squeezed state and the two-mode squeezed state are introduced in this section.

A single-mode squeezed state is created through the single-mode squeezed operator

$$S_1(r) = \exp\left[\frac{1}{2}(r^* a^2 - r a^{\dagger 2})\right], \tag{1.22}$$

where $r = |r| \exp(i\phi)$ is the complex squeezing factor. $S_1(r)$ satisfies the following

properties:

$$
\begin{aligned}
&S_1^\dagger(r)S_1(r) = S_1(r)S_1^\dagger(r) = I,\\
&S_1^\dagger(r)a^\dagger S_1(r) = a^\dagger \cosh|r| - ae^{-i\phi}\sinh|r|,\\
&S_1^\dagger(r)aS_1(r) = \Big(S_1^\dagger(r)a^\dagger S_1(r)\Big)^\dagger = a\cosh|r| - a^\dagger e^{i\phi}\sinh|r|.
\end{aligned}
\tag{1.23}
$$

One detailed calculation is shown below:

$$
\begin{aligned}
&S_1^\dagger(r)a^\dagger S_1(r) = \exp\left[\frac{1}{2}(ra^{\dagger 2} - r^*a^2)\right]a^\dagger \exp\left[\frac{1}{2}(r^*a^2 - ra^{\dagger 2})\right]\\
&= a^\dagger + [\frac{1}{2}(ra^{\dagger 2} - r^*a^2), a^\dagger] + \frac{1}{2!}[\frac{1}{2}(ra^{\dagger 2} - r^*a^2), [\frac{1}{2}(ra^{\dagger 2} - r^*a^2), a^\dagger]] + \cdots\\
&= a^\dagger - \frac{r^*}{2}(aaa^\dagger - aa^\dagger a + aa^\dagger a - a^\dagger aa) + \frac{1}{2!}[\frac{1}{2}(ra^{\dagger 2} - r^*a^2), [\frac{1}{2}(ra^{\dagger 2} - r^*a^2), a^\dagger]] + \cdots\\
&= a^\dagger - r^*a - \frac{1}{2!}[\frac{1}{2}(ra^{\dagger 2} - r^*a^2), r^*a] + \cdots = a^\dagger - |r|e^{-i\phi}a + \frac{|r|^2}{2!}a^\dagger - e^{-i\phi}\frac{|r|^3}{3!}a + \cdots\\
&= a^\dagger(1 + \frac{|r|^2}{2!} + \cdots) - ae^{-i\phi}(r + \frac{|r|^3}{3!} + \cdots)\cdots = a^\dagger\cosh|r| - ae^{-i\phi}\sinh|r|,
\end{aligned}
\tag{1.24}
$$

with Taylor expansions

$$
\cosh x = \sum_{n=0}^{\infty}\frac{x^{2n}}{(2n)!},\ \text{and}\ \sinh x = \sum_{n=0}^{\infty}\frac{x^{2n+1}}{(2n+1)!}. \tag{1.25}
$$

Operating $S_1(r)$ on a coherent state gives a squeezed coherent state; i.e., $|\alpha, r\rangle_1 = S_1(r)D_1(\alpha)|0\rangle_1$. When the coherent amplitude $\alpha = 0$ (no coherent seeding), the state is a single-mode squeezed vacuum state (SMSV), whose expansion using Fock states

can be calculated using the disentangling theorem [64]:

$$
\begin{aligned}
|r\rangle_1 &= S_1(r)|0\rangle_1 = \exp\left[\frac{1}{2}(ra^{\dagger 2} - r^* a^2)\right]|0\rangle_1 \\
&= \exp\left[\frac{1}{2}e^{i\phi}\tanh|r|a^{\dagger 2}\right]\exp\left[-2\ln\cosh|r|\left(\frac{1}{2}a^\dagger a + \frac{1}{4}\right)\right]\exp\left[-\frac{1}{2}e^{-i\phi}\tanh|r|a^2\right]|0\rangle_1 \\
&= \frac{1}{\sqrt{\cosh|r|}}\sum_{n=0}^{\infty}\left(e^{i\phi}\tanh|r|\right)^n\frac{\sqrt{(2n)!}}{2^n n!}|2n\rangle_1.
\end{aligned}
\tag{1.26}
$$

The photons in SMSV tend to appear in pairs in the same mode. In other words, only even-photon-number components exist in SMSV. The mean photon number for SMSV is $\bar{n}_{\mathrm{SMSV}} = \sinh^2|r|$ and the variance is $\Delta^2 n_{\mathrm{SMSV}} = \sinh^4|r| + \sinh^2|r|$.

The two-mode squeezed state, on the other hand, is related to the two-mode squeezed operator

$$
S_{12}(r) = \exp\left(r^* a_1 a_2 - r a_1^\dagger a_2^\dagger\right), \tag{1.27}
$$

which satisfies

$$
\begin{aligned}
&S_{12}^\dagger(r)S_{12}(r) = S_{12}(r)S_{12}^\dagger(r) = I, \\
&S_{12}^\dagger(r)a_1(a_2)S_{12}(r) = a_1(a_2)\cosh|r| - a_2^\dagger(a_1^\dagger)e^{i\phi}\sinh|r| \\
&S_{12}^\dagger(r)a_1^\dagger(a_2^\dagger)S_{12}(r) = a_1^\dagger(a_2^\dagger)\cosh|r| - a_2(a_1)e^{-i\phi}\sinh|r|.
\end{aligned}
\tag{1.28}
$$

Applying $S_{12}(r)$ on coherent states in either mode or both modes gives the two-mode squeezed coherent state $|\alpha, r\rangle_{12} = S_{12}(r)D_1(\alpha_1)D_2(\alpha_2)|0\rangle_{12}$. When $\alpha_1 = \alpha_2 = 0$ (no coherent seeding in either arm), the state is a two-mode squeezed vacuum state

(TMSV), which can also be written in the Fock state basis as

$$|r\rangle_{12} = S_{12}(r)|0\rangle_{12} = \frac{1}{\cosh|r|}\sum_{n=0}^{\infty}\left(e^{i\phi}\tanh|r|\right)^n|n,n\rangle_{12}. \tag{1.29}$$

Similar to SMSV, only even total-photon-number terms exist here. Nevertheless, the photons in TMSV occupy equally in two different modes, which could be different spatial modes, orthogonal polarization modes, or both. Actually, combining the two modes of a TMSV on a balanced beam splitter converts it into two spatially-separated SMSVs, which will be proved after the introduction of beam splitters in the next section. The mean photon number ${}_{12}\langle r|a_i^\dagger a_i|r\rangle_{12} = \sinh^2|r|$ and the variance ${}_{12}\langle r|a_i^\dagger a_i a_i^\dagger a_i|r\rangle_{12} - {}_{12}\langle r|a_i^\dagger a_i|r\rangle_{12}^2 = \sinh^4|r| + \sinh^2|r|$ for each mode i $(i = 1, 2)$ of the TMSV is the same as those in the corresponding SMSV.

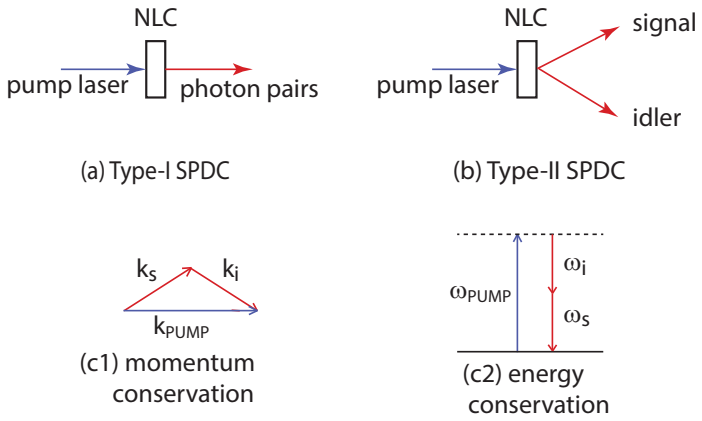

Figure 1.1. The schematic setup of Type-I and Type-II SPDC.

Experimentally, the squeezed vacuum state can be generated using a nonlinear $\chi^{(2)}$ crystal (NLC) through a spontaneous parametric down-conversion process (SPDC) [65], as shown in Fig. 1.1(a) and (b), in accordance with the laws of conservation of momentum and energy as shown in (c1) and (c2). When a high intensity

pumping laser beam is injected into an NLC, some photons undergo spontaneous down-conversion and exit from the crystal in pairs. For the type-I SPDC, the output photon pairs have the same polarization and exit in the same spatial location, which is essentially an SMSV. For the type-II SPDC, the output photon pairs are emitted into two orthogonal modes–the signal mode and idler mode–in three possibilities: (1) the same polarization but different exiting angles emitted from the same spatial location, (2) the same exiting angle but different polarizations, or (3) different polarizations and different exiting angles. All of these possibilities can be represented using the TMSV. Since the output photons in the signal mode and the idler mode are identical (other than certain temporal or spatial walk-offs that can be compensated), type-II SPDC is commonly considered as a heralded single photon generator with the triggering of single photon detection at the other arm [61]. In order to generate squeezed coherent state, in addition to the pump laser, one/two seeding coherent laser beams should be injected into the system, accordingly.

1.3.4 The NOON state

The mathematical expressions of the state of interest in this dissertation–the NOON state–are given in this section. A two-mode NOON state with mean photon number N can be written as

$$|\mathrm{NOON}\rangle_{12} = \frac{1}{\sqrt{2}}(|N0\rangle_{12} + |0N\rangle_{12}), \tag{1.30}$$

which is a superposition of two possibilities: all the N photons either exist in mode 1 or in mode 2. This state is different from the N-photon Fock state, in the way that the N photons in the NOON state are entangled in two orthogonal modes 1 and 2 with equal probability, while the N photons in the latter appear in a single mode with 100% probability. There has been plenty of work done on the generation of two-mode NOON states, and this work will be summarized in Chapter 3.

With more attention on the simultaneous multiple phase estimation, there is the requirement for multi-mode NOON state:

$$|\mathrm{NOON}\rangle_{12\cdots d} = \frac{1}{\sqrt{d}}(|N0\cdots0\rangle \pm |0N0\cdots0\rangle \pm \cdots \pm |0\cdots0N\rangle)_{12\cdots d}, \tag{1.31}$$

where d is the mode number. The N photons in the d-mode NOON state exist in d orthogonal modes simultaneously, and the quantum states for different modes are not separable.

1.4. Basic optical devices

After introducing several important states of light, the basic optical devices utilized to generate NOON states are discussed in this section. These devices are beam splitters, phase shifters, and photon detectors. Moreover, an important unit called the Fock state filter is described. This filter plays an important role in the proposed multi-mode NOON state generation methods.

A beam splitter (BS) is an optical device, which takes one or more incident light beams and splits them into two or more modes. In this dissertation, only beam split-

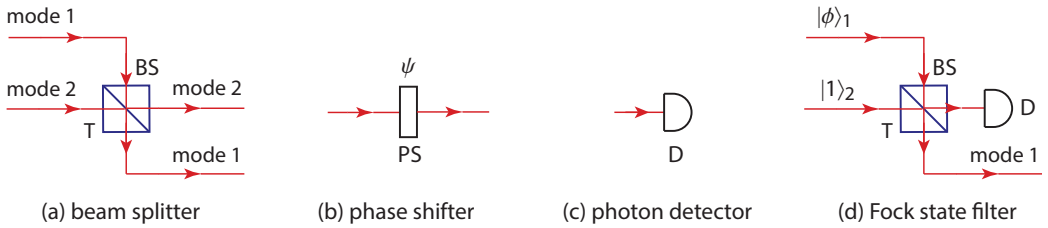

Figure 1.2. Notations of (a) a beam splitter, (b) a phase shifter, (c) a photon detector, and (d) a Fock state filter.

ters with two input modes and two output modes are discussed, where one of the input modes could be a vacuum mode. Beam splitters can be polarizing or non-polarizing. A polarizing beam splitter (PBS) is defined by the two orthogonal polarizations, such as horizontal and vertical (HV). Normally, a PBS transmits horizontally-polarized photons and reflects vertically-polarized photons. A non-polarizing beam splitter redistributes the incident photons in two spatial modes. The notation of a BS is shown in Fig. 1.2(a). The term "beam splitter," or "BS," refers to a non-polarizing beam splitter in this dissertation.

Conventionally, a BS in modes 1 and 2 with transmissivity $T = \cos^2\theta$ can be represented using a unitary operator

$$U_{12}(\theta) = e^{i\theta(a_1^\dagger a_2 + a_2^\dagger a_1)}, \tag{1.32}$$

or using the operator transformation formulae

$$\begin{aligned} a_1^\dagger &\xrightarrow{\text{BS}} \cos\theta a_1^\dagger + i\sin\theta a_2^\dagger \\ a_2^\dagger &\xrightarrow{\text{BS}} \cos\theta a_2^\dagger + i\sin\theta a_1^\dagger, \end{aligned} \tag{1.33}$$

where a $\pi/2$ phase difference is introduced into the reflected arm. The two rep-

resentations in Eqs. (1.32) and (1.33) are equivalent to each other; for example, $U_{12}(\theta)a_1^\dagger U_{12}^\dagger(\theta) = \cos\theta a_1^\dagger + i\sin\theta a_2^\dagger$.

It can be shown that when two single photons $|1,1\rangle_{12}$ are combined on a balanced 50:50 BS with $T = 1/2$, the output state has the form

$$\begin{aligned} U_{12}(\frac{\pi}{4})|1,1\rangle_{12} &= U_{12}(\frac{\pi}{4})a_1^\dagger a_2^\dagger|0,0\rangle_{12} \\ &= \left(\cos\frac{\pi}{4}a_1^\dagger + i\sin\frac{\pi}{4}a_2^\dagger\right)\left(\cos\frac{\pi}{4}a_2^\dagger + i\sin\frac{\pi}{4}a_1^\dagger\right)|0,0\rangle_{12} \\ &= \frac{i}{2}\left(a_1^{\dagger 2} + a_2^{\dagger 2}\right)|0,0\rangle_{12} = \frac{i}{\sqrt{2}}(|2,0\rangle_{12} + |0,2\rangle_{12}), \end{aligned} \tag{1.34}$$

where the $|1,1\rangle_{12}$ term is canceled due to interference and the two photons can only appear in mode 1 or mode 2. This is a simple but important example of quantum interference in which a 2-mode 2-photon NOON state is generated. The phenomenon is called the Hong-Ou-Mandel effect (HOM) [66].

Another interesting phenomenon involving BS is that combining the two output modes of a TMSV on a 50:50 BS gives two spatially-separated SMSVs. This is also

mentioned in Section 4.4.2. The proof is as follows:

$$
\begin{aligned}
U_{12}(\frac{\pi}{4})|r\rangle_{12} &= e^{\frac{\pi}{4}(a_1^\dagger a_2 + a_2^\dagger a_1)} \frac{1}{\cosh|r|} \sum_{n=0}^{\infty} \left(e^{i\phi}\tanh|r|\right)^n |n,n\rangle_{12} \\
&= \frac{1}{\cosh|r|} \sum_{n=0}^{\infty} e^{\frac{\pi}{4}(a_1^\dagger a_2 + a_2^\dagger a_1)} e^{in\phi} \tanh^n|r| \frac{a_1^{\dagger n} a_2^{\dagger n}}{n!} |0,0\rangle_{12} \\
&= \frac{1}{\cosh|r|} \sum_{n=0}^{\infty} e^{in\phi} \tanh^n|r| \frac{(a_1^\dagger + ia_2^\dagger)^n (a_2^\dagger + ia_1^\dagger)^n}{2^n n!} |0,0\rangle_{12} \\
&= \frac{1}{\cosh|r|} \sum_{n=0}^{\infty} e^{in\phi} \tanh^n|r| \frac{i^n}{2^n n!} \sum_{m=0}^{n} \frac{n!}{m!(n-m)!} a_1^{\dagger 2m} a_2^{\dagger 2(n-m)} |0,0\rangle_{12} \\
&= \frac{1}{\cosh|r|} \sum_{m=0}^{\infty}\sum_{n'=0}^{\infty} e^{i(m+n')\phi} \tanh^{(m+n')}|r| \frac{i^{(m+n')}}{2^{(m+n')}(m+n')!} \frac{(m+n')!}{m!n'!} a_1^{\dagger 2m} a_2^{\dagger 2n'} |0,0\rangle_{12} \\
&= \frac{1}{\sqrt{\cosh|r|}} \sum_{m=0}^{\infty} e^{im\phi} \tanh^m|r| \frac{i^m}{2^m m!} a_1^{\dagger 2m} |0\rangle_1 \frac{1}{\sqrt{\cosh|r|}} \sum_{n=0}^{\infty} e^{in\phi} \tanh^n|r| \frac{i^n}{2^n n!} a_2^{\dagger 2n} |0\rangle_2 \\
&= |r'\rangle_1 |r'\rangle_2,
\end{aligned}
\tag{1.35}
$$

where $r' = |r|\exp(\phi + \pi/2)$.

A phase shifter (PS) modulates the phase parameter on a certain mode, as shown in Fig. 1.2(b). The phase shift ψ is accomplished by the operator $\exp(i\psi a^\dagger a)$ with $a^\dagger$ being the field operator to that mode.

A photon detector is used to detect the photons in one mode. In discrete-variable quantum information processing (QIP), two types of photon detectors are commonly used: single photon detectors (also called on-off detectors) and photon-number-resolving (PNR) detectors. A schematic of a generic photon detector is shown in Fig. 1.2(c). PNR detectors are theoretically sensitive enough to measure exactly N photons, and they are able to distinguish between n- and $(n+1)$-photon events

$(n = 1, 2, \cdots)$, whose measurement process can be written using the measurement operator $\Pi_N = |N\rangle\langle N|$. Since all of the current measurement processes are destructive, the post-measurement state after the detection on a certain mode is calculated by tracing out the measuring mode after applying the measurement operator on the state. For example, the evolution of the state $|\phi\rangle_{12}$ after detecting N photons in mode 1 can be expressed [67] as

$$\rho_{12} \to \rho_2 = \mathrm{Tr}_1\left(\Pi_N^{(1)}\rho_{12}\right) = \mathrm{Tr}_1\left(|N\rangle_1\langle N|\phi\rangle_{12}\langle\phi|\right) \tag{1.36}$$

with $\rho_{12} = |\phi\rangle_{12}\langle\phi|$, where the trace operation on any operator O is calculated as $\mathrm{Tr}(O) = \sum_{i=0}^{\infty}\langle i|O|i\rangle$ and ρ_2 is the density operator of the post-measured state. On the other hand, the commonly called single photon detector or, more properly, the on-off detector, does not resolve the photon number. For such a detector with perfect efficiency, the off event corresponds to $|0\rangle\langle 0|$, whereas the on event corresponds to $\sum_{n\geq 1}\Pi_n$. In this dissertation, when a single photon detector is mentioned, this refers to a PNR detector that registers the one-photon event only and ignores the other events (zero-photon or multi-photon events). However, in practice, when the events of more than one photon have small probability amplitudes, an on-off detector acts pretty well as a single photon detector.

In the proposed strategies of creating the multi-mode NOON state, there is an important unit that has been utilized frequently, called the Fock state filter (FSF) [68]. It can filter out a certain Fock state component from the incident beam and modulate the amplitude of the other components– with the help of a single photon catalyst, a

beam splitter with certain transmissivity, and a single photon detector. The setup of the FSF is shown in Fig. 1.2(d). A detailed analysis of the FSF is conducted below.

Considering an input state as an arbitrary coherent superposition of the Fock states in mode 1

$$|\phi\rangle_1 = \sum_{n=0}^{\infty} C_n |n\rangle_1 = \sum_{n=0}^{\infty} C_n \frac{a_1^{\dagger n}}{\sqrt{n!}} |0\rangle_1, \tag{1.37}$$

the output state after combining $|\phi\rangle_1$ with a single photon state in mode 2 on a beam splitter is

$$\begin{aligned} U_{12}(\theta)|\phi\rangle_1|1\rangle_2 &= \sum_{n=0}^{\infty} \frac{C_n}{\sqrt{n!}} U_{12}(\theta) a_1^{\dagger n} a_2^{\dagger} |0,0\rangle_{12} \\ &= \sum_{n=0}^{\infty} \frac{C_n}{\sqrt{n!}} (\cos\theta a_1^{\dagger} + i \sin\theta a_2^{\dagger})^n (\cos\theta a_2^{\dagger} + i \sin\theta a_1^{\dagger}) |0,0\rangle_{12}. \end{aligned} \tag{1.38}$$

When there is one and only one photon detected at detector D, the un-normalized state in output mode 1 is then

$$\begin{aligned} |\phi\rangle_1^{\text{un-norm}} &= \mathrm{Tr}_2\Big[\Pi_{N=1}^{(2)} \sum_{n=0}^{\infty} \frac{C_n}{\sqrt{n!}} (\cos\theta a_1^{\dagger} + i \sin\theta a_2^{\dagger})^n (\cos\theta a_2^{\dagger} + i \sin\theta a_1^{\dagger}) |0,0\rangle_{12}\Big] \\ &= \mathrm{Tr}_2\Big[|1\rangle_2\langle 1| \sum_{n=0}^{\infty} \frac{C_n}{\sqrt{n!}} \\ &\quad \Big(ni \sin\theta a_2^{\dagger} \cos^{n-1}\theta a_1^{\dagger(n-1)} i \sin\theta a_1^{\dagger} + \cos\theta a_2^{\dagger} \cos^n\theta a_1^{\dagger n}\Big) |0,0\rangle_{12}\Big] \\ &= \sum_{n=0}^{\infty} \frac{C_n}{\sqrt{n!}} \cos^{n+1}\theta \left(1 - n\tan^2\theta\right) a_1^{\dagger n} |0\rangle_1 \\ &= \sum_{n=0}^{\infty} C_n \cos^{n+1}\theta \left(1 - n\tan^2\theta\right) |n\rangle_1. \end{aligned} \tag{1.39}$$

If the transmissivity of the BS is chosen to be $T = k/(k+1)$ (i.e., $\theta = \arctan 1/\sqrt{k}$),

the probability of the k photon component $|k\rangle$ appearing in the output state $|\phi\rangle_1'^{\text{un-norm}}$ is zero. In other words, the k photon term is filtered out after the FSF. Comparing Eq. (1.39) with Eq. (1.37), one can see that the amplitudes of the other components are modulated by

$$\cos^{n+1}\theta\left(1-n\tan^2\theta\right)=\left(\frac{k}{k+1}\right)^{\frac{n+1}{2}}\left(1-\frac{n}{k}\right). \tag{1.40}$$

It should be noted that the FSF functions by multi-photon interference. It can be regarded as a generalization of the HOM effect, which corresponds to the case of $k=1$.

1.5. Measurement methods: pre-selection and post-selection

In this section, two general types of measurements commonly considered in the studies of QIP are introduced: pre-selection and post-selection. QIP schemes based on pre-selection usually involve the explicit generation of the required quantum state, while those associated with post-selection do not separate the required state from the undesired components until the final detection stage, since all current measurement techniques are destructive. Concretely, for multiple phase estimation with the NOON state, the pre-selection scheme usually exploits the fixed-photon-number states, such as Fock states, as the light sources (by triggering certain heralded modes), extracts the NOON components from the photon sources explicitly, and uses it to probe the target. That is, the NOON state is formed before interacting with the target. On the other hand, the post-selection approach exploits nondeterministic-photon-number

states–such as coherent states and squeezed states–as the photon sources, and only the information carried by the functional NOON components are post-selected after the quantum state is used to probe a target, with both the NOON and non-NOON components present in the quantum state during the interaction with the target.

Pre-selection may be preferred for various reasons. One reason is that the number of photons actually interacting with the target is exact as that of the photons needed to be measured afterwards, if it can be exploited efficiently. In practice, post-selection is more commonly utilized in QIP experiments since it is more feasible to produce and manipulate nondeterministic-photon-number states. Both approaches are deemed effective when they can accomplish the same QIP task. In the following discussion, the post-selection approach is regarded to be as effective as pre-selection in generating the multi-mode NOON state.

Chapter 2: Applications of NOON states in quantum metrology and quantum imaging

Before introducing the proposed generation approaches for multi-mode NOON states, the advantages of NOON states in quantum metrology will be discussed in this chapter.

Quantum metrology aims at studying the ultimate measurement precision of physical parameters, and this precision is limited by quantum theory [28, 69]. In the case of quantum phase estimation in imaging, a target can be characterized by the phase shifts in light when the light passes through the object (known as the phase object). The phase imaging is assumed in Chapters 3 and 4. In this case, the performance of the measurement and estimation is reflected by two factors–resolution and sensitivity–and these factors depend on the properties of the probing states, the interaction of the states with the target, and the strategy of measurement. Resolution involves the ability to distinguish two different pixels of the object, while sensitivity denotes the signal-to-noise ratio of a single pixel. Compared to classical imaging, measurements using quantum light (the NOON state in this dissertation) can enhance the ultimate measurement precision, and hence obtain super-resolution and super-sensitivity.

On account of the diffraction of light, the resolution achieved with classical light

is limited by the wavelength λ of the light; this limitation is called the Rayleigh-Abbe diffraction limit [70]. When the quantum property entanglement of the NOON state is introduced into the system, super-resolving measurements can be attained, and the resolution can reach the de Broglie resolution λ/N, where N is the mean photon number of the illumination light source. The N times resolution enhancement is essential in quantum optics, which has been demonstrated in many studies [22,24–26].

The measurement sensitivity is bounded by the quantum Cramér-Rao bound (QCRB) [69, 71], which sets the lower bound of the estimation uncertainty with any possible measurement strategy, and it is denoted using the measurement variance in this dissertation. It is visualized as the visibility of interference fringes in experiments. In virtue of the discreteness of photons, there are always fluctuations in determining the photon counts at the detectors, which leads to the fact that the uncertainty of estimation can never reach zero. Nevertheless, it is of great importance to look for an optimal measurement that can minimize the uncertainty in quantum estimation theory. It has been proved that, when using classical light sources, the uncertainty (noise variance) is bounded by the standard quantum limit (SQL) of precision with a scaling of $1/N$. On the other hand, when taking quantum properties such as entanglement and squeezing into consideration, one can beat the SQL and approach the Heisenberg limit (HL) with a scaling of $1/N^2$, which has an N times benefit over its classical counterpart. Extensive theoretical and experimental work has been conducted to show the super-sensitivity of the single phase estimation problem, especially with the two-mode NOON state [27, 72]. Practically, the current understanding of super-sensitive quantum measurements has been applied to applications of differ-

ent kinds, such as quantum microscopy, material characterization, etc. Recently, the improved efficiency of measuring multiple phases simultaneously using multi-mode entangled states compared to the independent estimation of multiple parameters has been reported [45, 55].

2.1. Super-resolving measurements using two-mode NOON states

In this section, two techniques of achieving super-resolution are discussed: the traditional quantum lithography method and the optical centroid measurement method.

2.1.1 The quantum lithography scheme

Quantum lithography (QL) has been studied as an approach for achieving super-resolution in quantum imaging, by exploiting quantum properties, including entanglement [3, 22, 73, 74]. It makes usage of quantum entangled states as the illuminating sources, and adopts either multi-photon absorption or coincidence detection to measure out the N-photon events with all of the N photons appearing at one single mode, in order to extract the information carried by the NOON state components.

One experimental demonstration of the two-mode NOON state with up to 3 photons in constructing super-resolving measurements [22] is shown as an example in this section. The experimental setup of NOON state generation is shown in Fig. 2.1(a). For the 3-photon scenario, the authors produced an HV-polarized NOON state by manipulating the polarizations of 3 single photons. This was experimentally implemented by combining two single photons (down-converted photons) coming from down-conversion with horizontal (H) and vertical (V) polarizations on

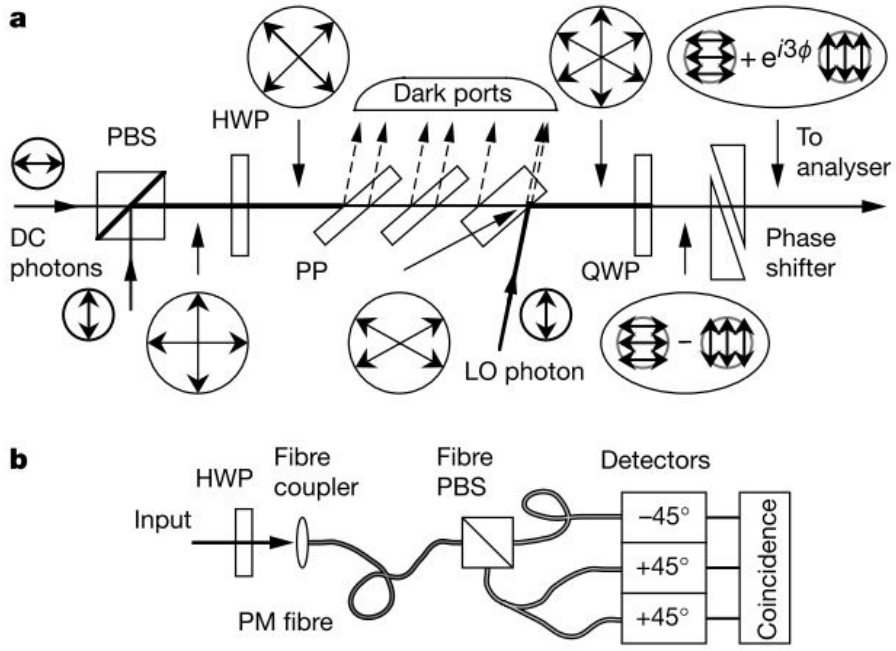

Figure 2.1. Production and detection of a 3-photon NOON state [22]. (a) The experimental generation setup of the 3-photon NOON state. (b) The measurement analyser for $|2,1\rangle_{\pm 45^\circ}$. HWP: half-wave plate. PP: partial polarizer. QWP: quarter-wave plate. PM fibre: polarization-maintaining fibre.

an HV-polarized PBS. Then the two photons pass through a half wave plate (HWP), and a partial polarizer (PP) performed by Brewster-angle interfaces which transmit H-polarized photons with transmissivity 1 and transmit V-polarized photons with transmissivity 1/3, followed by the selection of no photon detected at the reflected beam. The state evolves as follows:

$$\begin{aligned} a_H^\dagger a_V^\dagger |0\rangle &\xrightarrow{\text{HWP}} \left(a_H^\dagger + a_V^\dagger\right)\left(a_H^\dagger - a_V^\dagger\right)|0\rangle \\ &\xrightarrow{\text{PP}} \left(a_H^\dagger + \frac{1}{\sqrt{3}}a_V^\dagger\right)\left(a_H^\dagger - \frac{1}{\sqrt{3}}a_V^\dagger\right)|0\rangle = a_{60^\circ}^\dagger a_{-60^\circ}^\dagger |0\rangle. \end{aligned} \tag{2.1}$$

Afterwards, another polarizer is adopted to combine a third H-polarized photon coming from the local-oscillator with the state above, developing a 3-photon NOON state

entangled in the left and right circular polarizations and followed by a quarter-wave plate (QWP) to transform the left/right circular polarizations to linear HV polarizations:

$$a^{\dagger}_{0^\circ} a^{\dagger}_{60^\circ} a^{\dagger}_{-60^\circ} |0\rangle \xrightarrow{\text{basis change}} |3,0\rangle_{LR} - |0,3\rangle_{LR} \xrightarrow{\text{QWP}} |3,0\rangle_{HV} - |0,3\rangle_{HV}. \tag{2.2}$$

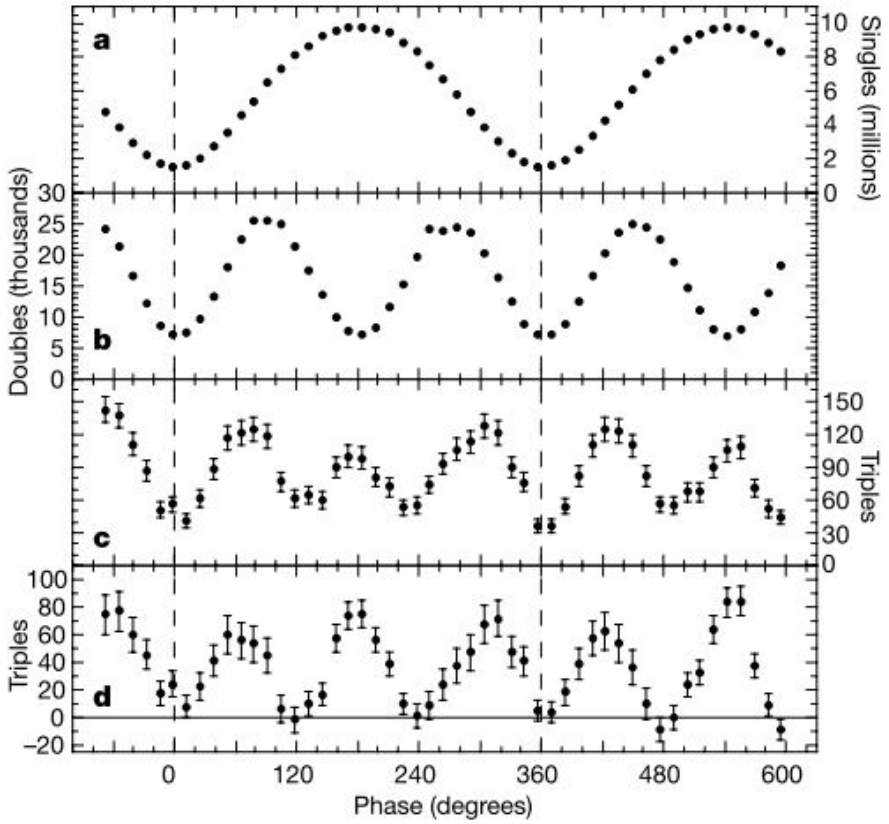

Figure 2.2. Super-resolving phase measurement [22] with (a) single detections of $|0,1\rangle_{\pm 45^\circ}$, (b) 2-fold coincidence detections of $|1,1\rangle_{\pm 45^\circ}$, (c) 3-fold coincidence detections of $|2,1\rangle_{\pm 45^\circ}$, and (d) 3-fold coincidence detections of $|2,1\rangle_{\pm 45^\circ}$ after the background subtraction.

In order to measure the NOON state generated above, Fig. 2.1(b) gives an example of measuring one of the NOON possibilities in $\pm 45^\circ$ bases when the phase parameter ϕ is added in the vertical mode. The measurement results with detected

photon number $N = 1, 2, 3$ are plotted in Fig. 2.2, where Fig. 2.2(a), Fig. 2.2(b), Fig. 2.2(c), and Fig. 2.2(d) correspond to the measurement using single detections of $|0,1\rangle_{\pm 45^\circ}$, 2-fold SPCD of $|1,1\rangle_{\pm 45^\circ}$, 3-fold SPCD of $|2,1\rangle_{\pm 45^\circ}$ and 3-fold SPCD of $|2,1\rangle_{\pm 45^\circ}$ after background subtraction of photons coming from unexpected down-converted or local oscillator, respectively.These plots illustrate that the wavelength of the phase measurement resulting from 3-fold SPCD is 1/3 times the wavelength with single photon detection. In other words, when using the produced 3-photon NOON state for phase estimation, the input 405-nm photons stimulate phase oscillation three times faster than when using single photons only. This corresponds to the 3 times the enhanced resolution, in theory. This demonstration of super-resolution over single infrared photons is encouraging, especially for imaging of light-sensitive targets, where high-intensity light or short-wavelength light may potentially be destructive to samples.

2.1.2 The optical centroid measurement scheme

The traditional QL procedure requires N-photon absorbers or N-fold coincidence detection in order to measure out the NOON components. The efficiency using this procedure is limited by the low multi-photon detection rate and the experimental infeasibility, especially for large N. With this in mind, Tsang proposed the use of optical centroid measurements (OCM) to supplant multi-photon absorption or coincidence detection. The resolution achieved using this OCM scheme can also beat the Rayleigh diffraction limit [24]. This OCM scheme uses all of the N-photon events (both NOON and non-NOON) measured by the optical intensity measurements, re-

gardless of the N-photon distribution, and this greatly improved the efficiency. Later, in 2011, Shin and colleagues reported a proof of principle experiment to demonstrate the enhanced resolution using the OCM scheme with 2 photons, and they proposed an improvement over OCM that involved the use of the photon-number-resolving (PNR) detectors [25]. In 2014, Rozema et al. further verified the phenomenon for 2-, 3-, and 4-photon scenarios [26].

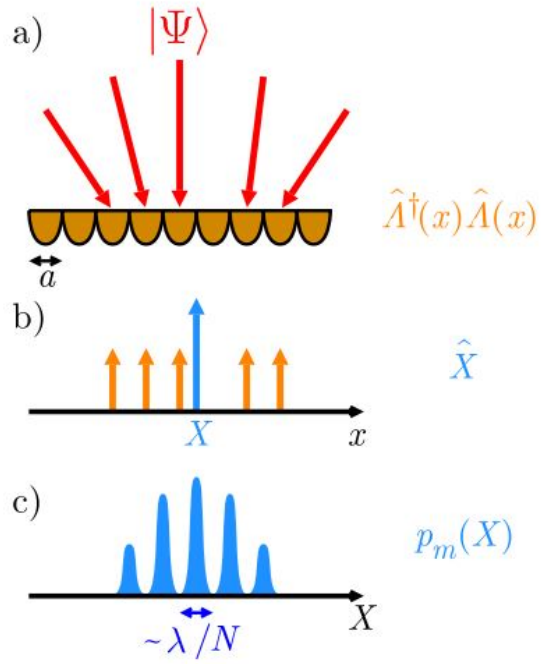

Figure 2.3. Optical centroid measurements [24]. (a) For the input state $|\Psi\rangle$, a spatially resolving intensity measurement $\hat{A}^\dagger(x)\hat{A}(x)$ is made using the photon counting detection array. (b) The centroid X is calculated from the measured intensity pattern. (c) The intensity marginal centroid distribution $p_m(x)$ can be obtained by repeating the measurements on X.

The OCM measurement scheme is sketched in Fig. 2.3, which consists of, respectively, (a) the spatially intensity measurement, (b) the calculated centroid from the measured intensity pattern, and (c) the intensity centroid distribution after repeated measurements. Instead of measuring the events with all N photons in the same mode

using multiple N-photon absorbers, OCM makes usage of a photon counting detector array, such that any N-photon event with any photon number distribution over the sensor array carrying the image information is measured by spatially resolving intensity measurements $\hat{A}^{\dagger}(x)\hat{A}(x)$, which can be denoted using the measurement operator $\Pi\left(x_1,\cdots,x_n\right)=|x_1,\cdots,x_n\rangle\langle x_1,\cdots,x_n|$ where x_i $(i=1,\cdots,n)$ is the intensity in pixel mode i and $\sum_{i=1}^{n}x_i=N$. The intensity centroid position is then calculated as $X=\frac{1}{N}\sum_{i=1}^{n}ix_i$, where each detection corresponds to an N-photon absorber registration at one mode, as in the traditional QL scheme. Eventually, the intensity marginal centroid distribution $p_m(x)$ can be obtained by repeating the measurements on X. As a result, more events are taken into account in OCM, which fundamentally guarantees the method's higher efficiency.

Note that the size of each pixel on the detection array is chosen to be small enough, such that the probability of more than one photon falling on the same pixel is much smaller than the probability of only one or zero photons. Under this assumption, single photon detectors can be substituted for the photon counting detectors in the detection array. Defining the momentum for each photon as k_n $(n=1,2,\cdots,N)$, they are restricted by the Rayleigh-Abbe diffraction limit to a finite bandwidth as $|k_n|\leq 2\pi\sin\theta/\lambda$. Using the OCM scheme, one can calculate that the minimum feature size of the marginal intensity centroid distribution is limited by the bandwidth of the total momentum $|K|=\sum_{n=1}^{N}|k_n|\leq 2\pi N\sin\theta/\lambda$, which leads to the de Broglie resolution with scaling λ/N.

The OCM scheme Tsang proposed theoretically overcame the difficulty with the NOON state measurements, and it inspired further experimental demonstrations of

this phenomenon. Later, the 2-photon super-resolution obtained using the OCM scheme was verified by Shin et al. [25]. As stated in Tsang's paper, the pixel size should be small enough such that one can neglect the events with more than 2 photons appearing in the same mode. Nevertheless, it is a difficult condition to obtain in practice. To address this, Shin et al. proposed the use of high-efficiency PNR detectors [75, 76], which have the ability to distinguish between different photon number states. They experimentally created a 2-photon NOON state using BBO crystal, and conducted the measurements using three approaches: the traditional QL approach, OCM with a single photon detector array, and OCM with a PNR detector array. Despite the fact that all three approaches attained the same twofold increase in the resolution, the OCM using PNR detectors had the highest fringe visibility, and hence it is the most efficient scheme of all three, followed by OCM with single photon detectors and, lastly, the traditional QL approach.

Later in 2014, Rozema and colleagues demonstrated super-resolution with the NOON state using OCM with up to four photons [26], where the NOON state is generated by combining a coherent light beam with a squeezed vacuum state, as discussed in Section 3.5. Moreover, they compared NOON-state interference with classical super-resolution attained using classical light with the OCM scheme. Despite the fact that both schemes can reach the twofold resolution enhancement, as shown in Fig. 2.4(a) and (b), it is illustrated in Fig. 2.4(c) that the visibility achieved using the NOON state (red) is higher, more stable, and independent of the photon number N when $N = 2, 3, 4$, compared with the exponentially decreasing visibility of the classical counterpart (blue).

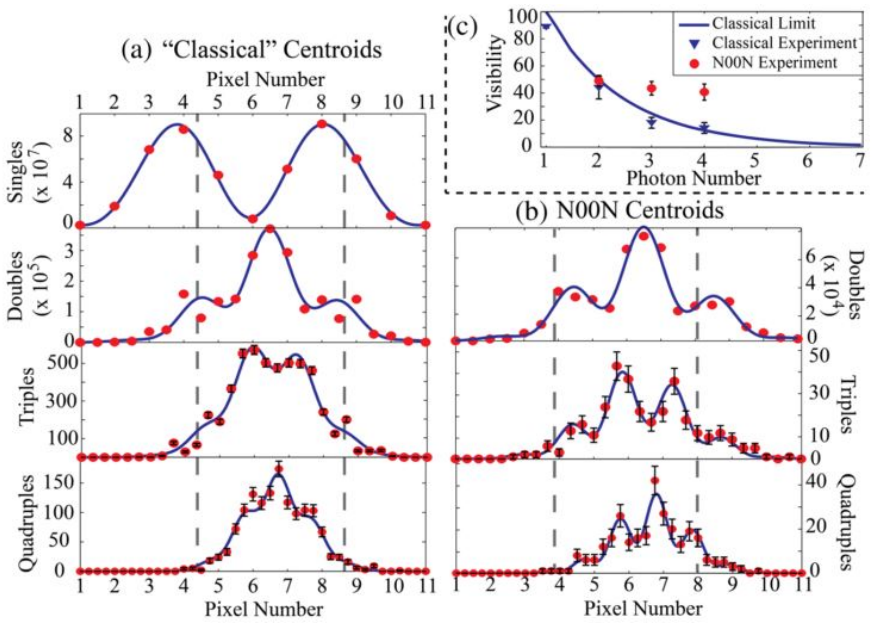

Figure 2.4. Plots of the centroid distributions with OCM using (a) classical light and (b) NOON states [26]. (c) A plot of visibility versus the photon number.

2.2. Super-sensitive imaging using NOON states

2.2.1 Single phase estimation using two-mode NOON states

In this section, the standard quantum limit and the Heisenberg limit are studied with regard to classical light sources [77] and two-mode NOON states, respectively.

The standard quantum limit

A Mach-Zehnder interferometer (MZI) is commonly utilized to measure and determine the relative phase shift between two modes. It has applications in high-precision spectroscopy [78] and optical interferometry [4, 79, 80]. The schematic setup is illustrated in Fig. 2.5. MZI has been applied in a wide range of fundamental studies on quantum entanglement, quantum computing, quantum cryptography and other

active research areas.

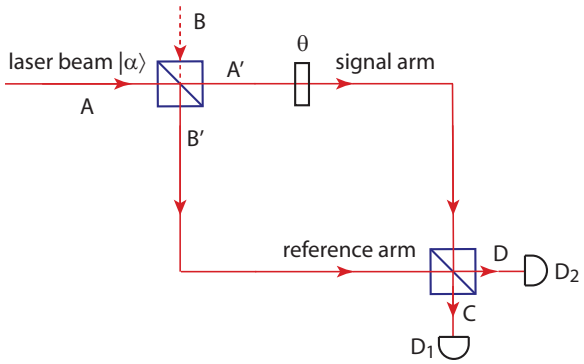

Figure 2.5. The schematic setup of Mach-Zehnder interferometer.

In classical optics, a laser beam, which is a coherent optical field, propagates into an interferometer with a phase difference θ between the signal arm and the reference arm. At the output end, θ is recovered by measuring the intensities of the two output pulses at D_1 and D_2, which are

$$n_C = \langle c^\dagger c \rangle = \frac{1-\cos\theta}{2} N, \;\; n_D = \langle d^\dagger d \rangle = \frac{1+\cos\theta}{2} N, \tag{2.3}$$

where $N = |\alpha|^2$ is the mean photon number of the input coherent state. Therefore, the information about the phase θ can be extracted from $\theta = \arccos\left((n_D - n_C)/N\right)$. The phase sensitivity is optimized at $\theta = (m+1/2)\pi$ with $m \in \mathcal{Z}$, since it maximizes the derivative of the photocurrent with a small change in θ. For small displacements around the optimal point, the phase shift θ is approximately

$$\theta = \frac{n_D - n_C}{N} - \frac{\pi}{2}. \tag{2.4}$$

Then the optimal variance of measuring θ is

$$\mathrm{Var}(\theta) = \frac{\mathrm{Var}(n_D) + \mathrm{Var}(n_C) - 2\mathrm{Cov}(n_D, n_C)}{N^2}. \tag{2.5}$$

When the optical field is stationary over time, the photon detection events are uncorrelated between the photo detectors; i.e., $\mathrm{Cov}(n_D, n_C) = 0$. The output states at modes C and D are still coherent states following the Poissonian distribution; i.e., $\mathrm{Var}(n_C) = n_C$ and $\mathrm{Var}(n_D) = n_D$. Therefore, when there is no loss in the system, the statistical variance of measuring the phase parameter θ is

$$|\delta\theta|^2_{\mathrm{SQL}} = \mathrm{Var}(\theta) = \frac{1}{N}, \tag{2.6}$$

which is the so-called standard quantum limit (SQL). The SQL sets a lowest bound of the measurement uncertainty one can approach using classical light sources only.

The Heisenberg limit

The SQL has been proved to be the best sensitivity achievable using pure classical sources, such as laser beams. However, in certain experimental applications, such as biomedical microscopy, where the target object is light-sensitive, high-intensity laser beams have the potential to damage the specimen. This leads to a reconsideration of the phase estimation problem in the photon scaling, taking advantage of the quantum entanglement and squeezing properties in order to achieve higher sensitivity with as few photons as possible. In the classical estimation theory, the uncertainty $|\delta\theta|^2$ of

estimating an unknown parameter θ is bounded by the Cramér-Rao inequality [81]:

$$|\delta\theta|^2 \geq \frac{1}{I(\theta)}, \tag{2.7}$$

with $I(\theta)$ the Fisher information defined as

$$I(\theta) = \int d\hat{\theta} \frac{1}{p(\hat{\theta}|\theta)} \left(\frac{\partial p(\hat{\theta}|\theta)}{\partial \theta} \right)^2, \tag{2.8}$$

in which $\hat{\theta}$ is the estimator of θ, and $p(\hat{\theta}|\theta)$ is the probability of obtaining the estimate $\hat{\theta}$ when the initial phase has the value θ. According to the Born rule, the probability is calculated as $p(\hat{\theta}|\theta) = \mathrm{Tr}(\rho_\theta \Pi_{\hat{\theta}})$, where ρ_θ is the density operator of the input state after interacting with phase θ and $\Pi_{\hat{\theta}}$ is the positive operator-valued measure (POVM) satisfying identity $\int d\hat{\theta} \Pi_{\hat{\theta}} = I$ that can always give a non-negative estimation probability.

To calulate the optimal sensitivity in the quantum picture, the symmetric logarithmic derivative (SLD) L_θ is introduced as a mathematical tool. It is defined as

$$\frac{L_\theta \rho_\theta + \rho_\theta L_\theta}{2} = \frac{\partial \rho_\theta}{\partial \theta}, \tag{2.9}$$

with $\partial\theta$ denoting the partial derivative with respect to θ. Substituting Eq. (2.9) into

Eq. (2.8), one can find the upper bound for the Fisher information:

$$
\begin{aligned}
I(\theta) &= \int d\hat{\theta} \frac{\mathrm{Re}(\mathrm{Tr}(\rho_\theta \Pi_{\hat{\theta}} L_\theta))^2}{\mathrm{Tr}(\rho_\theta \Pi_{\hat{\theta}})} \\
&\leq \int d\hat{\theta} \left| \frac{\mathrm{Tr}(\rho_\theta \Pi_{\hat{\theta}} L_\theta)}{\sqrt{\mathrm{Tr}(\rho_\theta \Pi_{\hat{\theta}})}} \right|^2 \\
&= \int d\hat{\theta} \left| \mathrm{Tr} \left(\frac{\sqrt{\rho_\theta}}{\sqrt{\mathrm{Tr}(\rho_\theta \Pi_{\hat{\theta}})}} \Pi_{\hat{\theta}} L_\theta \sqrt{\rho_\theta} \right) \right|^2 \\
&\leq \int d\hat{\theta} \mathrm{Tr} \left(\frac{\sqrt{\rho_\theta}}{\sqrt{\mathrm{Tr}(\rho_\theta \Pi_{\hat{\theta}})}} \Pi_{\hat{\theta}} \frac{\sqrt{\rho_\theta}}{\sqrt{\mathrm{Tr}(\rho_\theta \Pi_{\hat{\theta}})}} \right) \mathrm{Tr} \left(\sqrt{\rho_\theta} L_\theta \Pi_{\hat{\theta}} L_\theta \sqrt{\rho_\theta} \right) \\
&= \int d\hat{\theta} 1 \cdot \mathrm{Tr} \left(\rho_\theta L_\theta \Pi_{\hat{\theta}} L_\theta \right) \\
&= \mathrm{Tr} \left(\rho_\theta L_\theta^2 \right),
\end{aligned}
\tag{2.10}
$$

where the second inequality comes from the Cauchy-Schwarz inequality. Therefore, in the quantum analogy, the Quantum Cramér-Rao inequality turns into

$$
|\delta\theta|^2 \geq \frac{1}{I(\theta)} \geq |\delta\theta|^2_{\mathrm{QCRB}} = \frac{1}{\mathrm{Tr} \left(\rho_\theta L_\theta^2 \right)}, \tag{2.11}
$$

where $|\delta\theta|^2_{\mathrm{QCRB}} = 1/\mathrm{Tr} \left(\rho_\theta L_\theta^2 \right)$ is so-called the quantum Cramér-Rao bound (QCRB). QCRB provides an ultimate bound on the uncertainty of precision, given any measurement system, although there are only specific measurements that can saturate this bound. The optimal measurement saturating the QCRB can always be obtained for single parameter estimation [71,82] and, recently, the necessary and sufficient conditions for optimal projective measurements acting on pure states are reported [83]. In addition, the optimal measurement depends on the choice of the metric. Another choice is to find the maximum-likelihood measurement that maximizes the likelihood

function. An example for the maximum-likelihood measurement of polarization of light is given in Appendix A.

When a two-mode NOON state $|\phi\rangle = 1/\sqrt{2}(|N0\rangle + |0N\rangle)_{A'B'}$ is probed, the state after passing the phase object in the signal arm can be written as $|\phi_\theta\rangle = 1/\sqrt{2}(\exp(iN\theta)|N0\rangle + |0N\rangle)$, where only the most common linear phase interaction is considered in this dissertation. Its SLD is simply calculated to be $L_\theta = 2(\partial|\phi_\theta\rangle\langle\phi_\theta| + |\phi_\theta\rangle\partial\langle\phi_\theta|)$ with $\partial|\phi_\theta\rangle = iN/\sqrt{2}\exp(iN\theta)|N0\rangle$. Then one can calculate

$$\langle\phi_\theta|\partial|\phi_\theta\rangle = \frac{iN}{2}, \text{ and } \partial\langle\phi_\theta|\partial|\phi_\theta\rangle = \frac{N^2}{2}, \tag{2.12}$$

Substituting $\rho_\theta = |\phi_\theta\rangle\langle\phi_\theta|$, L_θ and Eq. (2.12) into the $|\Delta\theta|^2_{\text{QCRB}}$ as in Eq. (2.11), one can calculate the lowest bound of the uncertainty

$$\begin{aligned}
|\delta\theta|^2_{\text{QCRB}} &= \frac{1}{\text{Tr}\,(\rho_\theta L_\theta^2)} = \frac{1}{4\text{Tr}\,(|\phi_\theta\rangle\langle\phi_\theta|(\partial|\phi_\theta\rangle\langle\phi_\theta| + |\phi_\theta\rangle\partial\langle\phi_\theta|)(\partial|\phi_\theta\rangle\langle\phi_\theta| + |\phi_\theta\rangle\partial\langle\phi_\theta|))} \\
&= \frac{1}{4\langle\phi_\theta|(\partial|\phi_\theta\rangle\langle\phi_\theta| + |\phi_\theta\rangle\partial\langle\phi_\theta|)(\partial|\phi_\theta\rangle\langle\phi_\theta| + |\phi_\theta\rangle\partial\langle\phi_\theta|)|\phi_\theta\rangle} \\
&= \frac{1}{4(\langle\phi_\theta|\partial|\phi_\theta\rangle\langle\phi_\theta|\partial|\phi_\theta\rangle + \langle\phi_\theta|\partial|\phi_\theta\rangle\partial\langle\phi_\theta|\phi_\theta\rangle + \partial\langle\phi_\theta|\partial|\phi_\theta\rangle + \partial\langle\phi_\theta|\phi_\theta\rangle\partial\langle\phi_\theta|\phi_\theta\rangle)} \\
&= \frac{1}{4(\frac{N^2}{2} + \frac{iN}{2}\frac{iN}{2})} = \frac{1}{N^2} = |\delta\theta|^2_{\text{HL}},
\end{aligned} \tag{2.13}$$

which is the so-called the Heisenberg limit. It has been proved that the NOON state can beat the standard quantum limit and reach the Heisenberg limit with an N times benefit, and hence it has the potential to achieve super-sensitivity in experiments. The super-sensitive measurements attained using NOON states have been experimentally

demonstrated with 4 photons in [29], and they have been verified in applications, such as optical coherence tomography of a biological sample [31], protein concentration sensing [32], and microscopy [35, 36].

2.2.2 Simultaneous multiple phase estimation using multi-mode NOON states [55]

Inspired by the single parameter estimation, there has recently been increased interest in simultaneous multi-phase estimation in view of the potential $O(d)$ improvement in estimation efficiency over the individual estimation of d phase shifts using d copies of two-mode NOON states [45]. Only the case in which each phase parameter corresponds to one spatial mode is investigated here since, when there are couplings among different parameters, it was found that quantum entanglement may not necessarily be advantageous [84, 85].

In this section, a class of multi-mode NOON-like states for multi-parameter quantum metrology in optical phase imaging is studied and the results were published in [55], in which the multi-mode NOON state is one specific case in that class. The analytical form of the QCRB attained using this class of state is calculated. In particular, the performances of four different quantum state scenarios are compared: multi-mode NOON states, entangled coherent states, entangled squeezed coherent states, and entangled squeezed vacuum states.

The model of the simultaneous multi-phase estimation following [45] is depicted in Fig. 2.6. The class of state studied here is a balanced $(d+1)$-mode NOON-like state, where the Fock state component $|N\rangle$ in the NOON state is substituted with a

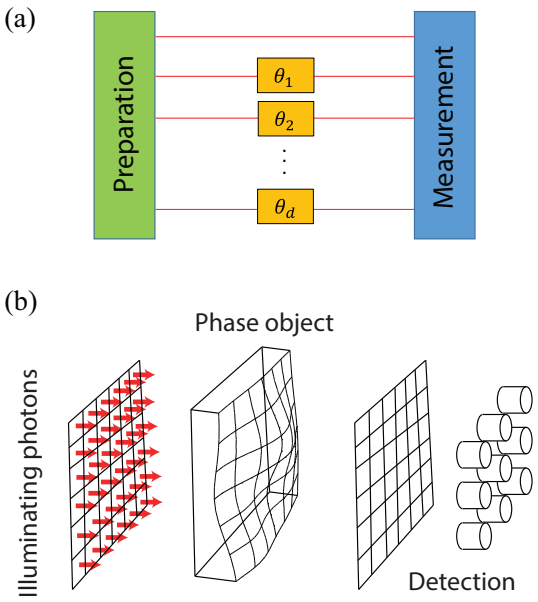

Figure 2.6. The model of the simultaneous multi-phase estimation [55]. (a) The schematic model of d-phase estimation. (b) The discretized phase imaging model.

state $|\psi\rangle$ with arbitrary photon statistics:

$$|\Psi\rangle = b \sum_{m=0}^{d} |0\rangle_0 |0\rangle_1 \cdots |\psi\rangle_m \cdots |0\rangle_d. \tag{2.14}$$

The normalization coefficient is given by

$$b = \frac{1}{\sqrt{d+1}\sqrt{1+d|\langle\psi|0\rangle|^2}} \tag{2.15}$$

where $|\langle\psi|0\rangle|^2$ could be nonzero. This is obtained from the identity property of a

quantum state $\langle\Psi|\Psi\rangle = 1$:

$$\begin{aligned}
1 = \langle\Psi|\Psi\rangle &= b^2\Big(\sum_{n=0}^{d}\langle 0|_0\langle 0|_1\cdots\langle\psi|_n\cdots\langle 0|_d\sum_{m=0}^{d}|0\rangle_0|0\rangle_1\cdots|\psi\rangle_m\cdots|0\rangle_d\Big) \\
&= b^2\Big(\sum_{n=m=0}^{d}\langle 0|_0\langle 0|_1\cdots\langle\psi|_m\cdots\langle 0|_d|0\rangle_0|0\rangle_1\cdots|\psi\rangle_m\cdots|0\rangle_d \\
&+ \sum_{n=0}^{d}\langle 0|_0\langle 0|_1\cdots\langle\psi|_n\cdots\langle 0|_d\sum_{m\neq n=0}^{d}|0\rangle_0|0\rangle_1\cdots|\psi\rangle_m\cdots|0\rangle_d\Big) \\
&= b^2\left((d+1)+(d+1)d\langle\psi|0\rangle\langle 0|\psi\rangle\right) = b^2(d+1)\left(1+d\langle|\psi|0\rangle|^2\right).
\end{aligned} \tag{2.16}$$

By convention, the $m = 0$ mode is chosen as the reference. The total mean photon number for this state is

$$\bar{n} \equiv \langle\Psi|\left(\sum_{m=0}^{d}a_m^\dagger a_m\right)|\Psi\rangle = \frac{\tilde{n}}{1+d\left|\langle\psi|0\rangle\right|^2}, \tag{2.17}$$

where $\tilde{n} = \langle\psi|a^\dagger a|\psi\rangle$ is the mean photon number for the single mode state $|\psi\rangle$. One can note that $\bar{n} \leq \tilde{n}$ is always true, which is owing to a finite probability of state $|\psi\rangle$ containing no photons. The equality is satisfied only when $|\langle\psi|0\rangle|^2 = 0$ as in the case, for example, of a NOON state. In practical sensing problems, $\bar{n}$ may be more meaningful than $\tilde{n}$ since it characterizes, on average, how many photons are used for the simultaneous parameter estimation.

The linear phase shift induced into the probing state is denoted as

$$U_{\boldsymbol{\theta}} = \exp\left(i\boldsymbol{\theta}\cdot\hat{\boldsymbol{H}}\right) = \exp\left(i\sum_{m=1}^{d}\theta_m\hat{H}_m\right) = \prod_{m=1}^{d}\exp\left(i\theta_m\hat{H}_m\right), \tag{2.18}$$

where $\boldsymbol{\theta} = (\theta_1, \theta_2..., \theta_d)$ represents d independent phases and $\hat{H}_m = a_m^\dagger a_m$ is the

photon number operator for the mode m. In writing Eq. (2.18), the assumption has been made that the reference mode has a phase set to zero, which can be practically realized by phase-locking the reference arm with some external reference [86]. The inclusion of the reference mode is to make the comparison with the multi-mode states reported in the previous works more explicit [45, 53]. The output state after the propagation process then reads as

$$\begin{aligned}|\Psi_{\boldsymbol{\theta}}\rangle = U_{\boldsymbol{\theta}}|\Psi\rangle &= \prod_{n=1}^{d} \exp\left(i\theta_n \hat{H}_n\right) b \sum_{m=0}^{d} |0\rangle_0 |0\rangle_1 \cdots |\psi\rangle_m \cdots |0\rangle_d \\ &= b \sum_{m=0}^{d} |0\rangle_0 \exp\left(i\theta_1 \hat{H}_1\right)|0\rangle_1 \cdots \exp\left(i\theta_m \hat{H}_m\right)|\psi\rangle_m \cdots \exp\left(i\theta_d \hat{H}_d\right)|0\rangle_d \\ &= b \sum_{m=0}^{d} |0\rangle_0 \cdots \exp\left(i\theta_m \hat{H}_m\right)|\psi\rangle_m \cdots |0\rangle_d.\end{aligned} \tag{2.19}$$

Given the probe state and the evolution operator, the QCRB can be calculated, which is inversely proportional to the quantum Fisher information:

$$|\delta\boldsymbol{\theta}|^2 \geq |\delta\boldsymbol{\theta}|^2_{\mathrm{QCRB}} = \mathrm{Tr}(I_{\boldsymbol{\theta}}^{-1}), \tag{2.20}$$

where $I_{\boldsymbol{\theta}}$ is the $d \times d$ quantum Fisher information matrix, which is calculated using the SLD in [87] as

$$[I_{\boldsymbol{\theta}}]_{l,m} = \frac{1}{2}\langle\Psi_{\boldsymbol{\theta}}|(L_l L_m + L_m L_l)|\Psi_{\boldsymbol{\theta}}\rangle. \tag{2.21}$$

The condition for the QCRB being saturated is $\mathrm{Im}\langle\Psi_{\boldsymbol{\theta}}|L_l L_m|\Psi_{\boldsymbol{\theta}}\rangle = 0$ [88], where $L_l = 2\left(|\partial_l\Psi_{\boldsymbol{\theta}}\rangle\langle\Psi_{\boldsymbol{\theta}}| + |\Psi_{\boldsymbol{\theta}}\rangle\langle\partial_l\Psi_{\boldsymbol{\theta}}|\right)$ is the symmetric logarithmic derivative over the

mode l. One can then calculate

$$\partial_l|\Psi_{\boldsymbol{\theta}}\rangle = ib|0\rangle_0 \cdots \hat{H}_l \exp\left(i\theta_l \hat{H}_l\right)|\psi\rangle_l \cdots |0\rangle_d, \tag{2.22}$$

$$\begin{aligned}
&\langle\Psi_{\boldsymbol{\theta}}|\partial_l|\Psi_{\boldsymbol{\theta}}\rangle \\
&= b \cdot ib \sum_{m=0}^{d} \langle 0|_0 \cdots \langle\psi|_m \exp\left(-i\theta_m \hat{H}_m\right) \cdots \langle 0|_d|0\rangle_0 \cdots \hat{H}_l \exp\left(i\theta_l \hat{H}_l\right)|\psi\rangle_l \cdots |0\rangle_d \\
&= ib^2 \langle 0|_1|0\rangle_1 \cdots \langle\psi|_l \exp\left(-i\theta_l \hat{H}_l\right) \hat{H}_l \exp\left(i\theta_l \hat{H}_l\right)|\psi\rangle_l \cdots \langle 0|_d|0\rangle_d \\
&= ib^2 \langle\psi|\hat{H}|\psi\rangle,
\end{aligned} \tag{2.23}$$

and

$$\begin{aligned}
&\partial_m\langle\Psi_{\boldsymbol{\theta}}|\partial_l|\Psi_{\boldsymbol{\theta}}\rangle \\
&= (-i)b \cdot ib \langle 0|_0 \cdots \langle\psi|_m \exp\left(-i\theta_m \hat{H}_m\right) \hat{H}_m \cdots \langle 0|_d ib|0\rangle_0 \cdots \hat{H}_l \exp\left(i\theta_l \hat{H}_l\right)|\psi\rangle_l \cdots |0\rangle_d \\
&= b^2 \delta_{lm} \langle 0|_0 \cdots \langle\psi|_m \exp\left(-i\theta_m \hat{H}_m\right) \hat{H}_m \cdots \langle 0|_d|0\rangle_0 \cdots \hat{H}_l \exp\left(i\theta_l \hat{H}_l\right)|\psi\rangle_l \cdots |0\rangle_d \\
&= b^2 \delta_{lm} \langle 0|_0|0\rangle_0 \cdots \langle\psi|_l \exp\left(-i\theta_l \hat{H}_l\right) \hat{H}_l \hat{H}_l \exp\left(i\theta_l \hat{H}_l\right)|\psi\rangle_l \cdots \langle 0|_d|0\rangle_d \\
&= b^2 \delta_{lm} \langle\psi|\hat{H}^2|\psi\rangle.
\end{aligned} \tag{2.24}$$

From Eqs. (2.23) and (2.24), one can see $\mathrm{Re}\left(\langle\Psi_{\boldsymbol{\theta}}|\partial_l\Psi_{\boldsymbol{\theta}}\rangle\right) = 0$ and $\mathrm{Im}\left(\langle\partial_m\Psi_{\boldsymbol{\theta}}|\partial_l\Psi_{\boldsymbol{\theta}}\rangle\right) =$

0, which leads to the saturation condition

$$
\begin{aligned}
&\mathrm{Im}\langle\Psi_{\boldsymbol{\theta}}|L_l L_m|\Psi_{\boldsymbol{\theta}}\rangle \\
&= 4\mathrm{Im}\langle\Psi_{\boldsymbol{\theta}}|\left(|\partial_l\Psi_{\boldsymbol{\theta}}\rangle\langle\Psi_{\boldsymbol{\theta}}| + |\Psi_{\boldsymbol{\theta}}\rangle\partial_l\langle\Psi_{\boldsymbol{\theta}}|\right)\left(|\partial_m\Psi_{\boldsymbol{\theta}}\rangle\langle\Psi_{\boldsymbol{\theta}}| + |\Psi_{\boldsymbol{\theta}}\rangle\partial_m\langle\Psi_{\boldsymbol{\theta}}|\right)|\Psi_{\boldsymbol{\theta}}\rangle \\
&= 4\mathrm{Im}\left(\langle\Psi_{\boldsymbol{\theta}}|\partial_l|\Psi_{\boldsymbol{\theta}}\rangle\langle\Psi_{\boldsymbol{\theta}}| + \partial_l\langle\Psi_{\boldsymbol{\theta}}|\right)\left(\partial_m|\Psi_{\boldsymbol{\theta}}\rangle + |\Psi_{\boldsymbol{\theta}}\rangle\partial_m\langle\Psi_{\boldsymbol{\theta}}|\Psi_{\boldsymbol{\theta}}\rangle\right) \\
&= 4\mathrm{Im}\big(\langle\Psi_{\boldsymbol{\theta}}|\partial_l|\Psi_{\boldsymbol{\theta}}\rangle(\langle\Psi_{\boldsymbol{\theta}}|\partial_m|\Psi_{\boldsymbol{\theta}}\rangle + \partial_m\langle\Psi_{\boldsymbol{\theta}}|\Psi_{\boldsymbol{\theta}}\rangle) + \partial_l\langle\Psi_{\boldsymbol{\theta}}|\partial_m|\Psi_{\boldsymbol{\theta}}\rangle \\
&\quad + \partial_l\langle\Psi_{\boldsymbol{\theta}}|\Psi_{\boldsymbol{\theta}}\rangle\partial_m\langle\Psi_{\boldsymbol{\theta}}|\Psi_{\boldsymbol{\theta}}\rangle\big) \\
&= 4\mathrm{Im}\big(0 + b^2\delta_{lm}\langle\psi|\hat{H}^2|\psi\rangle + (-i)b^2\langle\psi|\hat{H}|\psi\rangle(-i)b^2\langle\psi|\hat{H}|\psi\rangle\big) \\
&= 4\mathrm{Im}\big(b^2\delta_{lm}\langle\psi|\hat{H}^2|\psi\rangle - b^4\langle\psi|\hat{H}|\psi\rangle^2\big) = 0
\end{aligned}
\tag{2.25}
$$

is always true for the entangled state considered here. Eventually the (l, m) element in the quantum Fisher information matrix can be calculated as

$$
\begin{aligned}
&[I_{\boldsymbol{\theta}}]_{l,m} = \frac{1}{2}\langle\Psi_{\boldsymbol{\theta}}|(L_l L_m + L_m L_l)|\Psi_{\boldsymbol{\theta}}\rangle \\
&= 2\left(b^2\delta_{lm}\langle\psi|\hat{H}^2|\psi\rangle - b^4\langle\psi|\hat{H}|\psi\rangle\langle\psi|\hat{H}|\psi\rangle + b^2\delta_{lm}\langle\psi|\hat{H}^2|\psi\rangle - b^4\langle\psi|\hat{H}|\psi\rangle\langle\psi|\hat{H}|\psi\rangle\right) \\
&= \left(4b^2\delta_{lm}\langle\psi|\hat{H}^2|\psi\rangle - 4b^4\langle\psi|\hat{H}|\psi\rangle^2\right),
\end{aligned}
\tag{2.26}
$$

which leads to the quantum Fisher information matrix

$$
I_{\boldsymbol{\theta}} = 4b^2\langle\hat{H}^2\rangle I - 4b^4\langle\hat{H}\rangle^2 O, \tag{2.27}
$$

where $\langle ...\rangle$ denotes $\langle\psi|...|\psi\rangle$ with the mode number index m in $\hat{H}$ omitted for simplicity, and I and O respectively represent the $d \times d$ identity matrix and the matrix

with all elements equal to 1. Using a mathematical tool for calculating the inverse of a matrix:

$$((p-q)I + qO)^{-1} = \frac{-q}{(p-q)(dq+p-q)}O + \frac{1}{p-q}I, \tag{2.28}$$

one can obtain the inverse of Eq. (2.27) by substituting $p = 4b^2\langle\hat{H}^2\rangle - 4b^4\langle\hat{H}\rangle^2$ and $q = -4b^4\langle\hat{H}\rangle^2$ into Eq. (2.28):

$$\begin{aligned}(I_{\boldsymbol{\theta}})^{-1} &= \frac{4b^4\langle\hat{H}\rangle^2}{4b^2\langle\hat{H}^2\rangle(-d4b^4\langle\hat{H}\rangle^2 + 4b^2\langle\hat{H}^2\rangle)}O + \frac{1}{4b^2\langle\hat{H}^2\rangle}I \\ &= \frac{\langle\hat{H}\rangle^2}{4\langle\hat{H}^2\rangle(\langle\hat{H}^2\rangle - db^2\langle\hat{H}\rangle^2)}O + \frac{1}{4b^2\langle\hat{H}^2\rangle}I.\end{aligned} \tag{2.29}$$

Finally, the expression of the quantum Cramér-Rao lower bound is obtained:

$$|\delta\boldsymbol{\theta}|^2_{\mathrm{QCRB}} = \mathrm{Tr}(I_{\boldsymbol{\theta}}^{-1}) = \frac{d}{4\langle\hat{H}^2\rangle}\left(\frac{1}{b^2} + \frac{1}{R-b^2d}\right), \tag{2.30}$$

with $R \equiv \langle\hat{H}^2\rangle/\langle\hat{H}\rangle^2$, which gives a lower bound of the total variance of measuring d phase parameters simultaneously.

Equation (2.30) gives the analytical form of the QCRB for any quantum probe with the form, as in Eq. (2.14). It should be noted that $|\delta\boldsymbol{\theta}|^2_{\mathrm{QCRB}}$ is strictly positive here, for if it were zero, the required condition would be

$$R = (d-1)b^2 = \left(\frac{d-1}{d+1}\right)\frac{1}{1+d|\langle\psi|0\rangle|^2} < 1, \tag{2.31}$$

which contradicts the nonnegativity of the variance $\langle\hat{H}^2\rangle - \langle\hat{H}\rangle^2$.

Specifically, four input scenarios are compared in the following under the assump-

tion that all input states are available: the multi-mode NOON state $|\Psi\rangle_N$ [45], the entangled coherent state (ECS) $|\Psi\rangle_{\rm c}$, the entangled squeezed vacuum state (ESVS) $|\Psi\rangle_{\rm sv}$, and the entangled squeezed coherent state (ESCS) $|\Psi\rangle_{\rm sc}$ [89]:

$$\begin{aligned}
|\Psi\rangle_N &= b_N \sum_{m=0}^{d} |0\rangle_0 |0\rangle_1 \cdots |N\rangle_m \cdots |0\rangle_d, \\
|\Psi\rangle_{\rm c} &= b_{\rm c} \sum_{m=0}^{d} |0\rangle_0 |0\rangle_1 \cdots |\alpha\rangle_m \cdots |0\rangle_d, \\
|\Psi\rangle_{\rm sv} &= b_{\rm sv} \sum_{m=0}^{d} |0\rangle_0 |0\rangle_1 \cdots |r\rangle_m \cdots |0\rangle_d, \\
|\Psi\rangle_{\rm sc} &= b_{\rm sc} \sum_{m=0}^{d} |0\rangle_0 |0\rangle_1 \cdots |\alpha', r'\rangle_m \cdots |0\rangle_d.
\end{aligned} \tag{2.32}$$

Note that the two-mode ESVS has been reported in [90,91]. Without loss of generality, the amplitudes α and α' and the squeeze factors r and r' are assumed to be real numbers. The mean photon numbers for the balanced multi-mode entangled states above are

$$\begin{aligned}
\bar{n}_N &= \tilde{n}_N = N, \\
\bar{n}_{\rm c} &= \frac{\tilde{n}_{\rm c}}{1 + d e^{-\alpha^2}} = \frac{\alpha^2}{1 + d e^{-\alpha^2}}, \\
\bar{n}_{\rm sv} &= \frac{\tilde{n}_{\rm sv}}{1 + d/\cosh r} = \frac{\sinh^2 r}{1 + d/\cosh r}, \\
\bar{n}_{\rm sc} &= \frac{\tilde{n}_{\rm sc}}{1 + d e^{-\alpha'^2(1-\tanh r')}/\cosh r'} = \frac{\alpha'^2 + \sinh^2 r'}{1 + d e^{-\alpha'^2(1-\tanh r')}/\cosh r'},
\end{aligned} \tag{2.33}$$

.

For the balanced multi-mode NOON state, its total minimum uncertainty takes a

simple form:

$$|\delta\boldsymbol{\theta}|_N^2 = \frac{d(d+1)}{2\bar{n}_N^2} = \frac{d(d+1)}{2\tilde{n}_N^2} = \frac{d(d+1)}{2N^2}, \tag{2.34}$$

calculated using $b_N = 1/\sqrt{d+1}$, $R_N = 1$ and Eq. (2.30), where the number of phases d and the photon number N are independent parameters. This bound when using the multi-mode NOON state is in the scaling of the Heisenberg limit with $O(1/N^2)$, and in the scaling of $O(d^2)$ with respect to the mode number d. On the other hand, under the same footing of the N-photon source, if d two-mode NOON states with N/d photons in each state are used to measure d parameters individually, the lowest uncertainty for each phase measurement is in the scaling of d^2/N^2. The total variance is then $|\delta\boldsymbol{\theta}|_{\text{ind}}^2 = d^3/N^2$. The simultaneous estimation of d phases then has an $O(d)$ advantage over the bound for individual estimation with the scaling $O(d^3)$ and hence the former is more efficient [45].

To compare the QCRB with respect to different quantum probes, the mean total photon number $\bar{n}$ given by Eq. (2.17) was chosen as the common footing. With this condition, Eq. (2.30) can be rewritten as a function of a defined factor $f \equiv \langle\hat{H}\rangle/\langle\hat{H}^2\rangle$:

$$|\delta\boldsymbol{\theta}|_{\text{QCRB}}^2 = \frac{d(d+1)}{4} f \left(\frac{1}{\bar{n}} + \frac{1}{\frac{(d+1)}{f} - d\bar{n}} \right). \tag{2.35}$$

It is noted that f is related solely to the expectations with respect to the single mode state $|\psi\rangle$, whereas d and $\bar{n}$ are the features of the entire multi-mode state $|\Psi\rangle$. When d and $\bar{n}$ are fixed, $|\delta\boldsymbol{\theta}|_{\text{QCRB}}^2$ is a monotonic increasing function of f. Due to the variance $(\langle\hat{H}^2\rangle - \langle\hat{H}\rangle^2) \geq 0$, one can get $0 \leq f \leq 1/\bar{n}$, where the upper bound is

derived as below:

$$f = \frac{\langle \hat{H} \rangle}{\langle \hat{H}^2 \rangle} \leq \frac{\langle \hat{H} \rangle}{\langle \hat{H} \rangle^2} = \frac{1}{\tilde{n}} = \frac{1}{\bar{n}(1 + d|\langle \psi|0 \rangle|^2)} \leq \frac{1}{\bar{n}}. \tag{2.36}$$

The upper bound is saturated when $\langle \hat{H}^2 \rangle = \langle \hat{H} \rangle^2$ and $|\langle \psi|0 \rangle|^2 = 0$, i.e., the NOON state, which leads to

$$|\delta \boldsymbol{\theta}|^2_{\mathrm{QCRB}} \leq \frac{d(d+1)}{2\bar{n}^2}. \tag{2.37}$$

This means that any entangled state $|\Psi\rangle$ in this class with $\langle \hat{H}^2 \rangle > \langle \hat{H} \rangle^2$ can achieve a lower estimation uncertainty than the NOON state with the same mean photon number (i.e., $|\delta \boldsymbol{\theta}|^2_{\mathrm{QCRB}} \leq |\delta \boldsymbol{\theta}|^2_N$).

In order to compare the QCRB among the four scenarios, their corresponding f factors are calculated:

$$\begin{aligned} &f_N = \frac{1}{\tilde{n}_N}, \quad f_{\mathrm{c}} = \frac{1}{\tilde{n}_{\mathrm{c}} + 1}, \quad f_{\mathrm{sc}} = \left(\tilde{n}_{\mathrm{sc}} + \frac{\alpha'^2 e^{2r'} + 2\sinh^2 r' \cosh^2 r'}{\alpha'^2 + \sinh^2 r'} \right)^{-1}, \\ &f_{\mathrm{sv}} = \frac{1}{\tilde{n}_{\mathrm{sv}} + 2\cosh^2 r}. \end{aligned} \tag{2.38}$$

When the mean total photon numbers are fixed (i.e., $\bar{n}_N = \bar{n}_{\mathrm{c}} = \bar{n}_{\mathrm{sc}} = \bar{n}_{\mathrm{sv}}$), the following equation sets have no solutions:

$$\begin{cases} \alpha^2 \geq \alpha'^2 + \sinh^2 r' \\ e^{-\alpha^2} \geq e^{-\alpha'^2(1-\tanh r')} / \cosh r' \end{cases} \tag{2.39}$$

$$\begin{cases} \alpha'^2 + \sinh^2 r' \geq \sinh^2 r \\ e^{-\alpha'^2(1-\tanh r')} / \cosh r' \geq 1/\cosh r \end{cases} \tag{2.40}$$

which prove that $\alpha^2 < \alpha'^2 + \sinh^2 r' < \sinh^2 r$, equivalent to

$$\tilde{n}_N < \tilde{n}_{\rm c} < \tilde{n}_{\rm sc} < \tilde{n}_{\rm sv}. \tag{2.41}$$

Under the conditions as in Eq. (2.41), one can obtain

$$1 < \frac{\alpha'^2 e^{2r'} + 2\sinh^2 r' \cosh^2 r'}{\alpha'^2 + \sinh^2 r'} < 2\cosh^2 r, \tag{2.42}$$

since $e^{2r'} > 1$ and $\cosh^2 r' > 1$. Using Eq. (2.41) and Eq. (2.42), it is easy to derive the inequalities $f_N > f_{\rm c} > f_{\rm sc} > f_{\rm sv}$, which leads to the relations of the QCRB for the four specific cases as

$$|\delta\boldsymbol{\theta}|_N^2 > |\delta\boldsymbol{\theta}|_{\rm c}^2 > |\delta\boldsymbol{\theta}|_{\rm sc}^2 > |\delta\boldsymbol{\theta}|_{\rm sv}^2. \tag{2.43}$$

The entangled squeezed vacuum state has the lowest uncertainty, followed by the entangled squeezed coherent state, the entangled coherent state, and the NOON state. This suggests that with the same number of photons, the entangled squeezed vacuum state can reach the highest sensitivity in quantum metrology.

To illustrate the inequality in Eq. (2.43) explicitly and more exactly, the QCRB for the four scenarios with respect to the mean total photon number $\bar{n}$ under the condition of $d = 5$ phases are plotted in Fig. 2.7. Since the mean photon number

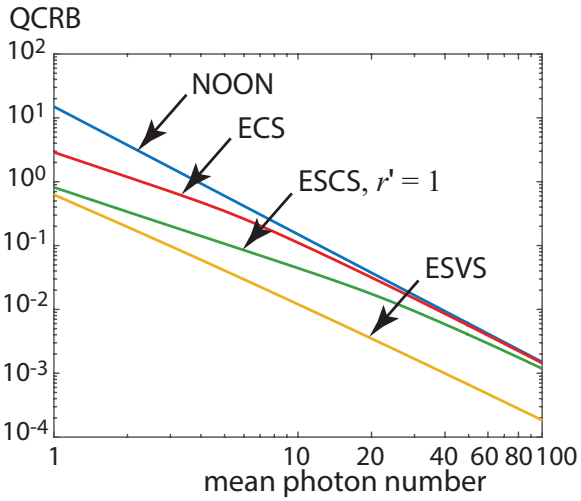

Figure 2.7. Plots of the QCRB [55] for the NOON state (blue), the ECS (red), the ESCS with $r' = 1$ (green), and the ESVS (yellow) with respect to the mean photon number $\bar{n}$ using Eqs. (2.35) and (2.38). The number of phases is taken to be 5. For the NOON state, the discrete points are interpolated to provide a better visualization.

of the squeezed coherent state depends on both α' and r', its squeeze factor $r' = 1$ is fixed for proper comparison. Note that Fig. 2.7 confirms the observation in the previous paragraph. Moreover, the ESVS QCRB is an order of magnitude smaller than the NOON QCRB for a wide range of the mean photon number, which stimulates future research interests on the entangled squeezed vacuum state and its experimental realization.

2.3. Summary

In this chapter, the super-resolving and super-sensitive single phase estimation using the two-mode NOON state were discussed. Both the quantum lithography scheme and the optical centroid measurement scheme were studied as methods for observing super-resolution interference fringes. The quantum standard limit and the Heisenberg limit were derived as the lower bounds of the measurement uncertainty using clas-

sical sources and quantum sources, respectively. Moreover, the potential of a class of multi-mode NOON-like states in efficiently achieving the Heisenberg limit with respect to sensitivity in simultaneous multi-phase estimation were studied. Among the four specific cases, the multi-mode entangled squeezed vacuum state has the lowest uncertainty under the footing of the same mean photon number, followed by the entangled squeezed coherent state, the entangled coherent state, and the NOON state.

Chapter 3: Generation of two-mode NOON states

In this chapter, several existing methods of generating two-mode NOON states are reviewed.

3.1. Method using cross-Kerr nonlinearity

In 2001, Gerry et al. [6] proposed a nonlinear scheme for generating two-mode NOON states aided by the cross-Kerr interaction. A cross-Kerr nonlinear medium with nonlinearity degree $\chi = \pi$ is embedded into a Mach-Zehnder interferometer, which is able to create an N-photon entanglement from an N-photon Fock state input with the help of a single photon state.

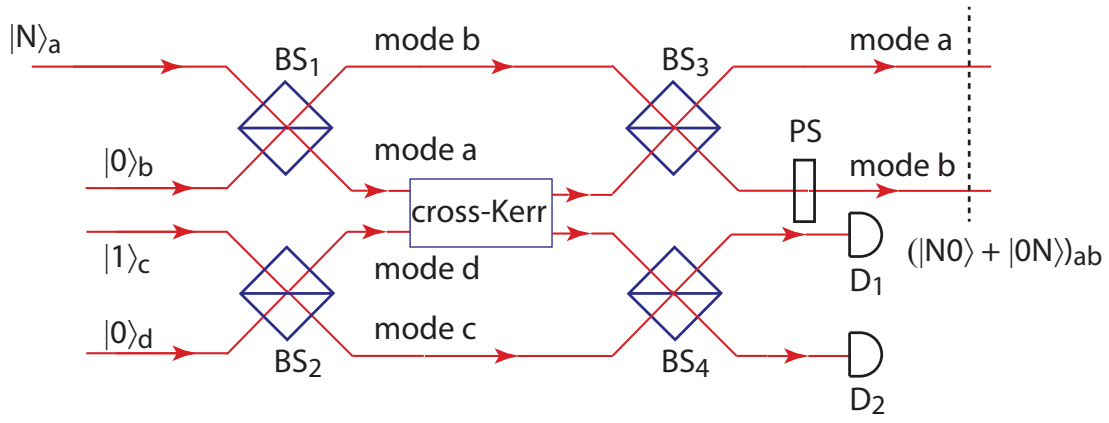

Figure 3.1. Nonlinear cross-Kerr method.

The experimental arrangement of the cross-Kerr nonlinearity method is sketched

in Fig. 3.1. It is composed of a Fock state input, a cross-Kerr nonlinear medium, a single photon input, four 50:50 beam splitters BS_j $(j = 1, 2, 3, 4)$, a phase shifter PS with $\psi = -N\pi/2$, and two single photon detectors D_1 and D_2. Mathematically, the cross-Kerr nonlinear effect applying on modes a and d can be represented by the unitary operation

$$U_{\mathrm{K}} = e^{i\chi a^\dagger a d^\dagger d}. \tag{3.1}$$

The degree of nonlinearity χ is proportional to the third-order nonlinear susceptibility $\chi^{(3)}$ and the length of the medium, which is here taken to be $\chi = \pi$. BS_1 and BS_3, BS_2 and BS_4 work conjugately with each other, where $\theta_1 = \theta_2 = -\theta_3 = -\theta_4 = \pi/4$.

The MZI that is composed of the cross-Kerr medium, BS_1, and BS_3 then acts as a Fredkin gate, which is calculated to be

$$U_{\mathrm{F}} = U_{ab}^\dagger U_{\mathrm{K}} U_{ab} = e^{\frac{i}{2}\chi d^\dagger d(a^\dagger a + b^\dagger b)} e^{\frac{1}{2}\chi d^\dagger d(ab^\dagger - a^\dagger b)}. \tag{3.2}$$

Then the output state after the Fock state and the single photon input passing through

the four beam splitters and the cross-Kerr medium evolves into

$$
\begin{aligned}
&U_{cd}^{\dagger}U_{\mathrm{F}}U_{cd}|N,0,1,0\rangle_{abcd}\\
&=e^{-i\frac{\pi}{4}(c^{\dagger}d+cd^{\dagger})}e^{\frac{i}{2}\chi d^{\dagger}d(a^{\dagger}a+b^{\dagger}b)}e^{\frac{1}{2}\chi d^{\dagger}d(ab^{\dagger}-a^{\dagger}b)}e^{i\frac{\pi}{4}(c^{\dagger}d+cd^{\dagger})}|N,0,1,0\rangle_{abcd}\\
&=e^{-i\frac{\pi}{4}(c^{\dagger}d+cd^{\dagger})}e^{\frac{i}{2}\chi d^{\dagger}d(a^{\dagger}a+b^{\dagger}b)}e^{\frac{1}{2}\chi d^{\dagger}d(ab^{\dagger}-a^{\dagger}b)}|N,0\rangle_{ab}\frac{1}{\sqrt{2}}\left(|1,0\rangle_{cd}+i|0,1\rangle_{cd}\right)\\
&=\frac{1}{\sqrt{2}}e^{-i\frac{\pi}{4}(c^{\dagger}d+cd^{\dagger})}e^{\frac{i}{2}\chi d^{\dagger}d(a^{\dagger}a+b^{\dagger}b)}\left(|N,0\rangle_{ab}|1,0\rangle_{cd}+ie^{\frac{1}{2}\chi(ab^{\dagger}-a^{\dagger}b)}\frac{a^{\dagger N}}{\sqrt{N!}}|0,0\rangle_{ab}|0,1\rangle_{cd}\right)\\
&=\frac{1}{\sqrt{2}}e^{-i\frac{\pi}{4}(c^{\dagger}d+cd^{\dagger})}e^{\frac{i}{2}\chi d^{\dagger}d(a^{\dagger}a+b^{\dagger}b)}\left(|N,0\rangle_{ab}|1,0\rangle_{cd}+i\frac{(\cos\frac{\chi}{2}a^{\dagger}+\sin\frac{\chi}{2}b^{\dagger})^{N}}{\sqrt{N!}}|0,0\rangle_{ab}|0,1\rangle_{cd}\right)\\
&=\frac{1}{\sqrt{2}}e^{-i\frac{\pi}{4}(c^{\dagger}d+cd^{\dagger})}\left(|N,0\rangle_{ab}|1,0\rangle_{cd}+ie^{\frac{i}{2}\chi(a^{\dagger}a+b^{\dagger}b)}|0,N\rangle_{ab}|0,1\rangle_{cd}\right)\\
&=\frac{1}{\sqrt{2}}\frac{1}{\sqrt{2}}\left(|N,0\rangle_{ab}(c^{\dagger}-id^{\dagger})|0,0\rangle_{cd}+ie^{\frac{i}{2}\chi N}|0,N\rangle_{ab}(d^{\dagger}-ic^{\dagger})|0,0\rangle_{cd}\right)\\
&=\frac{1}{\sqrt{2}}\frac{1}{\sqrt{2}}\left(|N,0\rangle_{ab}(|1,0\rangle_{cd}-i|0,1\rangle_{cd})+e^{i\frac{\pi}{2}N}|0,N\rangle_{ab}(i|0,1\rangle_{cd}+|1,0\rangle_{cd})\right)\\
&=\frac{1}{2}\left[\left(|N,0\rangle_{ab}+e^{i\frac{\pi}{2}N}|0,N\rangle_{ab}\right)|1,0\rangle_{cd}-i\left(|N,0\rangle_{ab}-e^{i\frac{\pi}{2}N}|0,N\rangle_{ab}\right)|0,1\rangle_{cd}\right].
\end{aligned}
\tag{3.3}
$$

After a phase shifter with $\psi=-N\pi/2$ is placed to the output mode b, whenever a photon is detected at D_1 or D_2, the heralded state in modes a and b is a two-mode NOON state:

$$
|\phi\rangle_{ab}^{(\mathrm{Kerr})}\propto\frac{1}{\sqrt{2}}|N0\rangle_{12}\pm|0N\rangle_{12}. \tag{3.4}
$$

In this setup, a quantum-optical Fredkin gate is adopted, combined with an auxiliary MZI, and they work together to generate a two-mode NOON state. Similarly, if the Fock state in mode a is changed into a coherent state $|\alpha\rangle$–under the same setup–a two-mode entangled coherent state proportional to $(|\alpha,0\rangle+|0,-i\alpha\rangle)$ can be obtained.

3.2. NOON state projective measurement

In 2005, a method of creating polarization-entangled NOON states using non-collinear type-II parametric down-conversion and NOON state projective measurement was proposed [12]. The state output from the non-collinear type-II SPDC process can be written as

$$|\psi\rangle = \frac{1}{\cosh^2 r} \sum_{n=0}^{\infty} \sqrt{n+1} \tanh^n r |\psi_n^-\rangle, \tag{3.5}$$

where $|\psi_n^-\rangle = 1/\sqrt{n+1} \sum_{m=0}^{n} (-1)^m |n-m, m\rangle_a |m, n-m\rangle_b$ with $|x, y\rangle_i$ representing x horizontally-polarized photons and y vertically-polarized photons in spatial mode i. If the photons in the two polarization modes of the spatial mode a is detected to be an HV-polarized NOON state by the projective measurement proportional to $(|N0\rangle_{HV} + |0N\rangle_{HV})(\langle N0|_{HV} + \langle 0N|_{HV})$ (or denoted using the field operators $(a_H^N \pm a_V^N)$), then the state in spatial mode b is heralded to be a NOON state also.

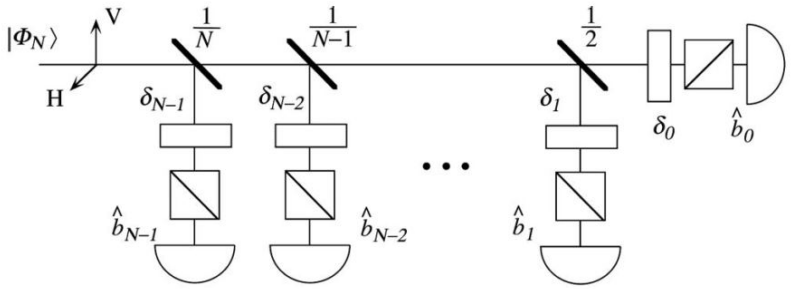

Figure 3.2. NOON state projective measurement [13].

The NOON state projective measurement can be expanded to

$$a_H^N \pm a_V^N = \prod_{n=0}^{N-1} (a_H - a_V e^{i\delta_n}) \tag{3.6}$$

with $\delta_n = 2\pi n/N$. This can be realized using the experimental setup illustrated in Fig. 3.2, where the to-be-measured state is split evenly into N beams and each beam is measured with a single photon detector corresponding to an operator $b_n = (a_H - a_V e^{i\delta_n})/\sqrt{2}$, with the help of PBSs and PSs. Whenever all of the N detectors click simultaneously, known as N-fold single photon coincidence detection (SPCD), an N-photon NOON event is detected. Applying this measurement scheme to spatial mode a of the non-collinear type-II squeezed state, as shown in Eq. (3.5), a heralded two-mode NOON state is obtained in mode b.

The drawback of this method is that the non-collinear type-II SPDC produces light sources with relatively low brightness because of the inefficient collection of the generated photons and the small nonlinear coefficient. In this regard, Nielsen et al. [15] proposed to exploit two type-II SPDC nonlinear crystals, each of which produces a TMSV entangled in horizontal and vertical polarizations. Then under the triggering of the NOON state projective detection on the vertical mode of the first NLC and the horizontal mode of the second one, the state in the remaining two modes are triggered to be a NOON state.

3.3. Method using dual-Fock states

In 2002, Kok et al. [9] proposed a method of generating two-mode NOON states using 2 independent N-photon Fock states, where the entanglement comes from repeatedly reducing one or two photons (depending on the parity of N) from either of the two input modes without the knowledge of their originating modes. This method, which works differently for even-N and odd-N, is discussed in detail below.

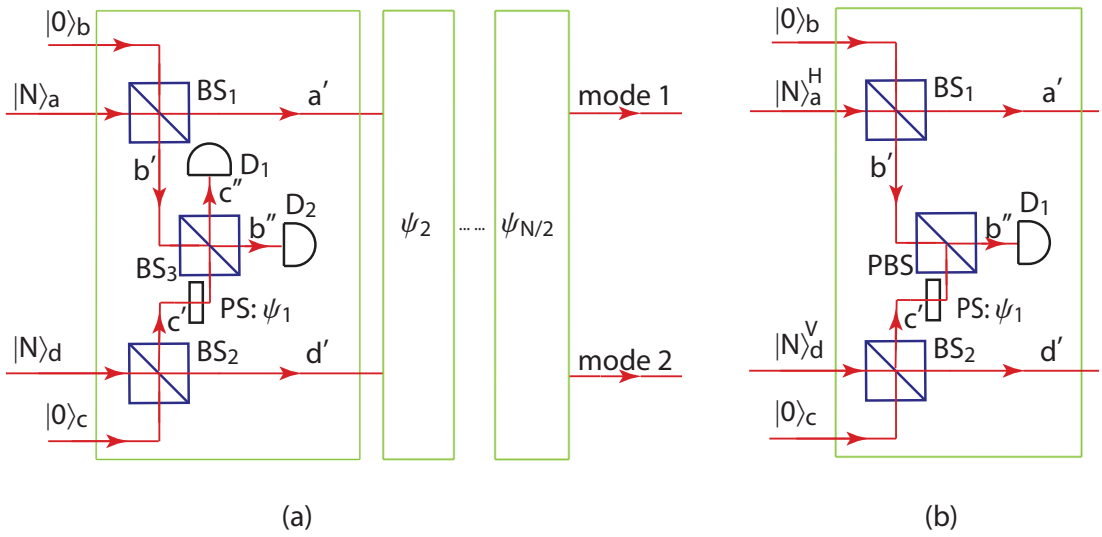

Figure 3.3. Method using dual-Fock states. (a) The full setup with even N. (b)The basic-block setup for odd N.

For the even-N NOON state generation, the experimental setup, which is composed of $N/2$ basic blocks, is sketched in Fig. 3.3(a). Each basic block contains two identical beam splitters BS_1 and BS_2, a 50:50 beam splitter BS_3, two single photon detectors D_1 and D_2, and one phase shifter PS. The transmissivity of both BS_1 and BS_2 for the kth block ($k = 1, 2, \cdots, N/2$) is $T_k = (N-k)/(N-k+1)$, which is optimally chosen in order to split two photons off from the dual-Fock states $|N, N\rangle_{ad}$ with the highest probability. Then the output modes b' and c' are recombined using a 50:50 beam splitter BS_3, whose outputs are measured by D_1 and D_2. Whenever a twofold SPCD is measured at D_1 and D_2, two photons are reduced, either from mode b' or mode c', as a consequence of the two-photon quantum interference, whose process can be written mathematically as $(a^2 - d^2)$. Similarly, when $N/2$ blocks with the corresponding T_k and phase shift $\psi_k = 2\pi k/N$ at mode c' are applied, a total of

N photons are reduced from either mode a or mode d, leading to a NOON state:

$$\left[\prod_{k=1}^{N/2}(a^2+e^{i2\psi_k}d^2)\right]|N,N\rangle_{ad}=(a^N\pm d^N)|N,N\rangle_{ad}\propto|N,0\rangle_{ad}\pm|0,N\rangle_{ad}, \tag{3.7}$$

where the upper (lower) sign applies to $N=2+4q$ ($N=4+4q$), with $q=0,1,2,\cdots$.

For odd-N, a new degree of freedom (polarization, in this case) is introduced into the experiment in order to avoid the non-detection triggering. The inputs are now instead dual-Fock states with orthogonal polarizations (e.g., horizontal and vertical polarizations). The main structure is still the same, except for some changes in the basic block, as shown in Fig. 3.3(b). Instead of reducing two photons, the kth block ($k=1,2,\cdots,N$) only reduces one photon each time, where the transmissivity of BS_1 and BS_2 are chosen to be $T_k'=(2N-k)/(2N-k+1)$. BS_3 is in lieu of by a PBS, which transmits horizontal photons and reflects vertical photons. A single photon detector is adopted to project one photon coming from either mode b' or mode c'. Repeating this process N times with the corresponding T_k and the same phase shift $\psi_k=2\pi k/N$ ($k=1,...,N$) produces a two-mode NOON state:

$$\left[\prod_{k=1}^{N}(a+e^{i\psi_k}d)\right]|N,N\rangle_{ad}=(a^N\pm d^N)|N,N\rangle_{ad}\propto|0N\rangle_{ad}\pm|N0\rangle_{ad}, \tag{3.8}$$

where the upper (lower) sign applies to $N=3+4q$ ($N=5+4q$), with $q=0,1,2,\cdots$.

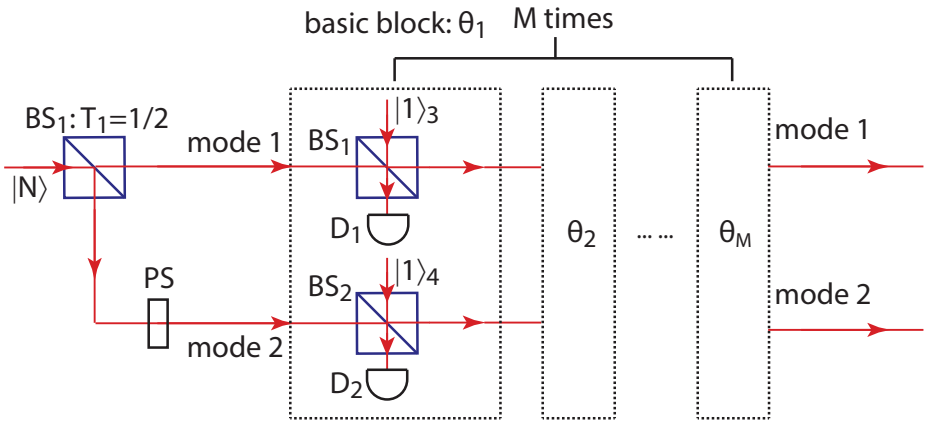

Figure 3.4. Method using a two-mode N-photon input.

3.4. Method using a two-mode N-photon state

In 2002, a method of two-mode NOON state generation, which is achieved by reducing the non-NOON components with the help of Fock state filters, was proposed independently by two groups [7,8]. Their setup is sketched in Fig. 3.4.

The input state for this procedure is a two-mode N-photon state,

$$|\psi\rangle_{12} = \sum_{n=0}^{N} c_n |n, N-n\rangle_{12}, \tag{3.9}$$

with $c_n = \sqrt{N!/\left(n!(N-n)!2^N\right)}$, created from splitting an N-photon Fock state using a 50:50 beam splitter and applying a PS with phase factor $e^{-i\pi N/2}$ in the reflected arm of the BS to cancel out the $\pi/2$ phase difference between the two arms. Then, $M = \lfloor N/2 \rfloor$ ($\lfloor\cdot\rfloor$ being the floor function) basic blocks (shown as dashed boxes) are deployed sequentially, the kth of which is composed of 2 FSFs with BS transmissivity $\cos^2\theta_k = k/(k+1)$. The state after adding 2 single photons in the kth block evolves

into a 4-mode state:

$$
\begin{aligned}
&U_{13}(\theta_k)U_{24}(\theta_k)|\psi\rangle_{12}|1,1\rangle_{34} = e^{i\theta_k(a_1^\dagger a_3 + a_1 a_3^\dagger)} e^{i\theta_k(a_2^\dagger a_4 + a_2 a_4^\dagger)} |\psi\rangle_{12}|1,1\rangle_{34} \\
&= \sum_{n=0}^{N} \frac{c_n}{\sqrt{n!(N-n)!}} \left(\cos\theta_k a_1^\dagger + i\sin\theta_k a_3^\dagger\right)^n \left(\cos\theta_k a_3^\dagger + i\sin\theta_k a_1^\dagger\right) \\
&\left(\cos\theta_k a_2^\dagger + i\sin\theta_k a_4^\dagger\right)^{N-n} \left(\cos\theta_k a_4^\dagger + i\sin\theta_k a_2^\dagger\right)|0\rangle_{1234}.
\end{aligned} \tag{3.10}
$$

Then the 2-fold SPCD at D_1 and D_2 projects the state into

$$
\begin{aligned}
&\sum_{n=0}^{N} \frac{c_n}{\sqrt{n!(N-n)!}} \left(ni\sin\theta_k a_3^\dagger(\cos\theta_k a_1^\dagger)^{n-1} i\sin\theta_k a_1^\dagger + \cos\theta_k a_3^\dagger(\cos\theta_k a_1^\dagger)^n\right) \\
&\left((N-n)i\sin\theta_k a_4^\dagger(\cos\theta_k a_2^\dagger)^{N-n-1} i\sin\theta_k a_2^\dagger + \cos\theta_k a_4^\dagger(\cos\theta_k a_2^\dagger)^{N-n}\right)|0\rangle_{1234} \\
&= \sum_{n=0}^{N} \frac{c_n}{\sqrt{n!(N-n)!}} \left(-n\sin^2\theta_k \cos\theta_k{}^{n-1} a_3^\dagger a_1^{\dagger n} + \cos^{n+1}\theta_k a_3^\dagger a_1^{\dagger n}\right) \\
&\left(-(N-n)\sin^2\theta_k \cos\theta_k{}^{N-n-1} a_4^\dagger a_2^{\dagger(N-n)} + \cos\theta_k{}^{N-n+1} a_4^\dagger a_2^{\dagger(N-n)}\right)|0\rangle_{1234} \\
&= \sum_{n=0}^{N} \frac{c_n}{\sqrt{n!(N-n)!}} \cos^{n+1}\theta_k \cos^{N-n+1}\theta_k \\
&\left(-n\tan^2\theta_k a_3^\dagger a_1^{\dagger(n)} + a_3^\dagger a_1^{\dagger n}\right)\left(-(N-n)\tan^2\theta_k a_4^\dagger a_2^{\dagger(N-n)} + a_4^\dagger a_2^{\dagger(N-n)}\right)|0\rangle_{1234} \\
&\xrightarrow{\text{reduce modes 3 and 4}} \\
&\sum_{n=0}^{N} \frac{c_n}{\sqrt{n!(N-n)!}} (\cos\theta_k)^{N+2} a_1^{\dagger n} a_2^{\dagger(N-n)} \left(1 - n\tan^2\theta_k\right)\left(1 - (N-n)\tan^2\theta_k\right)|0\rangle_{1234} \\
&= \sum_{n=0}^{N} c_n (\cos\theta_k)^{N+2} \left(1 - n\tan^2\theta_k\right)\left(1 - (N-n)\tan^2\theta_k\right)|n, N-n\rangle_{12}.
\end{aligned} \tag{3.11}
$$

It is seen that when θ_k is chosen to be $\arctan(1/\sqrt{k})$, $(1 - k\tan^2\theta_k) = 0$, and hence any events with k or $(N-k)$ photons in the output state can be canceled out.

When this state passes through each block from $k = 1$ to $k = M = \lfloor N/2 \rfloor$ with $\theta_k = \arctan(1/\sqrt{k})$, all terms with 1 and $(N-1)$, 2 and $(N-2)$, to $\lfloor N/2 \rfloor$ and $\lceil N/2 \rceil$ photons are discarded, eventually leaving the state as a two-mode N-photon NOON state.

This method for the even-N scenario can be simplified by combining 2 Fock states on the 50:50 BS, such that only even-photon-number components exist in the output. Under this settings, only $M = \lfloor N/4 \rfloor$ sets of basic FSF blocks are required to cancel out the non-NOON components.

3.5. Method of mixing a coherent state with a squeezed vacuum state

Almost all of the previous work on NOON state generation requires fixed-photon-number states, i.e., Fock states. In 2007, Hofmann and Ono [16] theoretically proposed a method with the illuminating sources being nondeterministic-photon-number states only. They showed that by combining the SMSV from type-I SPDC and photons from a coherent laser, one can generate an arbitrary-photon-number NOON state with fidelity higher than 90% under the post-selection of total N-photon components. This was later demonstrated experimentally by Afek et al. [23].

A schematic setup and a detailed experimental layout of the state preparation and NOON detection are shown in Fig. 3.5(a) and Fig. 3.5(b), respectively, where the PNR detections at D_1 and D_2 are achieved by detecting single photons after splitting the output into multiple modes. They defined the pair amplitude ratio of the coherent intensity $|\alpha|^2$ and $\tanh|r|$: $\gamma = |\alpha|^2/\tanh|r|$, which determines the fidelity of the output state from combining a coherent state $|\alpha\rangle$ and an SMSV $|r\rangle$ on a balanced

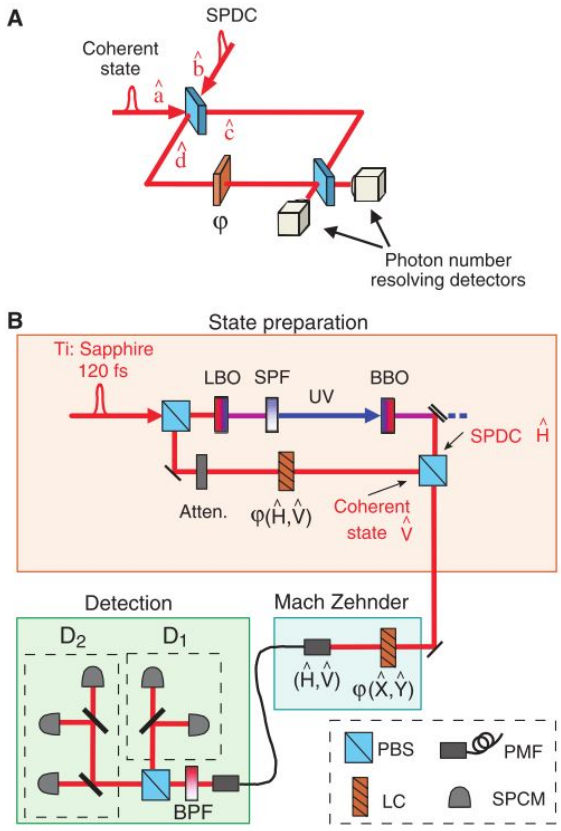

Figure 3.5. Method using a coherent state and a squeezed vacuum state [23]. (a) A schematic setup of the MZI using a coherent state and a squeezed vacuum state from SPDC. (b) A detailed layout of the state preparation and detection. LBO: lithium triborate crystal. BBO: barium borate crystal. BPF: bandpass filter. PMF: polarization-maintaining fiber. LC: liquid crystal.

BS with the prefect NOON state. By optimizing the parameter γ with respect to each photon number N, it is demonstrated that the output of combining these two states gives rise to perfect NOON states with up to $N = 3$. The fidelity for higher-N scenarios is larger than 90% for most of the cases. Later on, follow-up work has shown that mixing the coherent state with other states–such as photon-subtracted squeezed vacuum state [92–94] and even/odd coherent states [95]–can further improve the performance.

Table 3.1. Comparisons among different methods for two-mode NOON state generation.

Section	Input requirement	Major strength	Major weakness
3.1	one $\|N\rangle$, one $\|1\rangle$	highest efficiency	high nonlinearity
3.2	non-collinear type-II SPDC	pre-selection only	infeasible input
3.3	two $\|N\rangle$	arbitrary N	low efficiency
3.4	one $\|N\rangle$, $O(N)$ $\|1\rangle$	arbitrary N	$O(N)$ FSFs required
3.5	one $\|\alpha\rangle$, one $\|r\rangle$	feasible inputs	post-selection required

3.6. Summary

The major strength and weakness of each of the previous methods for the generation of two-mode NOON states are summarized in Table 3.1. Method 3.1 is the least feasible method due to the requirement of a high degree of cross-Kerr nonlinearity $\chi = \pi$ in spite of its potentially highest generation efficiency. Method 3.2 requires an infeasible light source produced by a non-collinear type-II SPDC process and a perfect NOON projective measurement, and these things are difficult to achieve in experiments. Methods 3.3 and 3.4 can potentially generate the NOON state with an arbitrary photon number N, but the main weakness of method 3.3 is its extremely low efficiency (shown in Section 4.2), and the main weakness of method 3.4 that it requires $O(N)$ number of Fock state filters. Method 3.5 is the most feasible method since it only requires experimentally-producible light sources, a coherent state from a laser, and a squeezed vacuum state from type-I SPDC. Since nondeterministic-photon-number states are utilized, proper post-selection is required to extract the NOON components after the quantum state interacts with the phase object.

Chapter 4: Generation of multi-mode NOON states

In this chapter, several scalable generation methods of multi-mode NOON states are proposed for the first time. Sections 4.1, 4.2, and 4.3.1 are the multi-mode extensions of two-mode NOON state generation, as summarized in Sections 3.1, 3.3, and 3.4, respectively. Sections 4.3 and 4.4 illustrate a handful of schemes assisted by Fock state filters, including a design for a 4-photon NOON state using single photons (Section 4.3.2), high-N NOON state generation using (1) d coherent states (Section 4.4.1), (2) d single-mode squeezed vacuum states (Section 4.4.2), and (3) one two-mode squeezed vacuum state (Section 4.4.3). Comparisons are made among these methods with regard to their feasibility and efficiency.

4.1. Method using cross-Kerr nonlinearity [96]

This method is inspired by the two-mode NOON state generation using cross-Kerr nonlinearity [6], as described in Section 3.1, where an N-photon entanglement between two spatial modes is created with the assistance of a cross-Kerr medium with nonlinearity degree $\chi = \pi$ embedded in an MZI. For future reference, in this dissertation, this process is referred to as the entanglement generator. In order to extend this method into the multi-mode scenario, a cascading layout (essentially a binary

tree) among multiple entanglement generators is deployed to successively add the entanglement mode into the system and eventually create an N-photon entanglement among multiple spatial modes.

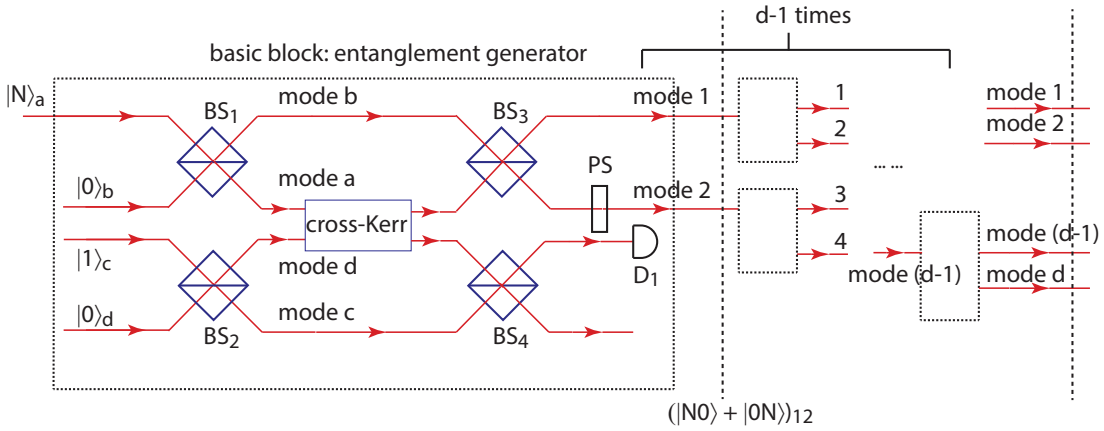

Figure 4.1. *d*-**mode NOON state generation using cross-Kerr nonlinearity.**

The experimental setup is sketched in Fig. 4.1. The setup is composed of $(d-1)$ entanglement generators (shown as dashed boxes), each of which is almost identical to the one in Section 3.1. It is important to point out that the N-photon Fock state input is outside the entanglement generator, and only one Fock state is required for the whole procedure. For the multi-mode scenario, only one detector is deployed in each entanglement generator as the pre-selection. This will be explained later.

From Eq. (3.3), one can obtain that the Fock state after the first generator triggering on the single photon detection at D_1 evolves as

$$|N\rangle_1 \rightarrow \frac{1}{2}(|N0\rangle_{12} + |0N\rangle_{12}), \tag{4.1}$$

which involves the entanglement of N photons in modes 1 and 2. Note that the right hand side of Eq. (4.1) is not normalized so as to show the probability amplitude

relative to the input state explicitly. This enables the intrinsic efficiency of the method to be calculated later. Then the scheme of adding more entanglement modes into the system is done by repeatedly applying another entanglement generator in a cascading configuration, where each of the output modes from the previous generator is aligned with the input of the following one. An example of adding one more entanglement mode is shown below, where mode 1 of the state in Eq. (4.1) is injected into the second generator. Together with the single photon $|1\rangle_c$ in the second generator, the state evolves as follows with mode 2 unchanged:

$$
\begin{aligned}
&\frac{1}{2}(|N0\rangle_{12}|1\rangle_c + |0N\rangle_{12}|1\rangle_c) \\
&\Big\downarrow |N\rangle_1|1\rangle_c \text{ creates another entanglement in modes 1 and 3} \\
&\frac{1}{2}\left(\frac{1}{2}\left(|N0\rangle_{12}|0\rangle_3 + |00\rangle_{12}|N\rangle_3\right) + |0N\rangle_{12}|1\rangle_c\right) \\
&\Big\downarrow |0\rangle_1|1\rangle_c \text{ triggers single photon detection at } \mathrm{D}_1 \text{ and gives vacuum in modes 1 and 3} \\
&\frac{1}{2}\left(\frac{1}{2}|N0\rangle_{12}|0\rangle_3 + \frac{1}{2}|00\rangle_{12}|N\rangle_3 + |0N\rangle_{12}|0\rangle_3\right) \\
&= \frac{1}{2}\left(\frac{1}{2}|N00\rangle_{123} + \frac{1}{2}|00N\rangle_{123} + |0N0\rangle_{123}\right),
\end{aligned}
\tag{4.2}
$$

which is a three-mode NOON state with unbalanced coefficients. Since the $|0\rangle_1|1\rangle_c$ term can only trigger a single photon detection at D_1, only one detector in each generator is required for the multi-mode scenario. In order to balance the amplitude for each NOON component $|N00\rangle_{123}$, $|00N\rangle_{123}$ and $|0N0\rangle_{123}$ in Eq. (4.2), a third generator with single photon $|1\rangle_{c'}$ is required with input aligned with mode 2 of the

state in Eq. (4.1) where modes 1 and 3 stay unchanged, and this leads to a balanced four-mode NOON state:

$$\begin{aligned}
&\frac{1}{2}\left(\frac{1}{2}|N00\rangle_{123}+\frac{1}{2}|00N\rangle_{123}+|0N0\rangle_{123}\right)|1\rangle_{c'}\\
&\Big\downarrow \text{same process as in Eq. (4.2), where entanglement in modes 2 and 4 is created}\\
&\frac{1}{2^2}\left(|N000\rangle_{1234}+|00N0\rangle_{1234}+|0N00\rangle_{1234}+|000N\rangle_{1234}\right).
\end{aligned} \tag{4.3}$$

Comparing this state with Eq. (4.1), an amplitude modulation of 1/2 is added after the second and third generator. This method can only be utilized to generate a NOON state with mode number $d = 2^m$ $(m = 1, 2, \cdots)$ since the amplitudes of the NOON components need to be balanced. For the d-mode NOON state generated eventually by repeating this process using $(d-1)$ entanglement generators aligned in the cascading configuration, as discussed above, the amplitude will be modulated by 1/2 m times with $m = \log d$, which gives a d-mode N-photon NOON state

$$\begin{aligned}
|\phi\rangle_{1\cdots d}^{(4.1)} &\propto \frac{1}{2^{\log d}}\big(|N0\cdots0\rangle+|0N0\cdots0\rangle+\cdots+|0\cdots0N\rangle\big)_{1\cdots d}\\
&= \frac{1}{d}\big(|N0\cdots0\rangle+|0N0\cdots0\rangle+\cdots+|0\cdots0N\rangle\big)_{1\cdots d}\\
&= \sqrt{p_{(4.1)}}\frac{1}{\sqrt{d}}\big(|N0\cdots0\rangle+|0N0\cdots0\rangle+\cdots+|0\cdots0N\rangle\big)_{1\cdots d}
\end{aligned} \tag{4.4}$$

triggered on a $(d-1)$-fold SPCD.

In order to facilitate the comparisons among different methods in the future, the intrinsic generation probability is calculated. This probability is also the percentage of the obtained NOON components with respect to unity of a normalized NOON

state, under the assumptions that all of the optical devices, including the detectors and the beam splitters have unity efficiency and are lossless, for the sake of simplicity. The generation efficiency for this method is then calculated to be

$$p_{(4.1)} = d|\frac{1}{d}|^2 = \frac{1}{d}. \tag{4.5}$$

It should be stated that the imperfection of resources can be compensated for by multiplying the efficiency for each device on the intrinsic generation efficiency as calculated above.

4.2. Method using d N-photon Fock states [96]

Based on a different entanglement generating scheme by reducing photons from one of the dual-Fock states without knowing the originating mode [9], as discussed in Section 3.3, another cascading method is proposed in this section. This method adopts a d N-photon Fock states to generate d-mode N-photon NOON state with $d = 2^m$ $(m = 1, 2, \cdots)$.

Figure 4.2(a) illustrates the full setup for the even-N NOON state generation, where each of the $(d-1)$ entanglement generators (shown as black dashed boxes) is almost the same as that in Fig. 3.3(a). It is noticeable that only the first generator has two Fock states as the input, while each of the others takes one Fock state inside the generator and one mode of state from the previous generator. The state passing

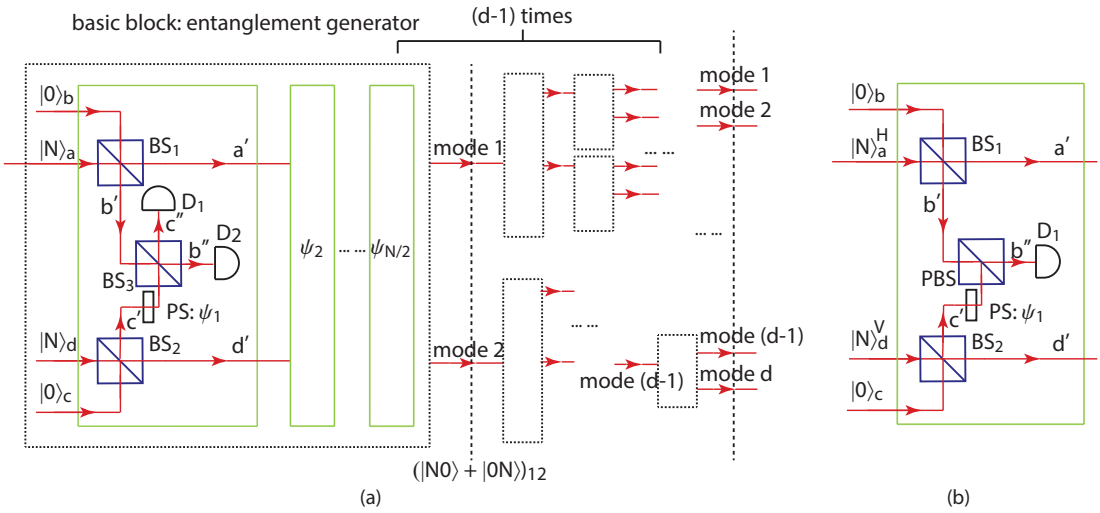

Figure 4.2. *d*-**mode NOON state generation using** d **Fock states. (a) The full setup with even** N**. (b) The sub-block setup inside the entanglement generator with odd** N**.**

through the first entanglement generator can be calculated as

$$|\phi\rangle_{12}^{(4.2,\text{even})} \propto \left[\bigotimes_{k=1}^{N/2} M_k\right] |N,N\rangle_{ad}, \tag{4.6}$$

where

$$M_k = {}_{b''c''}\langle 11|e^{i\psi_k c'^\dagger c'} U(\theta_k) = \frac{i}{\sqrt{2}}\Big({}_{b'c'}\langle 20| + e^{i2\psi_k}{}_{b'c'}\langle 02|\Big)U(\theta_k) \tag{4.7}$$

is the measurement operator for the kth sub-block. ${}_{b''c''}\langle 11|$ denotes the 2-fold SPCD at D_1 and D_2, $e^{i\psi_k c'^\dagger c'}$ is the phase shift operator with $\psi_k = 2\pi k/N$ added on mode c', and $U(\theta_k) = \exp\left[i\theta_k(a^\dagger b + ab^\dagger + c^\dagger d + cd^\dagger)\right]$ is the unitary operator for the combined BS_1 and BS_2 with transmissivity $T_k = \cos^2\theta_k = (N-k)/(N-k+1)$. Note that this expression is equivalent to the post-measurement state, as in Eq. (1.36), where the state notation instead of the corresponding density operator is used for calculation here. Using the mathematical induction in Appendix B, Eq. (4.6) can be calculated

to be

$$
\begin{aligned}
|\phi\rangle_{12}^{(4.2,\mathrm{even})} &\propto \left(-\frac{i}{2}\right)^{N/2}\left[\prod_{k=1}^{N/2}\sin^2\theta_k\cos^{2(N-k)}\theta_k(a^2+e^{i2\psi_k}d^2)\right]|N,N\rangle_{ad} \\
&= \left(-\frac{i}{2}\right)^{N/2}\prod_{k=1}^{N/2}\sin^2\theta_k\cos^{2(N-k)}\theta_k\left(a^N\pm d^N\right)|N,N\rangle \\
&= \left(-\frac{i}{2}\right)^{N/2}\sqrt{N!}(\frac{1}{N})(\frac{1}{N-1})\cdots(\frac{1}{N/2+1}) \\
&\quad (\frac{N-1}{N})^{(N-1)}(\frac{N-2}{N-1})^{(N-2)}\cdots(\frac{N/2}{N/2+1})^{N/2}\left(|0N\rangle\pm|N0\rangle\right) \\
&= \left(-\frac{i}{2}\right)^{N/2}\sqrt{N!}(\frac{1}{N})(\frac{1}{N-1})\cdots(\frac{1}{N/2+1}) \\
&\quad (\frac{1}{N})^{(N-1)}(N-1)(N-2)\cdots(\frac{N}{2}+1)(\frac{N}{2})^{N/2}\left(|N0\rangle\pm|0N\rangle\right) \\
&= c_{(4.2)a}(|N0\rangle\pm|0N\rangle)_{12},
\end{aligned}
\tag{4.8}
$$

where

$$
c_{(4.2)a} = \frac{(-i)^{N/2}\sqrt{N!}}{2^N N^{N/2}}. \tag{4.9}
$$

The upper (lower) sign in Eq. (4.8) applies to $N = 2+4q$ ($N = 4+4q$) with $q = 0, 1, 2, \cdots$.

The way to extend this method to the multi-mode case is similar to that in Section 4.1. When the output mode 1 of the first generator is aligned with the input of the next block, together with another Fock state $|N\rangle_3$ from the second generator, the input then becomes a superposition of $|N0N\rangle_{123}$ and $|0NN\rangle_{123}$. The first term creates another entanglement between modes 1 and 3: $c_{(4.2)a}(|N00\rangle_{123}+|00N\rangle_{123})$, while the second term is transferred into $c_{(4.2)b}|0N0\rangle_{123}$, with the coefficient

$$
c_{(4.2)b} = \left(\frac{-i}{2}\right)^{N/2}\frac{\sqrt{N!}}{N^{N/2}}. \tag{4.10}
$$

Similar to the method in Section 4.1, when this process is repeated $(d-1)$ times with $d = 2^m$, $m = 1, 2, \cdots$, the d-mode NOON state is finally obtained:

$$|\phi\rangle_{1\cdots d}^{(4.2,\text{even})} \propto c_{(4.2)a}^{\log_2 d} c_{(4.2)b}^{d-\log_2 d-1} \left(|N0\cdots0\rangle \pm |0N0\cdots0\rangle \pm \cdots \pm |0\cdots0N\rangle\right)_{1\cdots d}, \quad (4.11)$$

whose generation probability is

$$p_{(4.2)}^{\text{even}} = d \left| c_{(4.2)a}^{\log_2 d} c_{(4.2)b}^{d-\log_2 d-1} \right|^2 = \frac{1}{d^{N-1}} \left(\frac{N!}{2^N N^N} \right)^{d-1}. \quad (4.12)$$

For odd-N, the polarization degree of freedom is required as stated in Section 3.3. The setup of the sub-block shown in Fig. 4.2(b) is exactly the same as that in Fig. 3.3(b). Its extension to multi-mode scenario is also the same as discussed above for even-N.

4.3. Methods using Fock state filters and fixed-photon-number states

4.3.1 Generation using an evenly-distributed N-photon state [96]

Inspired by paper [8], a method of creating the d-mode N-photon NOON state using a d-mode evenly-distributed N-photon state source is presented. The main idea is to utilize FSFs to cancel out non-NOON components from an input containing both NOON components and non-NOON components. Since a fixed-photon-number state is chosen as the incident beam, only pre-selection is needed.

The required d-mode evenly-distributed N-photon state can be created by splitting an N-photon Fock state using $(d-1)$ beam splitters, as shown in the green box

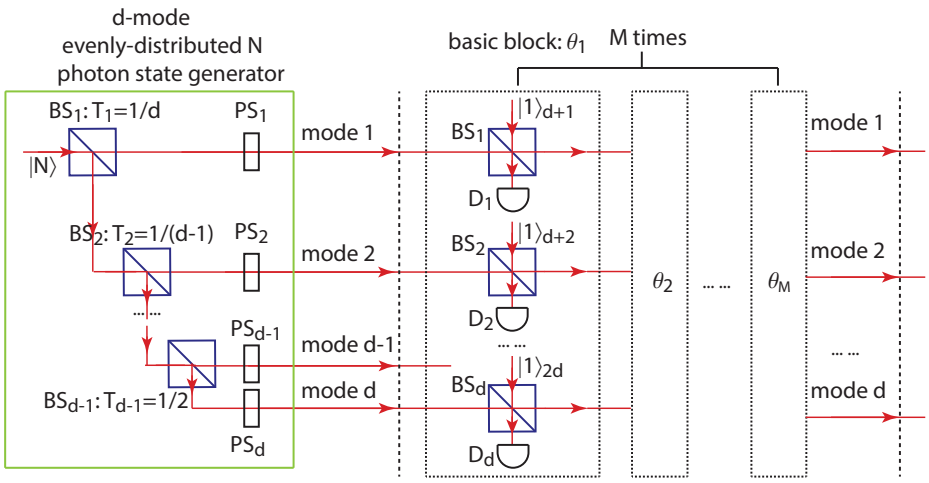

Figure 4.3. *d*-**mode NOON state generation using an evenly-distributed** *N*-**photon state.**

in Fig. 4.3, where the jth BS (U_j) has transmissivity $T_j = 1/(d+1-j)$, ($j = 1, 2, \cdots, d-1$). The transmissivity of each BS is optimally chosen to split one photon off from the incident beam each time with the highest probability. This splitting setup has the same effect as applying a 50:50 BS on each output mode of the previous BS to split it into two modes. In the latter case, the mode number has to be $d = 2^m$ ($m = 1, 2, \cdots$) such that the amplitudes for the NOON components are balanced. This splitting strategy is adopted in Section 4.4.3. Since a beam splitter usually introduces a $\pi/2$ phase shift to the reflected beam, a phase shifter (PS_j) is applied to each mode to cancel out this effect. The unitary operation of the d phase shifters is given by $U_{\mathrm{PS}} = \prod_{j=1}^{d} \exp\left[-i\frac{\pi}{2} a_j^\dagger a_j (j-1)\right]$. Then the state after this splitting and

phase shifting process is an evenly-distributed N-photon state:

$$\begin{aligned}|\psi\rangle_{1\cdots d}^{(4.3.1)} &= U_{\rm PS}U_{d-1}\cdots U_1|N\rangle_1 = \frac{1}{\sqrt{N!}d^{N/2}}\left(a_1^\dagger + a_2^\dagger + \cdots + a_d^\dagger\right)^N|0\rangle_{1\cdots d} \\ &= \frac{1}{d^{N/2}}\sum_{n_1+n_2+\cdots+n_d=N}\sqrt{C_{n_1,\ldots,n_d}^N}|n_1,...,n_{d-1},n_d\rangle_{1\cdots d} \\ &= |\psi\rangle_{1\cdots d}^{\rm NOON} + |\psi\rangle_{1\cdots d}^{\text{non-NOON}},\end{aligned} \tag{4.13}$$

which contains both the NOON component (un-normalized)

$$|\psi\rangle_{1\cdots d}^{\rm NOON} = \frac{1}{d^{N/2}}\left(|N0\cdots0\rangle + \cdots + |0\cdots0N\rangle\right)_{1\cdots d}, \tag{4.14}$$

and the non-NOON component (un-normalized)

$$|\psi\rangle_{1\cdots d}^{\text{non-NOON}} = \frac{1}{d^{N/2}}\sum_{\substack{n_1+n_2+\cdots+n_d=N,\\ n_1\neq N,\cdots,n_d\neq N}}\sqrt{C_{n_1,\ldots,n_d}^N}|n_1,...,n_{d-1},n_d\rangle_{1\cdots d}. \tag{4.15}$$

The coefficient $C_{n_1,\ldots,n_d}^N = N!/\left(n_1!n_2!...n_d!\right)$ denotes the multinomial distribution.

This state is then fed into $M_1 = \lfloor N/2\rfloor$ sets of FSFs (the black dashed boxes), where the kth set contains d FSFs with BS transmissivity $k/(k+1)$. The state after adding d single photons in the kth block evolves into a $2d$-mode state:

$$\begin{aligned}&\left[\bigotimes_{j=1}^d U_{j,d+j}^k\right]|\psi\rangle_{1\cdots d}|1,\cdots,1\rangle_{d+1,\ldots,2d} \\ &= \frac{1}{d^{N/2}}\sum_{\substack{n_1+n_2+\\ \ldots+n_d=N}}\frac{\sqrt{N!}}{n_1!n_2!...n_d!}\Big[\prod_{j=1}^d\left(\cos\theta_k a_j^\dagger + i\sin\theta_k a_{d+j}^\dagger\right)^{n_j} \\ &\quad\left(\cos\theta_k a_{d+j}^\dagger + i\sin\theta_k a_j^\dagger\right)\Big]|0\rangle_{1\cdots2d}.\end{aligned} \tag{4.16}$$

Then the d-fold SPCD at $\{\mathrm{D}_j\}$ projects the state into

$$|\psi\rangle_{1\cdots d}^{(4.3.1),k} \propto \frac{1}{d^{N/2}} \sum_{n_1+n_2+\cdots+n_d=N} \sqrt{\frac{N!}{n_1!n_2!...n_d!}} (\cos\theta_k)^{N+d} \Big[\prod_{j=1}^{d} \left(1 - n_j \tan^2\theta_k\right)\Big] |n_1, \cdots, n_d\rangle_{1\cdots d}. \tag{4.17}$$

When this state $|\psi\rangle_{1\cdots d}^{(3.4)}$ in Eq. (4.13) passes through each block from $k = 1$ to $k = M_1 = \lfloor N/2 \rfloor$ with $\theta_k = \arctan(1/\sqrt{k})$, the kth block cancels out all the non-NOON components with k or $(N-k)$ photons in any mode, since the total photon number in the system is fixed at N. Eventually only the terms with N photons in one mode, and vacuum in all the other modes, survive. This is essentially a d-mode N-photon NOON state:

$$|\phi\rangle_{1\cdots d}^{(4.3.1)} \propto c_{(4.3.1)}(|N0\cdots0\rangle + |0N0\cdots0\rangle + \cdots + |0\cdots0N\rangle)_{1\cdots d}, \tag{4.18}$$

where

$$\begin{aligned} c_{(4.3.1)} &= \frac{1}{d^{N/2}} \prod_{k=1}^{M_1} \left[(\cos\theta_k)^{N+d} \left(1 - N\tan^2\theta_k\right)\right] \\ &= \frac{(-1)^{M_1}(N-1)!}{d^{N/2}\sqrt{M_1+1}^{N+d}(N-M_1-1)!M_1!}. \end{aligned} \tag{4.19}$$

The intrinsic generation probability of the d-mode N-photon NOON state using this method is then

$$p_{(4.3.1)} = d|c_{(4.3.1)}|^2 = \frac{(N-1)!^2}{d^{N-1}(M_1+1)^{N+d}(N-M_1-1)!^2 M_1!^2}. \tag{4.20}$$

4.3.2 Generation of a 4-photon NOON state using single photons

In this section, a specific scenario of generating a 4-photon d-mode NOON state with $d = 2^m$ $(m = 2, 3, \cdots)$ is illustrated using indistinguishable single photon sources. Theoretically, it is possible to reach an even higher photon-number NOON state using a similar process of mixing single photons, as given in this section, but only the 4-photon case is discussed here, since the coherent mixture of multiple perfect single photons becomes more and more challenging and costly with an increasing photon number.

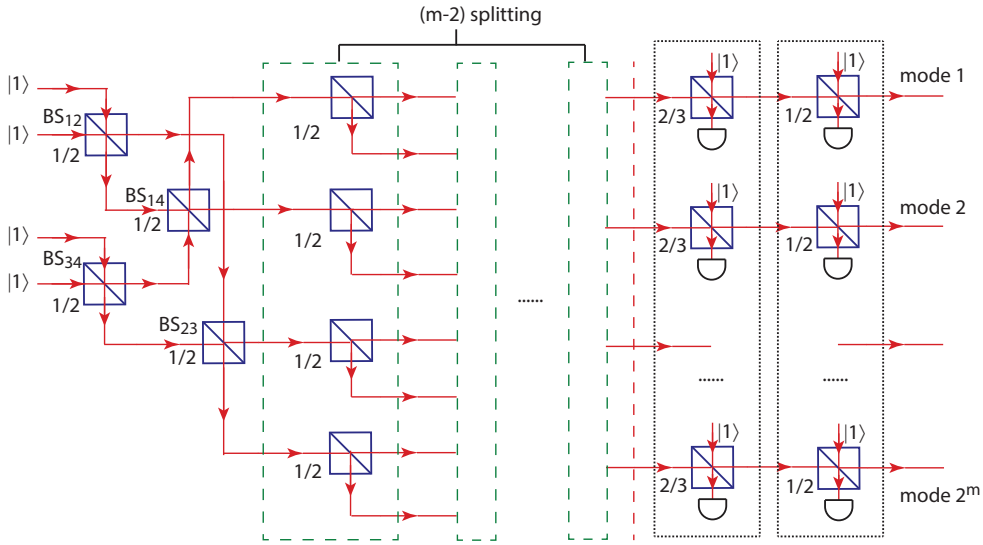

Figure 4.4. 4-photon NOON state generation using single photons.

The setup is sketched in Fig. 4.4, where 4 single photon states are combined using four identical 50:50 BSs (BS_{12}, BS_{34}, BS_{23}, and BS_{14}), such that there is a non-zero possibility that all 4 photons simultaneously appear in every one of the four modes.

The state evolves into

$$
\begin{aligned}
&U_{14}U_{23}U_{12}U_{34}|1,1,1,1\rangle_{1234} \\
&= \frac{1}{16}\left[a_1^{\dagger 4} + a_2^{\dagger 4} + a_3^{\dagger 4} + a_4^{\dagger 4}\right]|0000\rangle_{1234} \\
&+ \frac{1}{8}\left[-a_1^{\dagger 2}a_3^{\dagger 2} + a_1^{\dagger 2}a_2^{\dagger 2} + a_1^{\dagger 2}a_4^{\dagger 2} + a_3^{\dagger 2}a_4^{\dagger 2} - a_2^{\dagger 2}a_4^{\dagger 2} + a_2^{\dagger 2}a_3^{\dagger 2} + 4a_1^{\dagger}a_3^{\dagger}a_2^{\dagger}a_4^{\dagger}\right]|0000\rangle_{1234} \\
&= \frac{\sqrt{6}}{8}(|4000\rangle_{1234} + |0400\rangle_{1234} + |0040\rangle_{1234} + |0004\rangle_{1234}) \\
&+ \frac{1}{4}(|2200\rangle_{1234} - |2020\rangle_{1234} + |2002\rangle_{1234} + |0220\rangle_{1234} - |0202\rangle_{1234} + |0022\rangle_{1234}) \\
&+ \frac{1}{2}|1111\rangle_{1234}.
\end{aligned}
\tag{4.21}
$$

The 4 modes of this state in Eq. (4.21) are then split into $d = 2^m$ modes by applying $(m-2)$ sets of 50:50 BSs (dashed green boxes) at each output mode, successively. Finally, two sets of FSFs with BS transmissivity 2/3 and 1/2 are adopted to cancel out the unexpected components with 1, 2 or 3 photons in each mode and leave the output state a 4-photon NOON state.

In order to show the efficiency of this method, a simplification is made in which only the amplitudes of events with 4 photons in one certain mode are calculated, since the non-NOON components will be canceled out by the FSFs. Since each set of splitting modulates the 4-photon NOON component by $\left(1/\sqrt{2}\right)^4$, the amplitude of

the NOON components after $(m-2)$ sets of the splitting process is calculated below:

$$\begin{aligned}
&\left[\prod_{k=1}^{d-4} U_k\right] \frac{\sqrt{6}}{8}(|4000\rangle_{1234} + |0400\rangle_{1234} + |0040\rangle_{1234} + |0004\rangle_{1234}) \\
&\rightarrow \left(\frac{1}{\sqrt{2}^4}\right)^{m-2} \frac{\sqrt{6}}{8}(|40\cdots0\rangle + |040\cdots0\rangle + \cdots + |0\cdots04\rangle)_{1\cdots d} \\
&= \frac{\sqrt{6}}{2^{2m-1}}(|40\cdots0\rangle + |040\cdots0\rangle + \cdots + |0\cdots04\rangle)_{1\cdots d}.
\end{aligned} \tag{4.22}$$

Then, after the amplitude modulation introduced by the two sets of FSFs, the state turns into

$$\begin{aligned}
&\frac{\sqrt{6}}{2^{2m-1}}(|40\cdots0\rangle + |040\cdots0\rangle + \cdots + |0\cdots04\rangle)_{1\cdots d} \\
&\rightarrow \frac{\sqrt{6}}{2^{2m-1}}\left[(\sqrt{\frac{2}{3}})^{d+4}(1-\frac{4}{2})\right]\left[(\sqrt{\frac{1}{2}})^{d+4}(1-\frac{4}{1})\right] \\
&\quad (|40\cdots0\rangle + |040\cdots0\rangle + \cdots + |0\cdots04\rangle)_{1\cdots d} \\
&= \frac{\sqrt{6}}{2^{2m-1}3^{2^{m-1}+1}}(|40\cdots0\rangle + |040\cdots0\rangle + \cdots + |0\cdots04\rangle)_{1\cdots d}.
\end{aligned} \tag{4.23}$$

The efficiency is then given by $(d = 2^m)$

$$p_{(4.3.2)} = d|\frac{\sqrt{6}}{2^{2m-1}3^{2^{m-1}+1}}|^2 = \frac{1}{2^{3m-3}3^{2^m+1}} = \frac{8}{d^3 3^{d+1}}. \tag{4.24}$$

Actually, this scheme can be simplified for the case of $d = 4$, as shown in Fig. 4.5, where a phase shifter with $\pi/2$ is applied after BS_{34} in mode 3, such that the 4 single

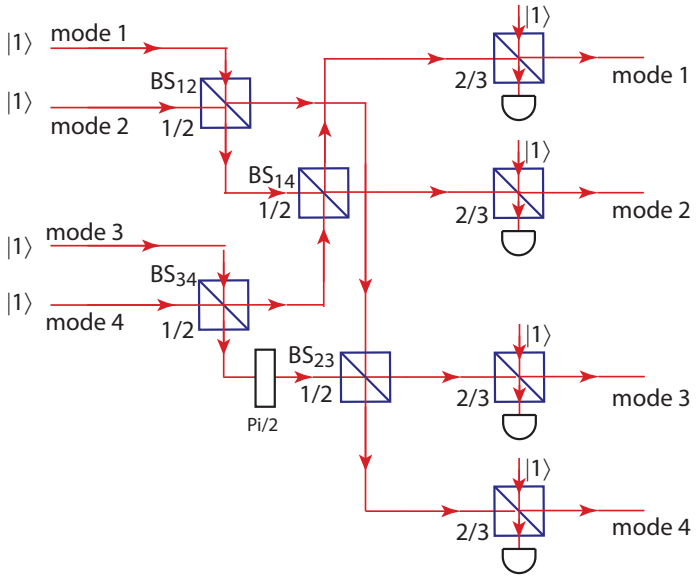

Figure 4.5. Four-mode 4-photon NOON state generation using single photons. Transmissivity as shown.

photons passing through 4 beam splitters and a phase shifter evolves into:

$$
\begin{aligned}
& U_{14}U_{23}e^{i\pi/2a_3^\dagger a_3}U_{12}U_{34}|1,1,1,1\rangle_{1234} \\
&= \frac{\sqrt{6}}{8}\left(|4000\rangle_{1234} - |0400\rangle_{1234} - |0040\rangle_{1234} + |0004\rangle_{1234}\right) \\
&+ \frac{1}{4}\left(|2002\rangle_{1234} - |0220\rangle_{1234}\right) \\
&+ \frac{\sqrt{2}i}{4}\left(|2110\rangle_{1234} - |1201\rangle_{1234} - |0112\rangle_{1234} + |1021\rangle_{1234}\right).
\end{aligned}
\tag{4.25}
$$

In this case, only one set of FSFs with BS transmissivity 1/2 is required to cancel out terms with 2 photons (i.e., all non-NOON components). The efficiency for this 4-mode 4-photon NOON state is 1.46×10^{-2}.

4.4. Methods using FSF and nondeterministic-photon-number states

In this section, a universal model for multi-mode NOON state generation using nondeterministic-photon-number states and post-selection with the assistance of Fock

state filters is proposed. The main difference between this section and Section 4.3 is that the illuminating light sources utilized in this section are easier to implement in experiments. These states include coherent states and squeezed vacuum states. Since such a state is usually the superposition of different photon-number components, the photon number of the state is not well determined, and hence proper post-selection of terms with the total number of photons equal to N is required in order to extract the N-photon NOON components for quantum metrology applications. In the following, we assume that the application is in estimating a phase object with $(d-1)$ unknown phases.

The universal model is sketched in Fig. 4.6(a). The model is composed of a d-mode input state, M basic blocks (dashed boxes), and a post-selection of total N-photon terms at the final stage after the state interacts with the phase object characterized by $(\varphi_1, \varphi_2, \cdots, \varphi_{d-1})$. Note that the dth mode is used as the reference mode. Each basic block then contains d identical FSFs (purple boxes), canceling unexpected non-NOON components from the probing state. The block number M is optimally determined according to the photon number distribution of the input d-mode state in order to minimize the number of FSFs required.

Specifically, three input scenarios are investigated in this section, which are (1) the coherent mixture of d coherent states (Fig. 4.6(b1)), (2) the coherent mixture of d single-mode squeezed vacuum states or $d/2$ two-mode squeezed vacuum states with the two modes of each TMSV combined on a 50:50 BS (even-N) (Fig. 4.6(b2)), and (3) one TMSV split into d modes (even-N) with canceled relative phase shifts among d arms ($d = 2^q$ with $q = 1, 2, \cdots$) (Fig. 4.6(b3)). These three input scenarios are

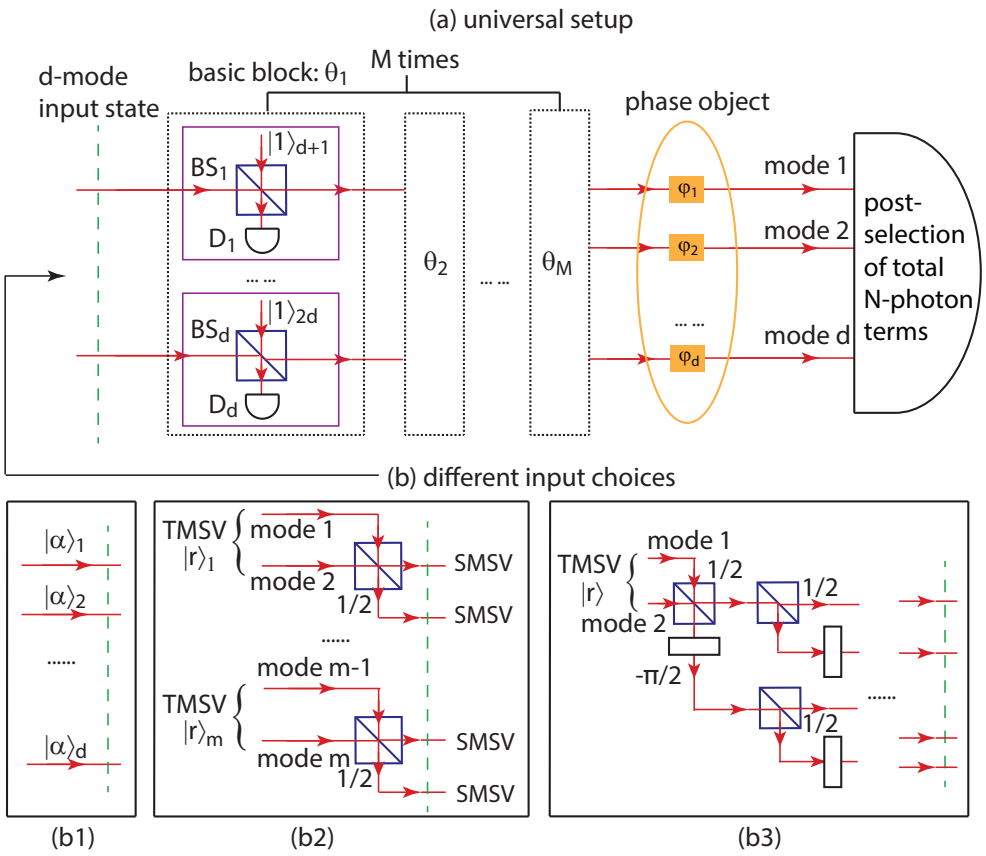

Figure 4.6. (a) The universal model for d-mode N-photon NOON state generation using FSFs, nondeterministic-photon-number states and post-selection. (b) Different input choices: (b1) a coherent mixture of d coherent states, (b2) a coherent mixture of d SMSVs or $d/2$ TMSVs, (b3) single TMSV split into d modes.

discussed in detail below, and the generation probability for each method is calculated.

4.4.1 Generation using d coherent states [96]

The first input choice being studied here is a coherent mixture of d identical coherent states, as shown in Fig. 4.6(b1), which is denoted as $|\alpha\rangle_1|\alpha\rangle_2\cdots|\alpha\rangle_d$. This work was published in [97, 98]. The detailed state transformation steps for this case are derived below, while simplification, as adopted in Section 4.3.2, is taken for the other two scenarios. The d coherent states passing through M basic blocks result in a

tensor product of d coherent-like states with missing 1- to M-photon terms. In order to generate a multi-mode NOON state with N photons, M is optimally chosen to be $M_1 = \lfloor N/2 \rfloor$, which minimizes the number of basic blocks required for each N. Under this configuration, when the post-selection on a total of N photons in all of the output modes is performed, one can project out the multi-mode NOON state in the final detection stage.

More explicitly, the state after adding d single photons using d beam splitters in the kth block can be written as

$$\begin{aligned}&\left[\bigotimes_{j=1}^{d} U^k_{j,d+j}\right] |\alpha, \cdots, \alpha\rangle_{1\cdots d} |1, \cdots, 1\rangle_{d+1,\ldots,2d} = \bigotimes_{j=1}^{d} \left[U^k_{j,d+j} |\alpha\rangle_j |1\rangle_{d+j}\right] \\ &= \bigotimes_{j=1}^{d} \left[e^{-\frac{|\alpha|^2}{2}} \sum_{n_j=0}^{\infty} \frac{\alpha^{n_j}}{n_j!} \left(\cos\theta_k a_j^\dagger + i \sin\theta_k a_{d+j}^\dagger\right)^{n_j} \left(\cos\theta_k a_{d+j}^\dagger + i \sin\theta_k a_j^\dagger\right) |0\rangle_{j,d+j} \right],\end{aligned} \tag{4.26}$$

where $U^k_{j,d+j} = \exp\left[i\theta_k (a_j^\dagger a_{d+j} + a_j a_{d+j}^\dagger)\right]$ is the unitary operator of BS_j with transmissivity $\cos^2\theta_k$ in the $j$the FSF ($j = 1, 2, \cdots, d$). A d-fold SPCD at $\{\mathrm{D}_j\}$ is then applied, projecting the state into

$$|\psi\rangle^{(4.4.1),k}_{1\cdots d} \propto \bigotimes_{j=1}^{d} \left[e^{-\frac{|\alpha|^2}{2}} \sum_{n_j=0}^{\infty} \frac{\alpha^{n_j}}{n_j!} \left[\cos^{n_j+1}\theta_k \left(1 - n_j \tan^2\theta_k\right)\right] a_j^{\dagger n_j} |0\rangle_j \right]. \tag{4.27}$$

Repeatedly applying this basic block M_1 times with different θ_k ($k = 1, \cdots, M_1$), the output state becomes

$$|\psi\rangle^{(4.4.1)}_{1\cdots d} \propto \bigotimes_{j=1}^{d} \left[e^{-\frac{|\alpha|^2}{2}} \sum_{n_j=0}^{\infty} \frac{\alpha^{n_j}}{n_j!} \left[\prod_{k=1}^{M_1} \cos^{n_j+1}\theta_k \left(1 - n_j \tan^2\theta_k\right)\right] a_j^{\dagger n_j} |0\rangle_j \right]. \tag{4.28}$$

If θ_k is chosen to be $\theta_k = \arctan(1/\sqrt{k})$ (i.e., $\cos^2\theta_k = k/(k+1)$), any term in $|\psi\rangle_{1\cdots d}^{(4.4.1)}$ with $n_j = k$ for any mode j is canceled out. In other words, the 1- to M_1-photon terms in any of the d modes disappear after the M_1 basic blocks, leaving the output state as

$$|\psi\rangle_{1\cdots d}^{(4.4.1)} \propto \bigotimes_{j=1}^{d} \left[e^{-\frac{|\alpha|^2}{2}} \left[\frac{1}{\sqrt{M_1+1}}|0\rangle_j + \sum_{n_j=M_1+1}^{\infty} \frac{\alpha^{n_j}}{\sqrt{n_j!}} \left(\frac{1}{M_1+1}\right)^{\frac{n_j+1}{2}} \frac{(n_j-1)!(-1)^{M_1}}{(n_j-M_1-1)!M_1!}|n_j\rangle_j \right] \right]. \tag{4.29}$$

Finally, after the output state (4.29) probes onto a target for multiple phase estimation, a post-selection on a total of exactly N photons in all the output modes $1\cdots d$ is performed as sketched in the right half of Fig. 4.6(a). Then only the NOON state components having all of the N photons in one mode $|N\rangle$ and no photons in any other mode $|0\rangle$ can contribute to the final detection. Eventually, the d-mode N-photon NOON state generated upon the post-selection and triggering can be obtained as

$$|\phi\rangle_{1\cdots d}^{(4.4.1)} \propto c_{(4.4.1)}(|N0\cdots0\rangle + |0N0\cdots0\rangle + \cdots + |0\cdots0N\rangle)_{1\cdots d}, \tag{4.30}$$

where

$$c_{(4.4.1)} = e^{-d\frac{|\alpha|^2}{2}} \frac{(-1)^{M_1}\alpha^N(N-1)!}{\sqrt{M_1+1}^{N+d}\sqrt{N!}(N-M_1-1)!M_1!}. \tag{4.31}$$

The intrinsic generation probability of the d-mode N-photon NOON state using d

coherent states is

$$p_{(4.4.1)} = d|c_{(4.4.1)}|^2 = \frac{de^{-d|\alpha|^2}|\alpha|^{2N}(N-1)!}{(M_1+1)^{N+d}N(N-M_1-1)!^2M_1!^2}, \tag{4.32}$$

which is a function of $|\alpha|^2$, N, and d. It can be maximized at $|\alpha^{\rm opt}_{(4.4.1)}|^2 = N/d$, giving

$$p^{\rm opt}_{(4.4.1)} = \frac{e^{-N}N^{N-2}N!}{d^{N-1}\,(M_1+1)^{N+d}\,(N-M_1-1)!^2M_1!^2}. \tag{4.33}$$

Under this optimization, the use of a coherent mixture of d coherent states with $|\alpha^{\rm opt}_{(4.4.1)}|^2 = N/d$ is equivalent to splitting a single coherent state with intensity $|\alpha_{\rm single}|^2 = N$ into balanced d modes.

4.4.2 Generation using d single-mode squeezed vacuum states [99]

In this section, the coherent mixture of d single-mode squeezed vacuum states is considered to be the probing state, which is equivalent to the coherent mixture of $m = d/2$ two-mode squeezed vacuum states with the two output modes of each TMSV combined on a 50:50 BS, in order to generate a d-mode NOON state with $N = 2n$ photons ($n = 1, 2, \cdots$). The phase of the SMSV or TMSV is chosen to be 0. This work is in preparation to be submitted soon.

It is interesting to note that the SMSVs contain the even-photon-number components only. That is to say, only even-photon-number non-NOON components need to be filtered out. This enables the reduction of the number of basic blocks to $M_2 = \lfloor N/4 \rfloor$, with BS transmissivity in the kth block being $T_2 = 2k/(2k+1)$.

Moreover, with this input choice, the generations of the multi-mode NOON states with $N = 4x$ and $N = 4x + 2$ ($x = 1, 2, \cdots$) require the same x basic blocks. The only difference is the post-selection of N photons in the readout. In other words, x basic blocks can be utilized to effectively generate NOON states with up to $(4x + 2)$ photons.

The coherent mixture of d SMSVs is shown in Fig. 4.6(b2). As a result of the post-selection of total N photons at the output ends, all of the events with less or more than N photons are discarded at the final detection stage. Under the condition of total N photons in all d modes, the probing state

$$\prod_{x=1}^{d} \frac{1}{\sqrt{\cosh r}} \sum_{y=0}^{N/2} \frac{(\tanh r)^y}{y! 2^y} a_x^{\dagger 2y} |0\rangle_x \tag{4.34}$$

then successively passes through $M_2 = \lfloor N/4 \rfloor$ sets of FSFs, where the BSs with transmissivity $2k/(2k+1)$ in the kth block filter out terms with $2k$ and $(N-2k)$ photons in any mode. Eventually, all of the even-photon-number non-NOON components with $2, 4, \cdots, (N-2)$ photons in each mode are discarded. This means that any term with $y = 1, 2, \cdots, (N/2-1)$ in Eq. (4.34) is canceled out after the FSFs, if only N-photon events are of concern. Therefore, only the term with all of the N photons coming from one SMSV

$$\sum_{x=1}^{d} \frac{1}{\sqrt{\cosh r}^d} \frac{(\tanh r)^{N/2}}{(N/2)! 2^{N/2}} a_x^{\dagger N} |0 \cdots 0\rangle \tag{4.35}$$

survives after the whole setup and post-selection. Then, counting in the amplitude

modulation on the NOON components introduced by the FSFs, the state evolves into

$$
\begin{aligned}
&|\phi\rangle_{1\cdots d}^{(4.4.2)} \\
&\propto \sum_{x=1}^{d} \frac{1}{\sqrt{\cosh r}^{d}} \frac{(\tanh r)^{N/2}}{(N/2)!2^{N/2}} \left[\prod_{k=1}^{M_2} \cos^{N+d}\theta_k'(1-N\tan^2\theta_k')\right] a_x^{\dagger N}|0\cdots 0\rangle \\
&= \sum_{x=1}^{d} \frac{(\tanh r)^{N/2}\sqrt{N!}(-1)^{M_2}2^{(N+d)M_2+1}M_2!^{N+d-1}}{\cosh^{d/2} r\sqrt{2}^{N} N(2M_2+1)!^{(N+d)/2}(N/2-M_2-1)!}|N\rangle_x|0\cdots 0\rangle,
\end{aligned}
\tag{4.36}
$$

with $\theta_k' = \arctan(1/\sqrt{2k})$. The generation efficiency is

$$
\begin{aligned}
p_{(4.4.2)} &= d\Big|\frac{(\tanh r)^{N/2}\sqrt{N!}(-1)^{M_2}2^{(N+d)M_2+1}M_2!^{N+d-1}}{\cosh^{d/2} r\sqrt{2}^{N} N(2M_2+1)!^{(N+d)/2}(N/2-M_2-1)!}\Big|^2 \\
&= d\frac{\tanh^N rN!}{\cosh^d rN^2}\frac{2^{2(N+d)M_2-N+2}M_2!^{2(N+d-1)}}{(2M_2+1)!^{N+d}(N/2-M_2-1)!^2},
\end{aligned}
\tag{4.37}
$$

which can be maximized at $\sinh^2 r_{(4.4.2)}^{\text{opt}} = N/d$, giving

$$
p_{(4.4.2)}^{\text{opt}} = \frac{d^{d/2+1}\sqrt{N}^{N-2}(N-1)!2^{2M_2(N+d)-N+2}M_2!^{2(N+d-1)}}{\sqrt{d+N}^{d+N}(2M_2+1)!^{N+d}(N/2-M_2-1)!^2}. \tag{4.38}
$$

4.4.3 Generation using one two-mode squeezed vacuum state [99]

Since any d-mode input state containing both NOON components and non-NOON components for a certain N has the potential to generate a NOON state with the help of FSFs, the scenario of using only one TMSV split into $d = 2^p$ modes ($p = 1, 2, \cdots$) is discussed in this section to generate a d-mode $N = 2n$ NOON state. $M_1 = \lfloor N/2 \rfloor$ basic blocks with BS transmissivity $k/(k+1)$ are used for this input choice.

Since the post-selection of total N photons is adopted, only the components in

the input with exactly $N = 2n$ photons

$$\frac{1}{\cosh r} \tanh^n r |n, n\rangle_{12} \tag{4.39}$$

are of interest. Modes 1 and 2 are then combined on a 50:50 BS, giving a state

$$e^{i\frac{\pi}{4}(a_1^\dagger a_2 + a_1 a_2^\dagger)} \frac{1}{\cosh r} \tanh^n r |n, n\rangle = \frac{(i \tanh r)^n}{\cosh r n! 2^n} \sum_{x=0}^{n} C_n^x a_1^{\dagger 2x} a_2^{\dagger 2(n-x)} |0, 0\rangle_{12}, \tag{4.40}$$

where only $x = 0$ and $x = n$ terms trigger the final NOON detection, with the same reason as in Section 4.4.2. Afterwards, balanced 50:50 BSs are applied on each of the output modes successively in order to split each mode into two modes. Phase shifters with $-\pi/2$ are adopted in each reflected arm of BSs to cancel out the relative phase difference. The contributed NOON components can be expressed as

$$\begin{aligned} &\frac{(i \tanh r)^n}{\cosh r n! 2^n} \frac{1}{\sqrt{2}^{N(\log_2 d - 1)}} \left(a_1^{\dagger N} + a_2^{\dagger N} + \cdots + a_d^{\dagger N} \right) |0, 0\rangle_{12} \\ &= \sum_{x=1}^{d} \frac{(i \tanh r)^n \sqrt{N!}}{\cosh r n! d^{N/2}} |N\rangle_x |0 \cdots 0\rangle. \end{aligned} \tag{4.41}$$

The above NOON state components, after M_1 sets of FSFs and amplitude modulation, turn into

$$\begin{aligned} &|\phi\rangle_{1 \cdots d}^{(4.4.3)} \\ &\propto \sum_{x=1}^{d} \frac{(i \tanh r)^n \sqrt{N!}}{\cosh r n! d^{N/2}} \prod_{k=1}^{M_1} \cos^{N+d} \theta_k (1 - N \tan^2 \theta_k) |N\rangle_x |0 \cdots 0\rangle \\ &= \sum_{x=1}^{d} \frac{(i \tanh r)^{N/2} \sqrt{N!} (-1)^{M_1} (N-1)!}{\cosh r \, (N/2)! d^{N/2} M_1! (N - M_1 - 1)! (M_1 + 1)^{(N+d)/2}} |N\rangle_x |0 \cdots 0\rangle. \end{aligned} \tag{4.42}$$

The efficiency is then

$$p_{(4.4.3)} = \frac{\tanh^N r N!(N-1)!^2}{\cosh^2 r d^{N-1}(N/2)!^2 M_1!^2 (N-M_1-1)!^2 (M_1+1)^{N+d}}, \tag{4.43}$$

which is optimized at $\sinh^2 r^{\text{opt}}_{(4.4.3)} = N/2$, giving

$$p^{\text{opt}}_{(4.4.3)} = \frac{2\sqrt{N}^N N!(N-1)!^2}{(N+2)^{N/2+1} d^{N-1}(N/2)!^2 (M_1+1)^{N+d}(N-M_1-1)!^2 M_1!^2}. \tag{4.44}$$

Both N and M_1 appear in the calculations in this section since they denote the photon number and the number of basic blocks, respectively, notwithstanding $N = 2M_1$. Note that this setup can be simplified for two-mode NOON state generation, since only even-photon-number terms exist in that case, which corresponds to Section 4.4.2.

4.5. Comparisons and summary

In this section, comparisons among the proposed methods of generating multi-mode NOON states are made with respect to their feasibility and efficiency. The major strength and weakness of each method are summarized in Table 4.1.

The cross-Kerr method in Section 4.1 requires the simultaneous application of multiple cross-Kerr nonlinear media, whose nonlinearity degree $\chi = \pi$ is extremely large and experimentally difficult to reach using current technologies. However, it has the highest generation efficiency $p_{(4.1)} = 1/d$, inversely proportional to the mode number d, and it requires relatively low number of single photon detectors, BSs and PSs. Such a large nonlinearity, if achieved, could be used to make an efficient optical

Table 4.1. Comparisons among the proposed methods for multi-mode NOON state generation.

Section	Input	Other resources	Major strength	Major weakness
4.1	one $\|N\rangle$ $(d-1)$ $\|1\rangle$	$(d-1)$ cross-Kerr media $(d-1)$ single photon detectors $4(d-1)$ BSs $(d-1)$ PSs	highest efficiency	high cross-Kerr nonlinearity
4.2 (even)	d $\|N\rangle$	$N(d-1)$ single photon detectors $3N(d-1)/2$ BSs $N(d-1)/2$ PSs	arbitrary N	low efficiency
4.3.1	one $\|N\rangle$ $d\lfloor N/2\rfloor$ $\|1\rangle$	$d\lfloor N/2\rfloor$ single photon detectors $(d\lfloor N/2\rfloor + d - 1)$ BSs d PSs	arbitrary N	low efficiency
4.3.2	$(2d+4)$ $\|1\rangle$	$2d$ single photon detectors $3d$ BSs	high efficiency with $d = 4$	works for 4-photon NOON state
4.4.1	d $\|\alpha\rangle$ $d\lfloor N/2\rfloor$ $\|1\rangle$	$d\lfloor N/2\rfloor$ single photon detectors $d\lfloor N/2\rfloor$ BSs	feasible input	low efficiency
4.4.2	d $\|r\rangle_1$ $d\lfloor N/4\rfloor$ $\|1\rangle$	$d\lfloor N/4\rfloor$ single photon detectors $d\lfloor N/4\rfloor$ BSs	high efficiency	coherent generation of multiple $\|r\rangle$
4.4.3	one $\|r\rangle_{12}$ $d\lfloor N/2\rfloor$ $\|1\rangle$	$d\lfloor N/2\rfloor$ single photon detectors $(d\lfloor N/2\rfloor + d - 1)$ BSs $(d-1)$ PSs	feasible input	low efficiency

quantum computer, but this is regarded as impossible with current technologies. Even though the nonlinear method seems promising, it is practically infeasible.

The method in Section 4.2 requires the coherent generation of d Fock states whose photon number N is exactly the mean photon number for the expected NOON state. The coherent generation of multiple Fock states is infeasible to achieve, and it requires more optical devices compared to other methods for fixed d and N. The action of reducing 1 or 2 photons successively from $N(d-1)$-fold SPCD in order to generate entanglement results in an extremely low efficiency that is not even comparable with the other methods.

With all the above concerns, the efficiency comparisons below are only made among the methods using a single Fock input in Section 4.3.1, a 4-photon NOON state generation using 4 single photons in Section 4.3.2, the methods using multiple coherent states in Section 4.4.1, multiple SMSVs or TMSVs in Section 4.4.2, and a single TMSV in Section 4.4.3.

The intrinsic generation efficiencies for these five input scenarios, under the assumption that all of the devices are lossless, is shown below with the corresponding

optimization conditions:

$$
\begin{aligned}
p_{(4.3.1)} &= \frac{(N-1)!^2}{d^{N-1}(M_1+1)^{N+d}(N-M_1-1)!^2 M_1!^2}, \\
p_{(4.3.2)} &= \frac{8}{d^3 3^{d+1}}, \\
p^{\text{opt}}_{(4.4.1)} &= \frac{e^{-N}N^{N-2}N!}{d^{N-1}\,(M_1+1)^{N+d}\,(N-M_1-1)!^2 M_1!^2}, \quad \text{where } |\alpha^{\text{opt}}_{(4.4.1)}|^2 = N/d, \\
p^{\text{opt}}_{(4.4.2)} &= \frac{d^{d/2+1}\sqrt{N}^{N-2}(N-1)!2^{2M_2(N+d)-N+2}M_2!^{2(N+d-1)}}{\sqrt{d+N}^{d+N}(2M_2+1)!^{N+d}(N/2-M_2-1)!^2}, \\
&\quad \text{where } \sinh^2 r^{\text{opt}}_{(4.4.2)} = N/d, \\
p^{\text{opt}}_{(4.4.3)} &= \frac{2\sqrt{N}^{N}N!(N-1)!^2}{(N+2)^{N/2+1}d^{N-1}(N/2)!^2(M_1+1)^{N+d}(N-M_1-1)!^2 M_1!^2}, \\
&\quad \text{where } \sinh^2 r^{\text{opt}}_{(4.4.3)} = N/2.
\end{aligned}
\tag{4.45}
$$

In Eq. (4.45), the generation efficiencies for the last three scenarios are optimized with respect to the coherent amplitude α of the coherent state or the squeezing factor r of the SMSV or TMSV, which are all attained when the mean total photon number of the d-mode probing state is N.

To illustrate the comparisons among the different methods more straightforwardly, the generation efficiencies for fixed photon number $N = 4$ and fixed mode number $d = 4$ are plotted in Fig. 4.7(a) and 4.7(b), respectively. Note that the efficiency of the four-mode 4-photon NOON state generation using single photons is calculated with the simplified setup in Fig. 4.5, in which only one set of FSFs is required. Generally speaking, the generation efficiency decreases exponentially with an increasing mode number d or photon number N. The method using single photons in Section 4.3.2 has the highest efficiency for the case of $d = 4$ and $N = 4$, although it drops quickly

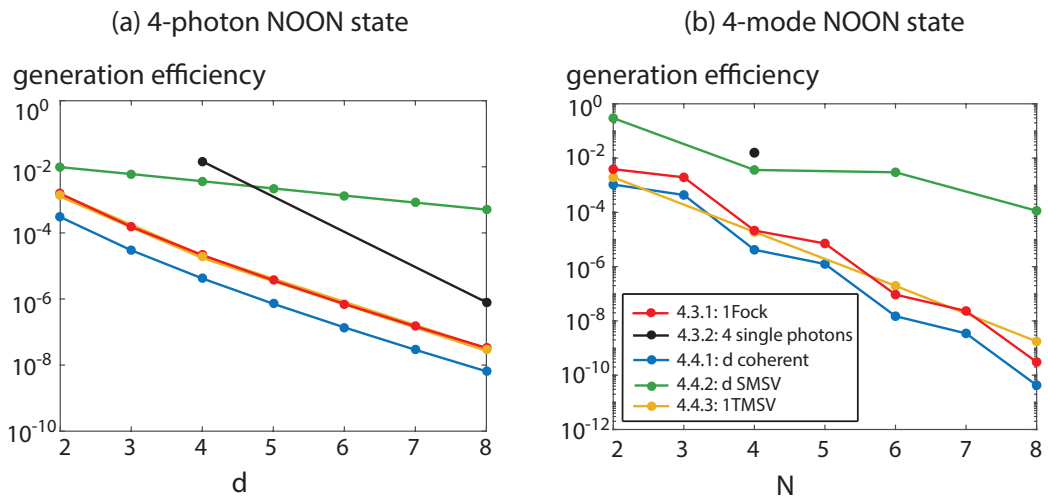

Figure 4.7. Generation efficiencies for (a) fixed photon number $N = 4$, and (b) fixed mode number $d = 4$. The discrete points are connected for better visualization.

with a higher mode number. Since a perfect single photon source usually requires a high-cost nonlinear crystal with a probabilistic triggering process or quantum dots, it is more meaningful to minimize the number of single photons required. In general, method 4.4.2, using a coherent mixture of d SMSVs or $d/2$ TMSVs (green), is the most efficient and stable method, followed by almost a tie between method 4.3.1 using a single Fock state (red) and method 4.4.3 using a single TMSV (yellow), and the least efficient method 4.4.1 using coherent states (blue), in general. It makes sense to some circumstance that the method using coherent states is least efficient, since classical light sources are adopted as the probing states. Recently, 15dB squeezed states of light were detected experimentally [100], corresponding to a squeezing factor $r \approx 2.4$. Given this, the optimization condition $\sinh^2 r^{\text{opt}}_{(4.4.2)} = N/d$ for method 4.4.2 is achievable when N and d are comparable. It is also more feasible in the sense that it requires relatively fewer FSFs, which necessitate single photon catalysts and single photon coincidence detection. As an example, using method 4.4.2, both the

four-mode 4-photon and four-mode 6-photon NOON generations require only 1 set of 4 FSFs. This is considerably easier than the other methods, which all require, respectively, 2 and 3 sets of 4 FSFs. This is also why the plot using scenario 4.4.2 in Fig. 4.7(b) displays a slower decline from the 4-photon case to the 6-photon case.

Chapter 5: Conclusion and future work

5.1. Conclusion

In this dissertation, three types of scalable generation methods of multi-mode NOON states are proposed. These methods can theoretically create NOON states with a high mode number d and a high photon number N. The first method, in Section 4.1, uses multiple cross-Kerr nonlinear media with strong nonlinearity degree $\chi = \pi$ to create an N-photon entanglement with the help of single photons. This method has the highest efficiency, but the nonlinearity requirement is very difficult to achieve. The second method, in Section 4.2, deploys multiple entanglement generators in a cascading configuration, and each generator creates an entanglement by reducing 1 or 2 photons successively from either of the dual-Fock state inputs, without the knowledge of which mode the photons come from. This method is the least efficient method, and it is infeasible in the sense that it requires multiple N-photon Fock states as the input. The third type of methods utilizes Fock state filters, which can cancel out the Fock state with any photon number k depending on the BS transmissivity. Within the methods using FSFs, four specific input scenarios are discussed: an evenly-distributed N-photon d-mode state in Section 4.3.1, a coherent mixture of d coherent states in Section 4.4.1, a coherent mixture of d single-mode squeezed vacuum states

(even-N) in Section 4.4.2, and one two-mode squeezed vacuum state (even-N) split into d modes in Section 4.4.3. The method using a coherent mixture of multiple SMSVs has the highest generation efficiency among these four scenarios, followed by almost a tie between the methods using an N-photon state and a single TMSV, and finally the method using coherent states has the lowest generation efficiency. The method using multiple SMSVs is also more feasible in the sense that it requires relatively fewer FSFs and its optimization is achievable when N and d are comparable. Specifically, an example of generating a four-mode 4-photon NOON state using single photons only is also discussed in Section 4.3.2, which is 4 times more efficient than the method using multiple SMSVs, despite its lower feasibility as a consequence of the single photon requirement. The efficiency of this method drops quickly as d increases.

The benefits of the NOON state in achieving super-resolution and super-sensitivity are discussed. Specifically, the simultaneous estimation of multiple phase parameters is studied using a whole class of multi-mode NOON-like entangled states, where the non-vacuum Fock component in the NOON state can be replaced by any photon-number-distribution state. It is shown that any state in that class can reach the Heisenberg limit with respect to the photon number N, and have an $O(d)$ efficiency enhancement over the individual estimation using multiple two-mode NOON states. Moreover, it is proved that under the same mean photon number, there are plenty of multi-mode entangled states, such as the entangled squeezed vacuum state, which can perform better than the multi-mode NOON state in quantum metrology.

5.2. Future work

The next step of the proposed theoretical work on multi-mode NOON state generation lies in its experimental realization, taking into consideration the imperfection of quantum states, and losses in beam splitters and the measurement process [39, 101]. Although it seems to be impossible to produce multi-mode NOON states with an arbitrary mode number or photon number at this point, in view of the low efficiency, it should be stated that no existing papers have demonstrated multi-mode NOON states with more than 2 photons. This means the realization of 3-/4-photon NOON states with three modes is already a breakthrough, if these states can be achieved effectively.

Now, the two experimental difficulties of the proposed work are the coherent generation of multiple single photons and the coincidence photon-number-resolving detections. The single photon generation has always been an active research field, for both quantum communication and quantum metrology, and this has been widely studied using quantum dots [102–108], or the recently-presented time multiplexing technique [109], in order to reach high levels of purity, indistinguishability, and efficiency. High-efficiency photon-number-resolving detectors have also been reported to be experimentally achievable with high photon number sensitivity [76,110,111]. With these developments, the experimental demonstration of the proposed theoretical work would be a promising future achievement.

References

[1] Schrödinger, E. Discussion of probability relations between separated systems. *Mathematical Proceedings of the Cambridge Philosophical Society* **31**, 555–563 (1935).

[2] Heisenberg, W. The actual content of quantum theoretical kinematics and mechanics (1927).

[3] Boto, A. N., Kok, P., Abrams, D. S. & Braunstein, S. L. Quantum interferometric optical lithography: exploiting entanglement to beat the diffraction limit. *Physical Review Letters* **85**, 2733–2736 (2000).

[4] Lee, H., Kok, P., Cerf, N. J. & Dowling, J. P. Linear optics and projective measurements alone suffice to create large-photon-number path entanglement. *Physical Review A* **65**, 030101 (2002).

[5] Greenberger, D. M., Horne, M. A. & Zeilinger, A. Going beyond Bell's theorem. In *Bell's Theorem, Quantum Theory and Conceptions of the Universe*, 69–72 (Springer, Dordrecht, 1989).

[6] Gerry, C. C. & Campos, R. A. Generation of maximally entangled photonic states with a quantum-optical Fredkin gate. *Physical Review A* **64**, 063814 (2001).

[7] Fiurášek, J. Conditional generation of N -photon entangled states of light. *Physical Review A* **65**, 053818 (2002).

[8] Zou, X. B., Pahlke, K. & Mathis, W. Generation of multi-photon entangled states by using linear optical elements. *Physics Review A* **306**, 014102 (2002).

[9] Kok, P., Lee, H. & Dowling, J. P. Creation of large-photon-number path entanglement conditioned on photodetection. *Physical Review A* **65**, 052104 (2002).

[10] Pryde, G. J. & White, A. G. Creation of maximally entangled photon-number states using optical fiber multiports. *Physical Review A* **68**, 052315 (2003).

[11] Shafiei, F., Srinivasan, P. & Ou, Z. Y. Generation of three-photon entangled state by quantum interference between a coherent state and parametric down-conversion. *Physical Review A* **70**, 043803 (2004).

[12] Eisenberg, H. S., Hodelin, J. F., Khoury, G. & Bouwmeester, D. Multiphoton path entanglement by nonlocal bunching. *Physical Review Letters* **94**, 090502 (2005).

[13] Sun, F. W., Ou, Z. Y. & Guo, G. C. Projection measurement of the maximally entangled N -photon state for a demonstration of the N -photon de Broglie wavelength. *Physical Review A* **73**, 023808 (2006).

[14] Kapale, K. T. & Dowling, J. P. Bootstrapping approach for generating maximally path-entangled photon states. *Physical Review Letters* **99**, 053602 (2007).

[15] Nielsen, A. E. B. & Mølmer, K. Conditional generation of path-entangled optical —N,0> + —0,N> states. *Physical Review A* **75**, 063803 (2007).

[16] Hofmann, H. F. & Ono, T. High-photon-number path entanglement in the interference of spontaneously down-converted photon pairs with coherent laser light. *Physical Review A* **76**, 031806 (2007).

[17] Ono, T. & Hofmann, H. F. Quantum enhancement of N-photon phase sensitivity by interferometric addition of down-converted photon pairs to weak coherent light. *Journal of Physics B: Atomic, Molecular and Optical Physics* **41**, 095502 (2008).

[18] Wolfgramm, F., Cere, A. & Mitchell, M. W. NOON states from cavity-enhanced down-conversion: high quality and super-resolution. *Journal of the Optical Society of America B* **27**, A25–A29 (2010).

[19] Kok, P. Creating large NOON states with imperfect phase control. *Optics and Spectroscopy* **111**, 520–522 (2011).

[20] Mullin, W. J. & Laloë, F. Creation of NOON states by double Fock-state/Bose-Einstein condensates. *Journal of Low Temperature Physics* **162**, 250–257 (2011).

[21] Walther, P. *et al.* De Broglie wavelength of a non-local four-photon state. *Nature* **429**, 158–161 (2004).

[22] Mitchell, M. W., Lundeen, J. S. & Steinberg, A. M. Super-resolving phase measurements with a multiphoton entangled state. *Nature* **429**, 161–164 (2004).

[23] Afek, I., Ambar, O. & Silberberg, Y. High-NOON states by mixing quantum and classical light. *Science* **328**, 879–881 (2010).

[24] Tsang, M. Quantum imaging beyond the diffraction limit by optical centroid measurements. *Physical Review Letters* **102**, 253601 (2009).

[25] Shin, H., Chan, K. W. C., Chang, H. J. & Boyd, R. W. Quantum spatial superresolution by optical centroid measurements. *Physical Review Letters* **107**, 083603 (2011).

[26] Rozema, L. A. *et al.* Scalable spatial superresolution using entangled photons. *Physical Review Letters* **112**, 223602 (2014).

[27] Kok, P., Braunstein, S. L. & Dowling, J. P. Quantum lithography, entanglement and Heisenberg-limited parameter estimation. *Journal of Optics B: Quantum and Semiclassical Optics* **6**, S811 (2004).

[28] Giovannetti, V., Lloyd, S. & Maccone, L. Quantum enhanced measurement: beating the standard quantum limit. *Science* **306**, 1330–1336 (2004).

[29] Nagata, T., Okamoto, R., O'Brien, J. L., Sasaki, K. & Takeuchi, S. Beating the standard quantum limit with four-entangled photons. *Science* **316**, 726–729 (2007).

[30] Okamoto, R. *et al.* Beating the standard quantum limit: phase super-sensitivity of N-photon interferometers. *New Journal of Physics* **10**, 073033 (2008).

[31] Nasr, M. B. *et al.* Quantum optical coherence tomography of a biological sample. *Optics Communications* **282**, 1154–1159 (2009).

[32] Crespi, A. *et al.* Measuring protein concentration with entangled photons. *Applied Physics Letters* **100**, 233704 (2012).

[33] Schwartz, O. *et al.* Superresolution microscopy with quantum emitters. *Nano Letters* **13**, 5832–5836 (2013).

[34] Cui, J. M., Sun, F. W., Chen, X. D., Gong, Z. J. & Cuo, G. C. Quantum statistical imaging of particles without restriction of the diffraction limit. *Physical Review Lettersc* **110**, 153901 (2013).

[35] Ono, T., Okamoto, R. & Takeuchi, S. An entanglement-enhanced microscope. *Nature Communications* **4**, 3426 (2013).

[36] Israel, Y., Rosen, S. & Silberberg, Y. Supersensitive polarization microscopy using NOON states of light. *Physical Review Letters* **112**, 103604 (2014).

[37] Lee, S.-Y., Lee, C.-w., Nha, H. & Kaszlikowski, D. Quantum phase estimation using a multi-headed cat state. *Journal of the Optical Society of America B* **32**, 1186–1192 (2015).

[38] Holland, M. J. & Burnett, K. Interferometric detection of optical phase shifts at the Heisenberg limit. *Physical Review Letters* **71**, 1355–1358 (1993).

[39] Datta, A. *et al.* Quantum metrology with imperfect states and detectors. *Physical Review A* **83**, 063836 (2011).

[40] Xiang, G. Y., Hofmann, H. F. & Pryde, G. J. Optimal multi-photon phase sensing with a single interference fringe. *Scientific Reports* **3**, 2684 (2013).

[41] Joo, J., Munro, W. J. & Spiller, T. P. Quantum metrology with entangled coherent states. *Physical Review Letters* **107**, 083601 (2011).

[42] Joo, J. *et al.* Quantum metrology for nonlinear phase shifts with entangled coherent states. *Physical Review A* **86**, 043828 (2012).

[43] Zhang, Y. R., Jin, G. R., Cao, J. P., Liu, W. M. & Fan, H. Unbounded quantum Fisher information in two-path interferometry with finite photon number. *Journal of Physics A: Mathematical and Theoretical* **46**, 035302 (2013).

[44] Shepard, S. R., Moxley, F. I. I. & Dowling, J. P. Quantum phase representation of Heisenberg limits and a minimally resourced quantum phase estimator. *Physical Review A* **93**, 033805 (2016).

[45] Humphreys, P. C., Barbieri, M., Datta, A. & Walmsley, I. A. Quantum enhanced multiple phase estimation. *Physical Review Letters* **111**, 070403 (2013).

[46] Yue, J. D., Zhang, Y. R. & Fan, H. Quantum-enhanced metrology for multiple phase estimation with noise. *Scientific Reports* **4**, 5933 (2014).

[47] Motes, K. R. *et al.* Linear optical quantum metrology with single photons: exploiting spontaneously generated entanglement to beat the shot-noise limit. *Physical Review Letters* **114**, 170802 (2015).

[48] Liu, J., Jing, X. X. & Wang, X. Quantum metrology with unitary parametrization processes. *Scientific Reports* **5**, 8565 (2015).

[49] Ciampini, M. A. *et al.* Quantum-enhanced multiparameter estimation in multiarm interferometers. *Scientific Reports* **6**, 28881 (2016).

[50] Knott, P. A. *et al.* Local versus global strategies in multiparameter estimation. *Physical Review A* **94**, 062312 (2016).

[51] Gagatsos, C. N., Branford, D. & Datta, A. Gaussian systems for quantum-enhanced multiple phase estimation. *Physical Review A* **94**, 042342 (2016).

[52] Szczykulska, M., Baumgratz, T. & Datta, A. Multi-parameter quantum metrology. *Advances in Physics: X* **1**, 621–639 (2016).

[53] Liu, J., Lu, X. M., Sun, Z. & Wang, X. Quantum multiparameter metrology with generalized entangled coherent state. *Journal of Physics A: Mathematical and Theoretical* **49**, 115302 (2016).

[54] Zhang, L., Chan, K. W. C. & Verma, P. K. Quantum multiple phase estimation using balanced multi-mode entangled states. In *Frontiers in Optics/Laser Science (FiO/LS)*, Paper JW4A.194 (Rochester, NY, 2016).

[55] Zhang, L. & Chan, K. W. C. Quantum multiparameter estimation with generalized balanced multimode NOON-like states. *Physical Review A* **95**, 032321 (2017).

[56] You, C. *et al.* Multiparameter estimation with single photons - linearly-optically generated quantum entanglement beats the shotnoise limit. *Journal of Optics* **19**, 124002 (2017).

[57] Walls, D. F. & Milburn, G. J. *Quantum otics* (Springer Science & Business Media, 2007).

[58] Hofheinz, M. *et al.* Generation of Fock states in a superconducting quantum circuit. *Nature* **454**, 310–314 (2008).

[59] Motes, K. R. *et al.* Efficient recycling strategies for preparing large Fock states from single-photon sources: applications to quantum metrology. *Physical Review A* **94**, 012344 (2016).

[60] Michler, P. *et al.* A quantum dot single-photon turnstile device. *Science* **290**, 2282–2285 (2000).

[61] Hong, C. K. & Mandel, L. Experimental realization of a localized one-photon state. *Physical Review Letters* **56**, 58 (1986).

[62] Scully, M. O. & Zubairy, M. S. *Quantum optics* (Cambridge University Press, 1997).

[63] Miller, W. *Symmetry groups and their applications* (Academic Press, 1973).

[64] Truax, D. R. Baker-Campbell-Hausdorff relations and unitarity of SU (2) and SU (1, 1) squeeze operators. *Physical Review D* **31**, 1988 (1985).

[65] Wu, L. A., Kimble, H. J., Hall, J. L. & Wu, H. Generation of squeezed states by parametric down conversion. *Physical Review Letters* **57**, 2520 (1986).

[66] Hong, C. K., Ou, Z. Y. & Mandel, L. Measurement of subpicosecond time intervals between two ohotons by interference. *Physical Review Letters* **59**, 2044 (1987).

[67] Nielsen, M. A. & Chuang, I. L. *Quantum computation and quantum information* (Cambridge university press, 2010).

[68] Sanaka, K., Resch, K. J. & Zeilinger, A. Filtering out photonic fock states. *Physical Review Letters* **96**, 083601 (2006).

[69] Helstrom, C. W. *Quantum detection and estimation theory* (Academic, New York, 1976).

[70] Born, M. & Wolf, E. *Principles of optics: electromagnetic theory of propagation, interference and diffraction of light* (Elsevier, 2013).

[71] Braunstein, S. L. & Caves, C. M. Statistical distance and the geometry of quantum states. *Physical Review Letters* **72**, 3439–3443 (1994).

[72] Lee, H., Kok, P. & Dowling, J. P. A quantum Rosetta stone for interferometry. *Journal of Modern Optics* **49**, 2325–2338 (2002).

[73] Agarwal, G. S., Boyd, R. W., Nagasako, E. M. & Bentley, S. J. Comment on "quantum interferometric optical lithography: exploiting entanglement to beat the diffraction limit". *Physical Review Letters* **86**, 1389 (2001).

[74] Giovannetti, V., Lloyd, S., MacCone, L. & Shapiro, J. H. Sub-Rayleigh-diffraction-bound quantum imaging. *Physical Review A* **79**, 013827 (2009).

[75] Achilles, D., Silberhorn, C., Sliwa, C., Banaszek, K. & Walmsley, I. A. Fiber-assisted detection with photon number resolution. *Optics letters* **28**, 2387–2389 (2003).

[76] Divochiy, A. & al, E. Superconducting nanowire photon number resolving detector at telecom wavelength. *Nature Photonics* **2**, 302 (2008).

[77] Taylor, M. A. & Bowen, W. P. Quantum metrology and its application in biology. *Physics Reports* **615**, 1–59 (2016).

[78] Bollinger, J. J., Itano, W. M., Wineland, D. J. & Heinzen, D. J. Optimal frequency measurements with maximally correlated states. *Physical Review A* **54**, R4649–R4652 (1996).

[79] Campos, R. A., Gerry, C. C. & Benmoussa, A. Optical interferometry at the Heisenberg limit with twin Fock states and parity measurements. *Physical Review A* **68**, 023810 (2003).

[80] Dowling, J. P. Correlated input-port, matter-wave interferometer: quantum-noise limits to the atom-laser gyroscope. *Physical Review A* **57**, 4736–4746 (1998).

[81] Cramér, H. *Mathematical methods of statistics (PMS-9)* (Princeton university press, 2016).

[82] Braunstein, S. L., Caves, C. M. & Milburn, G. J. Generalized uncertainty relations: Theory, examples, and Lorentz invariance. *Annals of Physics* **247**, 135–173 (1995).

[83] Pezzè, L. *et al.* Optimal measurements for simultaneous quantum estimation of multiple phases. *Physical Review Letters* **119**, 130504 (2017).

[84] Baumgratz, T. & Datta, A. Quantum enhanced estimation of a multidimensional field. *Physical Review Letters* **116**, 030801 (2016).

[85] Kok, P., Dunningham, J. & Ralph, J. F. Role of entanglement in calibrating optical quantum gyroscopes. *Physical Review A* **95**, 012326 (2017).

[86] Jarzyna, M. & Demkowicz-Dobrzański, R. Quantum interferometry with and without an external phase reference. *Physical Review A* **85**, 011801 (2012).

[87] Paris, M. G. A. Quantum estimation for quantum technology. *International Journal of Quantum Information* **7**, 125–137 (2009).

[88] Matsumoto, K. A new approach to the Cramér–Rao-type bound of the pure-state model. *Journal of Physics A: Mathematical and Theoretical* **35**, 3111 (2002).

[89] Agarwal, G. S. *Quantum Optics* (Cambridge University Press, 2013).

[90] Knott, P. A., Proctor, T. J., Hayes, A. J., Cooling, J. P. & Dunningham, J. A. Practical quantum metrology with large precision gains in the low-photon-number regime. *Physical Review A* **93**, 033859 (2016).

[91] Lee, S.-y., Lee, C.-w., Lee, J. & Nha, H. Quantum phase estimation using path-symmetric entangled states. *Scientiific Reports* **6**, 30306 (2016).

[92] Birrittella, R., Mimih, J. & Gerry, C. C. Multiphoton quantum interference at a beam splitter and the approach to Heisenberg-limited interferometry. *Physical Review A* **86**, 063828 (2012).

[93] Birrittella, R. & Gerry, C. C. Quantum optical interferometry via the mixing of coherent and photon-subtracted squeezed vacuum states of light. *Journal of the Optical Society of America B* **31**, 586–593 (2014).

[94] Gong, Q. K. *et al.* Intramode-correlation-enhanced phase sensitivities in an SU(1,1) interferometer. *Physical Review A* **96**, 033809 (2017).

[95] Sivakumar, S. Superposed coherent states improve fidelity of NOON states generated in post-selection. *Canadian Journal of Physics* **93**, 373–376 (2015).

[96] Zhang, L. & Chan, K. W. C. Scalable generation of multi-mode NOON states for quantum multiple-phase estimation. *arXiv* 1712.00128 (2017).

[97] Zhang, L. & Chan, K. W. C. Generation of multi-mode NOON states with three photons using linear optics. In *Frontiers in Optics/Laser Science (FiO/LS)*, Paper JW4A.22 (Washington D.C., 2017).

[98] Zhang, L. & Chan, K. W. C. Generation of multi-mode high-NOON states. In *Quantum Communication, Measurement and Computing (QCMC)* (Baton Rouge, LA, 2018).

[99] Zhang, L. & Chan, K. W. C. Universal multi-mode NOON state generation using nondeterministic-photon-number inputs and post-selection (in preparation, 2018).

[100] Vahlbruch, H., Mehmet, M., Danzmann, K. & Schnabel, R. Detection of 15 dB squeezed states of light and their application for the absolute calibration of photoelectric quantum efficiency. *Physical Review Letters* **117**, 110801 (2016).

[101] Ono, T. & Hofmann, H. F. Effects of photon losses on phase estimation near the Heisenberg limit using coherent light and squeezed vacuum. *Physical Review A* **81**, 033819 (2010).

[102] Reimer, M. E. *et al.* Bright single-photon sources in bottom-up tailored nanowires. *Nature Communications* **3**, 737 (2012).

[103] Wei, Y. J. *et al.* Deterministic and robust generation of single photons from a single quantum dot with 99.5% indistinguishability using adiabatic rapid passage. *Nano Letters* **14**, 6515–6519 (2014).

[104] Kuhlmann, A. V. *et al.* Transform-limited single photons from a single quantum dot. *Nature Communications* **6**, 8204 (2015).

[105] Somaschi, N. *et al.* Near-optimal single-photon sources in the solid state. *Nature Photonics* **10**, 340–345 (2016).

[106] Ding, X. *et al.* On-Demand single photons with high extraction efficiency and near-unity indistinguishability from a resonantly driven quantum dot in a micropillar. *Physical Review Letters* **116**, 020401 (2016).

[107] Wang, H. *et al.* Near-transform-limited single photons from an efficient solid-state quantum emitter. *Physical Review Letters* **116**, 213601 (2016).

[108] Wang, H. *et al.* High-efficiency multiphoton boson sampling. *Nature Photonics* **11**, 361–365 (2017).

[109] Kaneda, F. & Kwiat, P. G. High-efficiency single-photon generation via large-scale active time multiplexing. *arXiv* 1803.04803 (2018).

[110] Lita, A. E., Miller, A. J. & Nam, S. W. Counting near-infrared single-photons with 95% efficiency. *Optics Express* **16**, 3032–3040 (2008).

[111] Calkins, B. *et al.* High quantum-efficiency photon-number-resolving detector for photonic on-chip information processing. *Optics Express* **21**, 22657–22670 (2013).

[112] Zhang, L., Chan, K. W. C. & Verma, P. K. Universal optimal estimation of the polarization of light with arbitrary photon statistics. *Physical Review A* **93**, 032137 (2016).

Appendix A: Universal optimal measure for the polarization estimation of light with arbitrary photon statistics [112]

As mentioned in Section 2.2.1, optimal measurement has different definitions depending on the choice of metric. One choice is the ability to saturate QCRB with respect to the uncertainty limit, and the other choice is the ability to maximize the likelihood function, where the measurement is called the maximum-likelihood POVM. In this appendix, a universal continuous optimal maximum-likelihood measurement of the polarization of light with arbitrary photon statistics is given as an example. This work was published in [112].

The polarization of light is an important resource with widespread applications. It is used for encoding information in quantum communication protocols, and it can provide additional information in remote sensing and microscopy. In the Fock basis, a polarized single photon is given by $|1\rangle_{\mathbf{r}} = a^\dagger_{\mathbf{r}}|0\rangle$, where

$$a^\dagger_{\mathbf{r}} = \cos\frac{\theta}{2}a^\dagger_H + e^{i\phi}\sin\frac{\theta}{2}a^\dagger_V, \tag{A.1}$$

in which θ and ϕ are the spherical coordinates of the polarization vector $\mathbf{r}$ on the Bloch sphere shown in Fig. A.1, and a_H and a_V are the annihilation operators for the north pole and the south pole, which are designated as the horizontal and vertical

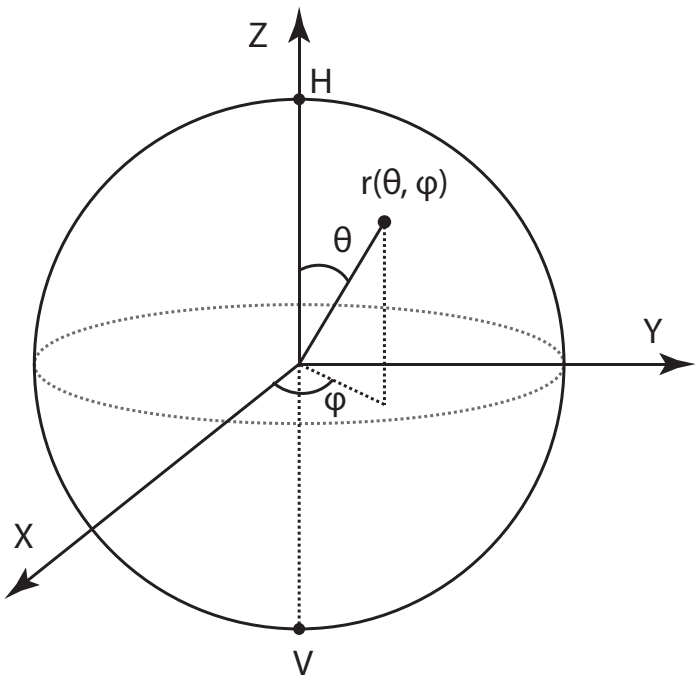

Figure A.1. Bloch sphere. θ and ϕ are spherical coordinates of the polarization vector r. H and V denote the horizontal and vertical polarizations, respectively.

polarizations, respectively.

The operator $a_{\mathbf{r}}$ satisfies the commutation relation

$$[a_{\mathbf{r}}, a^{\dagger}_{\mathbf{r}'}] = {}_{\mathbf{r}}\langle 1|1\rangle_{\mathbf{r}'} \equiv f_{\mathbf{r}\mathbf{r}'}. \tag{A.2}$$

Note that $|f_{\mathbf{r}\mathbf{r}'}|^2 = \frac{1}{2}(1 + \mathbf{r}\cdot\mathbf{r}')$ is the fidelity between two pure qubits with polarizations $\mathbf{r}$ and $\mathbf{r}'$. The n photon Fock state basis is then produced by applying the creation operator $a^{\dagger}_{\mathbf{r}}$ successively, i.e.,

$$|n\rangle_{\mathbf{r}} = \frac{a^{\dagger n}_{\mathbf{r}}}{\sqrt{n!}}|0\rangle. \tag{A.3}$$

It can be shown that ${}_{\mathbf{r}}\langle n|m\rangle_{\mathbf{r}'} = f^{n}_{\mathbf{r}\mathbf{r}'}\delta_{nm}$, where δ_{nm} is the Kronecker delta.

The light source considered here is a multi-photon light beam with a fixed but unknown polarization vector $\mathbf{r}_0$ and the different photon number modes are incoherent with each other. Its density operator is generally written as

$$\rho(\mathbf{r}_0) = \sum_{n=0}^{\infty} P_n |n\rangle_{\mathbf{r}_0}\langle n|, \tag{A.4}$$

in which P_n is the probability of the occurrence of n photons.

The operator

$$\Pi(\mathbf{r}) = \sum_{n=0}^{\infty} \frac{n+1}{4\pi} |n\rangle_{\mathbf{r}}\langle n|, \tag{A.5}$$

is then found to be a continuous measurement that can generate a maximum-likelihood estimate $\mathbf{r}$ of any polarization $\mathbf{r}_0$ of state $\rho(\mathbf{r}_0)$ on the Bloch sphere, i.e., $\mathbf{r}_{0_{\mathrm{ML}}} = \arg\max_{\mathbf{r}\in S} P(\mathbf{r}|\mathbf{r}_0) = \mathbf{r}$, which is obtained by maximizing the likelihood function

$$\begin{aligned} P(\mathbf{r}|\mathbf{r}_0) &= \mathrm{Tr}\left[\Pi(\mathbf{r})\rho(\mathbf{r}_0)\right] = \mathrm{Tr}\left[\sum_{n=0}^{\infty} \frac{n+1}{4\pi} |n\rangle_{\mathbf{r}}\langle n| \sum_{n=0}^{\infty} P_n |n\rangle_{\mathbf{r}_0}\langle n|\right] \\ &= \sum_{n=0}^{\infty} \frac{n+1}{4\pi} P_n \langle n|_{\mathbf{r}}|n\rangle_{\mathbf{r}_0}\langle n|_{\mathbf{r}_0}|n\rangle_{\mathbf{r}} = \sum_{n=0}^{\infty} \frac{n+1}{4\pi} P_n |\langle n|_{\mathbf{r}}|n\rangle_{\mathbf{r}_0}|^2 = \sum_{n=0}^{\infty} \frac{n+1}{4\pi} P_n \left|f_{\mathbf{r}\mathbf{r}_0}\right|^{2n}. \end{aligned} \tag{A.6}$$

According to quantum estimation theory [69], the maximum-likelihood POVM $\Pi(\mathbf{r})$ satisfies the following conditions:

$$\left[\Upsilon - W(\mathbf{r})\right]\Pi(\mathbf{r}) = \Pi(\mathbf{r})\left[\Upsilon - W(\mathbf{r})\right] = 0 \tag{A.7}$$

and

$$\Upsilon - W(\mathbf{r}) \geq 0, \tag{A.8}$$

where

$$W(\mathbf{r}) \equiv \int_S d\mathbf{r}_0 \; p(\mathbf{r}_0) C(\mathbf{r}, \mathbf{r}_0) \rho(\mathbf{r}_0) = \frac{\rho(\mathbf{r})}{4\pi} \tag{A.9}$$

is the Hermitian risk operator with a uniform prior distribution $p(\mathbf{r}_0) = 1/4\pi$ and a delta cost function $C(\mathbf{r}, \mathbf{r}_0) = \delta(\mathbf{r} - \mathbf{r}_0)$. Here Υ is a Hermitian Lagrange operator defined by

$$\Upsilon \equiv \int_S d\mathbf{r} \; W(\mathbf{r}) \Pi(\mathbf{r}). \tag{A.10}$$

Note that the integration is over the Bloch surface S with $d\mathbf{r} = \sin\theta d\theta d\phi$. The proof of Eq. (A.5) satisfying the conditions (A.7) and (A.8) is shown below. First of all, it should be noted that Eq. (A.5) forms a legitimate continuous POVM (in $\mathbf{r}$), *viz.*, $\Pi(\mathbf{r}) > 0$ and

$$\int_S \Pi(\mathbf{r}) d\mathbf{r} = I, \tag{A.11}$$

where

$$I \equiv \sum_{n=0}^{\infty} I_n \equiv \sum_{n=0}^{\infty} \left[\sum_{m=0}^{n} |m\rangle_H \langle m| \otimes |n-m\rangle_V \langle n-m| \right] = \sum_{n=0}^{\infty} |n\rangle_H \langle n| \otimes \sum_{m=0}^{\infty} |m\rangle_V \langle m| \tag{A.12}$$

is the identity operator of the infinite dimensional Fock space and I_n is the identity operator of the n photon subspace. In addition, substituting Eqs. (A.9) and (A.5)

into Eq. (A.10), one obtains

$$\begin{aligned}\Upsilon &= \int_S d\mathbf{r}\frac{\rho(\mathbf{r})}{4\pi}\sum_{n=0}^{\infty}\frac{n+1}{4\pi}|n\rangle_{\mathbf{r}}\langle n| = \int_S d\mathbf{r}\frac{\sum_{n=0}^{\infty}P_n|n\rangle_{\mathbf{r}}\langle n|}{4\pi}\sum_{n=0}^{\infty}\frac{n+1}{4\pi}|n\rangle_{\mathbf{r}}\langle n| \\ &= \sum_{n=0}^{\infty}\frac{n+1}{16\pi^2}P_n\int_S d\mathbf{r}|n\rangle_{\mathbf{r}}\langle n| = \sum_{n=0}^{\infty}\frac{n+1}{16\pi^2}P_n\frac{4\pi I_n}{n+1} = \frac{1}{4\pi}\sum_{n=0}^{\infty}P_nI_n,\end{aligned} \tag{A.13}$$

which is Hermitian; i.e., $\Upsilon = \Upsilon^\dagger$. Then substituting Eqs. (A.9), (A.5) and (A.10) into Eq. (A.7), one obtains

$$\begin{aligned}\Pi(\mathbf{r})\left[\Upsilon - W(\mathbf{r})\right] &= \sum_{n=0}^{\infty}\frac{n+1}{4\pi}|n\rangle_{\mathbf{r}}\langle n|\left[\frac{1}{4\pi}\sum_{n=0}^{\infty}P_nI_n - \frac{\rho(\mathbf{r})}{4\pi}\right] \\ &= \frac{P_n}{4\pi}\sum_{n=0}^{\infty}\frac{n+1}{4\pi}|n\rangle_{\mathbf{r}}\langle n|\left(\sum_{n=0}^{\infty}I_n - \sum_{n=0}^{\infty}|n\rangle_{\mathbf{r}}\langle n|\right) \\ &= \frac{P_n}{4\pi}\left(\sum_{n=0}^{\infty}\frac{n+1}{4\pi}|n\rangle_{\mathbf{r}}\langle n| - \sum_{n=0}^{\infty}\frac{n+1}{4\pi}|n\rangle_{\mathbf{r}}\langle n||n\rangle_{\mathbf{r}}\langle n|\right) = 0,\end{aligned} \tag{A.14}$$

which verifies Eq. (A.7). To prove Eq. (A.8), I first organize the operator $\Upsilon - W(\mathbf{r})$ into a more suggestive form:

$$\Upsilon - W(\mathbf{r}) = \frac{1}{4\pi}\sum_{n=0}^{\infty}P_n\left(I_n - |n\rangle_{\mathbf{r}}\langle n| \otimes |0\rangle_{-\mathbf{r}}\langle 0|\right), \tag{A.15}$$

where the polarization $-\mathbf{r}$ is perpendicular to $\mathbf{r}$. Now I_n can be expanded in any orthogonal polarization basis:

$$I_n = \sum_{m=0}^{n}|m\rangle_{\mathbf{r}}\langle m| \otimes |n-m\rangle_{-\mathbf{r}}\langle n-m|. \tag{A.16}$$

Therefore $\Upsilon - W(\mathbf{r})$ is a non-negative definite operator. So far, both Eqs. (A.7)

and (A.8) have been proven, and hence $\Pi(\mathbf{r})$ in Eq. (A.5) is a maximum-likelihood POVM.

Appendix B: Proof of Eq. (4.8) using the mathematical induction

In order to prove Eq. (4.8), mathematical induction can be utilized. Given the to-be-proved equation

$$\prod_{k=1}^{x} M_k|NN\rangle_{ad} = \left(-\frac{i}{2}\right)^x \prod_{k=1}^{x} \sin^2\theta_k \cos^{2(N-k)}\theta_k \prod_{k=1}^{x}\left(a^2 + e^{i2\psi_k}d^2\right)|NN\rangle_{ad}, \quad \text{(B.1)}$$

the base case at $x = 1$ is calculated as follows:

$$\begin{aligned}
M_1|N,N\rangle_{ad} &= \frac{i}{\sqrt{2}}({}_{b'c'}\langle 20| + e^{i2\psi_k}{}_{b'c'}\langle 02|)U(\theta_1)\frac{a^{\dagger N}d^{\dagger N}}{N!}|0\rangle \\
&= \frac{i}{\sqrt{2}}({}_{b'c'}\langle 20| + e^{i2\psi_k}{}_{b'c'}\langle 02|)\frac{(\cos\theta_1 a'^{\dagger} + i\sin\theta_1 b'^{\dagger})^N(\cos\theta_1 d'^{\dagger} + i\sin\theta_1 c'^{\dagger})^N}{N!}|0\rangle \\
&= -\frac{i}{\sqrt{2}}({}_{b'c'}\langle 20| + e^{i2\psi_k}{}_{b'c'}\langle 02|)\frac{C_N^2}{N!} \\
&\quad \left(\sin\theta_1{}^2\cos\theta_1{}^{2N-2}a'^{\dagger(N-2)}b'^{\dagger 2}d'^{\dagger N} + \cos\theta_1{}^{2N-2}\sin\theta_1{}^2 a'^{\dagger N}c'^{\dagger 2}d'^{\dagger(N-2)}\right)|0\rangle \\
&= -i\frac{C_N^2\sin\theta_1{}^2\cos\theta_1{}^{2N-2}}{N!}\left(a'^{\dagger(N-2)}d'^{\dagger N}|00\rangle_{a'd'} + e^{i2\psi_k}a'^{\dagger N}d'^{\dagger(N-2)}|00\rangle_{a'd'}\right) \\
&= -i\frac{C_N^2\sin\theta_1{}^2\cos\theta_1{}^{2N-2}}{N!}\sqrt{(N-2)!N!}\left(|N-2,N\rangle_{a'd'} + e^{i2\psi_k}|N,N-2\rangle_{a'd'}\right) \\
&= -\frac{i}{2}\sin^2\theta_1\cos^{2(N-1)}\theta_1(a'^2 + e^{i2\psi_k}d'^2)|N,N\rangle_{a'd'} \\
&= -\frac{i}{2}\sin^2\theta_1\cos^{2(N-1)}\theta_1(a^2 + e^{i2\psi_k}d^2)|N,N\rangle_{ad},
\end{aligned} \quad \text{(B.2)}$$

which satisfies Eq. (B.1). Then assuming Eq. (B.1) holds for $x = y$ with $y = 2, 3, \cdots, N/2 - 1$:

$$\prod_{k=1}^{y} M_k |NN\rangle_{ad} = \left(-\frac{i}{2}\right)^y \prod_{k=1}^{y} \sin^2\theta_k \cos^{2(N-k)}\theta_k \prod_{k=1}^{y} \left(a^2 + e^{i2\psi_k} d^2\right) |NN\rangle_{ad}, \quad \text{(B.3)}$$

one can calculate the case with $x = y + 1$:

$$\begin{aligned}
&\prod_{k=1}^{y+1} M_k |NN\rangle_{ad} = M_{y+1} \prod_{k=1}^{y} M_k |NN\rangle_{ad} \\
&= \frac{i}{\sqrt{2}} ({}_{b'c'}\langle 20| + e^{i2\psi_{y+1}} {}_{b'c'}\langle 02|) U(\theta_{y+1}) \left(-\frac{i}{2}\right)^y \\
&\quad \prod_{k=1}^{y} \sin^2\theta_k \cos^{2(N-k)}\theta_k \prod_{k=1}^{y} \left(a^2 + e^{i2\psi_k} d^2\right) |NN\rangle \\
&= \left(-\frac{i}{2}\right)^y \prod_{k=1}^{y} \sin^2\theta_k \cos^{2(N-k)}\theta_k \frac{i}{\sqrt{2}} {}_{b'c'}(\langle 20| + e^{i2\psi_{y+1}} \langle 02|) U(\theta_{y+1}) \\
&\quad \sum_{m=0}^{y} \frac{N!}{(N-2m)!(N-2y+2m)!} \\
&\quad \sum_{\substack{C_y^m \text{ combs of } m \ x_i \\ x_i \in [1,y],\ x_i \neq x_j}} e^{i2\left(\psi_{x_1} + \psi_{x_2} + \ldots + \psi_{x_m}\right)} a^{\dagger(N-2y+2m)} d^{\dagger(N-2m)} |0,0\rangle \\
&= \left(-\frac{i}{2}\right)^y \prod_{k=1}^{y} \sin^2\theta_k \cos^{2(N-k)}\theta_k \frac{i}{\sqrt{2}} {}_{b'c'}(\langle 20| + e^{i2\psi_{y+1}} \langle 02|) \\
&\quad \sum_{m=0}^{y} \frac{N!}{(N-2m)!(N-2y+2m)!} \sum_{x_i \in [1,y],\ x_i \neq x_j} e^{i2\left(\psi_{x_1} + \psi_{x_2} + \ldots + \psi_{x_m}\right)} \\
&\quad (\cos\theta_{y+1} a^\dagger + i \sin\theta_{y+1} b^\dagger)^{(N-2y+2m)} (\cos\theta_{y+1} d^\dagger + i \sin\theta_{y+1} c^\dagger)^{(N-2m)} |0,0\rangle
\end{aligned} \quad \text{(B.4)}$$

$$
\begin{aligned}
&= -\left(-\frac{i}{2}\right)^{y} \prod_{k=1}^{y} \sin^2\theta_k \cos^{2(N-k)}\theta_k \sin^2\theta_{y+1}\cos^{2(N-y-1)}\theta_{y+1}\frac{i}{\sqrt{2}}b'c'\big(\langle 20| + e^{i2\psi_{y+1}}\langle 02|\big) \\
&\quad \sum_{m=0}^{y} \frac{N!}{(N-2m)!(N-2y+2m)!} \sum_{x_i\in[1,y],\ x_i\neq x_j} e^{i2\left(\psi_{x_1}+\psi_{x_2}+\ldots+\psi_{x_m}\right)} \\
&\quad \big(C^2_{N-2y+2m} a^{\dagger(N-2y+2m-2)} b^{\dagger 2} d^{\dagger(N-2m)} + C^2_{N-2m} a^{\dagger(N-2y+2m)} c^{\dagger 2} d^{\dagger(N-2m-2)}\big)|0,0\rangle \\
&= -i\left(-\frac{i}{2}\right)^{y} \prod_{k=1}^{y+1} \sin^2\theta_k \cos^{2(N-k)}\theta_k \sum_{m=0}^{y} \frac{N!}{(N-2m)!(N-2y+2m)!} \\
&\quad \sum_{x_i\in[1,y],\ x_i\neq x_j} e^{i2\left(\psi_{x_1}+\psi_{x_2}+\ldots+\psi_{x_m}\right)} \\
&\quad \big(C^2_{N-2y+2m} a^{\dagger(N-2y+2m-2)} d^{\dagger(N-2m)} + C^2_{N-2m} e^{i2\psi_{y+1}} a^{\dagger(N-2y+2m)} d^{\dagger(N-2m-2)}\big)|0,0\rangle \\
&= \left(-\frac{i}{2}\right)^{y+1} \prod_{k=1}^{y+1} \sin^2\theta_k \cos^{2(N-k)}\theta_k \sum_{m=0}^{y} \sum_{x_i\in[1,y],\ x_i\neq x_j} e^{i2\left(\psi_{x_1}+\psi_{x_2}+\ldots+\psi_{x_m}\right)} \\
&\quad \Big(\frac{N!}{(N-2m)!(N-2y+2m-2)!} a^{\dagger(N-2y+2m-2)} d^{\dagger(N-2m)} \\
&\quad + \frac{N!}{(N-2y+2m)!(N-2m-2)!} e^{i2\psi_{y+1}} a^{\dagger(N-2y+2m)} d^{\dagger(N-2m-2)}\Big)|0,0\rangle \\
&= \left(-\frac{i}{2}\right)^{y+1} \prod_{k=1}^{y+1} \sin^2\theta_k \cos^{2(N-k)}\theta_k \\
&\quad \Big(\sum_{m=0}^{y} \sum_{x_i\in[1,y],\ x_i\neq x_j} e^{i2\left(\psi_{x_1}+\psi_{x_2}+\ldots+\psi_{x_m}\right)} \frac{N! a^{\dagger(N-2y+2m-2)} d^{\dagger(N-2m)}}{(N-2m)!(N-2y+2m-2)!} \\
&\quad + \sum_{m'=1}^{y+1} \sum_{x_i\in[1,y],\ x_i\neq x_j} e^{i2\left(\psi_{x_1}+\psi_{x_2}+\ldots+\psi_{x_{m'-1}}\right)} \frac{e^{i2\psi_{y+1}} N! a^{\dagger(N-2y+2m'-2)} d^{\dagger(N-2m')}}{(N-2y+2m'-2)!(N-2m')!}\Big)|0,0\rangle
\end{aligned}
\tag{B.5}
$$

$$
\begin{aligned}
&= \left(-\frac{i}{2}\right)^{y+1} \prod_{k=1}^{y+1} \sin^2\theta_k \cos^{2(N-k)}\theta_k \Bigg(\frac{a^{\dagger(N-2y-2)} d^{\dagger(N)}}{(N-2y-2)!} + \\
&\sum_{m=1}^{y} \Big(\sum_{x_i \in [1,y]}^{x_i \neq x_j} e^{i2\left(\psi_{x_1}+\psi_{x_2}+\ldots+\psi_{x_m}\right)} + \sum_{x_i \in [1,y]}^{x_i \neq x_j} e^{i2\left(\psi_{x_1}+\psi_{x_2}+\ldots+\psi_{x_{m-1}}+\psi_{y+1}\right)} \Big) \\
&\frac{N! a^{\dagger(N-2y+2m-2)} d^{\dagger(N-2m)}}{(N-2y+2m-2)!(N-2m)!} \\
&+ e^{i2\left(\psi_1+\psi_2+\ldots+\psi_{x_y}+\psi_{y+1}\right)} \frac{a^{\dagger(N)} d^{\dagger(N-2y-2)}}{(N-2y-2)!} \Bigg) |0,0\rangle \\
&= \left(-\frac{i}{2}\right)^{y+1} \prod_{k=1}^{y+1} \sin^2\theta_k \cos^{2(N-k)}\theta_k \Bigg(\frac{a^{\dagger(N-2y-2)} d^{\dagger(N)}}{(N-2y-2)!} \\
&+ \sum_{m=1}^{y} \sum_{x_i \in [1,y+1],\ x_i \neq x_j} e^{i2\left(\psi_{x_1}+\psi_{x_2}+\ldots+\psi_{x_m}\right)} \frac{N! a^{\dagger(N-2y+2m-2)} d^{\dagger(N-2m)}}{(N-2y+2m-2)!(N-2m)!} \\
&+ e^{i2\left(\psi_1+\psi_2+\ldots+\psi_{x_y}+\psi_{y+1}\right)} \frac{a^{\dagger(N)} d^{\dagger(N-2y-2)}}{(N-2y-2)!} \Bigg) |0,0\rangle \\
&= \left(-\frac{i}{2}\right)^{y+1} \prod_{k=1}^{y+1} \sin^2\theta_k \cos^{2(N-k)}\theta_k \sum_{m=0}^{y+1} \sum_{x_i \in [1,y+1]}^{x_i \neq x_j} e^{i2\left(\psi_{x_1}+\psi_{x_2}+\ldots+\psi_{x_m}\right)} \\
&\frac{N! a^{\dagger(N-2y+2m-2)} d^{\dagger(N-2m)}}{(N-2y+2m-2)!(N-2m)!} |0,0\rangle \\
&= \left(-\frac{i}{2}\right)^{y+1} \prod_{k=1}^{y+1} \sin^2\theta_k \cos^{2(N-k)}\theta_k \prod_{k=1}^{y+1} (a^2 + e^{i2\psi_k} d^2) |NN\rangle_{ad}.
\end{aligned}
\tag{B.6}
$$

Therefore, Eq. (B.1) is proved to be valid for any $x \leq N/2$. When $x = N/2$, it gives Eq. (4.8).